

**ANALYSIS OF ABDOMINAL SLOW POTENTIALS
DURING MOTION SICKNESS**

by

Brian W. Rague

S.B., Massachusetts Institute of Technology

(1984)

SUBMITTED IN PARTIAL FULFILLMENT
OF THE REQUIREMENTS OF THE
DEGREE OF

MASTER OF SCIENCE IN
AERONAUTICS AND ASTRONAUTICS

at the

MASSACHUSETTS INSTITUTE OF TECHNOLOGY

May 1987

© Massachusetts Institute of Technology 1987

Signature of Author _____

Department of Aeronautics and Astronautics
May 8, 1987

Certified by _____

Dr. Charles M. Oman
Thesis Supervisor, Department of Aeronautics and Astronautics

Accepted by _____

Prof. Harold Y. Wachman
Chairman, Department Graduate Committee



Room 14-0551
77 Massachusetts Avenue
Cambridge, MA 02139
Ph: 617.253.2800
Email: docs@mit.edu
<http://libraries.mit.edu/docs>

DISCLAIMER OF QUALITY

Due to the condition of the original material, there are unavoidable flaws in this reproduction. We have made every effort possible to provide you with the best copy available. If you are dissatisfied with this product and find it unusable, please contact Document Services as soon as possible.

Thank you.

Some pages in the original document contain pictures, graphics, or text that is illegible.

ANALYSIS OF ABDOMINAL SLOW POTENTIALS
DURING MOTION SICKNESS

by

BRIAN WILLIAM RAGUE

Submitted to the Department of Aeronautics and Astronautics
on May 8, 1987 in partial fulfillment of the
requirements for the Degree of Master of Science in
Aeronautics and Astronautics

ABSTRACT

The purpose of this investigation was to quantitatively characterize changes in gastric myoelectrical activity in subjects experiencing motion sickness. Gastric electrical activity can be recorded cutaneously via surface electrodes placed on the abdomen, a method called electrogastrography (EGG).

Six healthy volunteers each participated in four repetitions of a standard motion sickness experiment. To induce motion sickness, subjects executed head movements in pitch and roll while rotating about an earth-vertical axis, thus producing a provocative Coriolis cross-coupled stimulus to the semicircular canals. A velocity staircase rotation profile was used. Subjects evaluated their sickness intensity using magnitude estimation of overall discomfort. Symptom endpoint was "halfway to vomiting." Symptoms were simultaneously scored according to the Pensacola Diagnostic method.

The stimulus successfully elicited moderate to severe symptoms in all test sessions. The EGG signal, sampled at 1 Hz, was obtained during the entire stimulus period and for at least 15 minutes prior to chair rotation. Running spectrum analysis of the recorded EGG's from all trials show a consistent loss in power of the 3 cycle/minute Basic Electrical Rhythm (BER) component by an average of 85% during motion sickness periods.

A dimensionless Spectrum Peak Index was proposed to detect EGG rhythm changes. A running average of the Spectrum Peak Index was calculated to obtain a measure of the duration and stability of decreases in BER magnitude. Parameters associated with this running average method were optimized to predict sickness. Using this method, running average EGG changes occurred more than one minute before the experimental endpoint was reached in 22 of 24 sessions. False positives occurred ~10% of the time in resting subjects. False negatives for subjects experiencing moderate or severe nausea occurred ~17% of the

time.

Although BER amplitude decrease was thus a reasonably consistent feature of sickness onset; it is not pathognomonic. Unequivocal tachygastric activity occurred in only 7 of the 24 trials, in contrast to a recent study by Stern, et.al. in which tachygastrias and motion sickness appeared more strongly correlated.

Thesis Supervisor: Dr. Charles M. Oman

Title: Sr. Research Engineer, Dept. of Aeronautics and Astronautics

Contents

1	Introduction	6
2	Background Issues	16
2.1	Electrical and Mechanical Activity of the Stomach	16
2.1.1	Anatomy of the stomach	16
2.1.2	Gastric action potentials	17
2.1.3	Propagation of action potentials	19
2.1.4	The interdigestive migrating complex	21
2.1.5	The cutaneous waveform	22
2.2	Motion Sickness	25
2.2.1	Organs for transducing motion	25
2.2.2	Etiology of motion sickness	26
2.2.3	Coriolis cross-coupled stimulation	30
2.2.4	Symptom scoring and magnitude estimation	34
2.3	EGG Processing and Analysis	43
2.3.1	Electrodes and electrode placement	43
2.3.2	Fourier Analysis and windowing	48
2.3.3	Power spectrum estimation	56
2.3.4	Running spectrum analysis	58
3	Materials and Methods	64
3.1	Subjects	64
3.2	EGG Recording	65
3.3	Signal Analysis and System Overview	67
3.4	Procedure	73
4	Results	75

CONTENTS

5

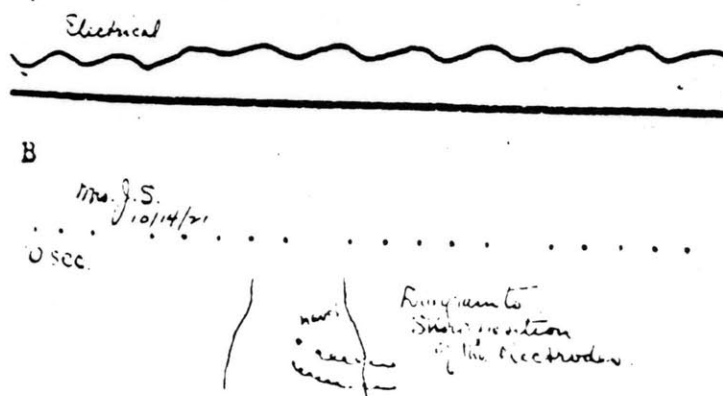
5 Analysis and Discussion	84
5.1 Spectrum Peak Index	84
5.2 Running Average Method Applied to the Spectrum Peak Index	88
5.3 The Usefulness of Tachygastrias in Motion Sickness Diagnosis	100
5.4 EGG Recording and Processing Methods	102
5.5 Summary	109
A Motion Sickness Questionnaire, Pre-Session Questionnaire, Magnitude Estimation Instructions, and Informed Consent Statement	112
B Symptom Scoring Definitions	120
C Lattice-C Programs used for EGG Real-Time Analysis	129
D Data	151
Bibliography	176
Acknowledgements	182

Chapter 1

Introduction

Gastric smooth muscle fibers generate electrical activity which can be recorded with surface electrodes placed on the abdomen. The signal from the stomach tissue that is measured is called the electrogastrogram, and the recording procedure is termed electrogastrography. The purpose of this investigation was to study cutaneous electrogastrogram recordings, using running spectrum analysis, in order to quantitatively characterize changes in gastric myoelectrical activity in subjects experiencing motion sickness. The consistency of the electrogastrogram response during periods of motion sickness stress is analyzed for the purpose of developing statistical criteria for diagnosis. The engineering objective of this research was to develop a microcomputer (PC/AT) based system capable of data acquisition and real-time signal processing of the electrogastrogram. Because PC/AT compatible systems are increasingly common in both research and clinical environments, the analysis software written for this investigation may be easily transported to computers in other laboratories doing electrogastrography. Throughout the following report, both electrogastrography and the electrogastrogram will be referred to as EGG.

The investigation of the EGG essentially began in 1922, when Walter Alvarez recorded the first electrogastrogram in a thin, elderly woman with a large cicatricial hernia[3]. The woman's abdominal wall was so thin that Alvarez was able to observe the rhythmic peri-



The first electrogastrogram, recorded by Alvarez.
The intervals between the dots represent 11 seconds.

Figure 1.1: First EGG (from Alvarez,1922).

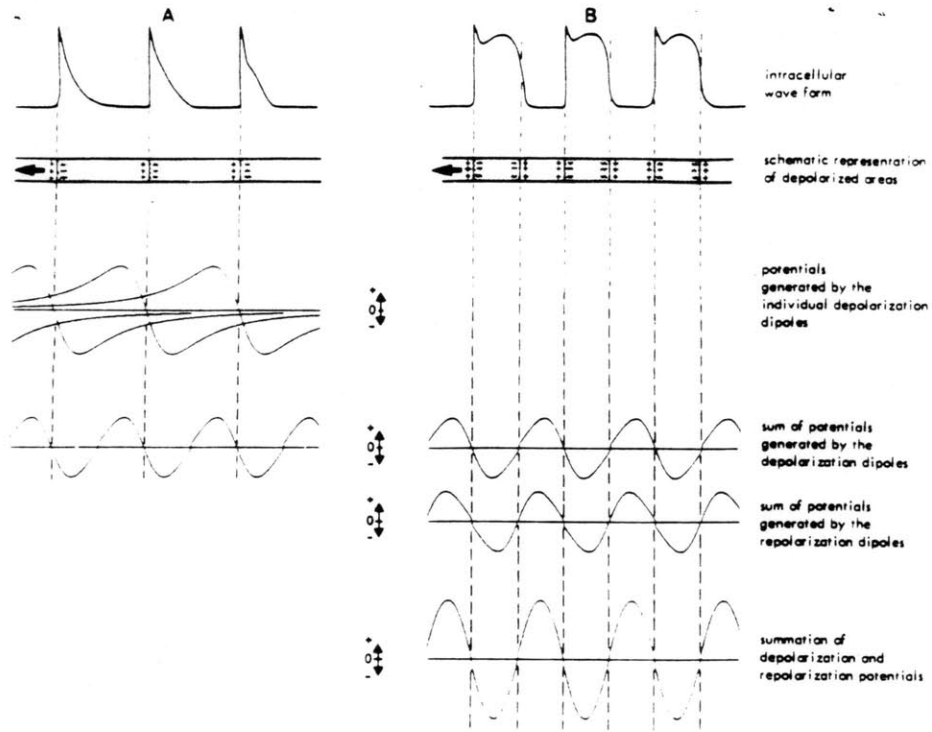
staltic movements associated with stomach contractions. During the recording session, he found a consistent correlation between the periodicity of the signal detected via the surface electrodes and the regular visible movements of the stomach. Figure 1.1 shows a sketch of this first EGG record as well as a diagram of electrode positions. As shown in the figure, the period of the EGG is about 20 seconds. This translates to a frequency of 0.05 hz or 3 cycle/minute (3 cpm). Subsequent EGG experiments verified the existence of this baseline gastric rhythm in normal, resting humans[11,12,54,66]. The 3 cpm frequency has been designated as Electrical Control Activity (ECA), Basic Electrical Rhythm (BER), slow wave activity, etc. In this paper, the baseline rhythm will usually be referred to as BER.

In 1975, Brown, et.al. analyzed EGG's of sixteen healthy volunteers[8]. The stomach's mechanical activity was simultaneously monitored by measuring intragastric pressure. The investigators found that 3 cpm activity occurs during periods of motor quiescence, i.e., no stomach contractions. Other observations from this study include a periodic component of

higher frequency (10 to 12 cpm) in 9 out of 32 recordings that was ascribed to the electrical activity of the small intestine. Also, after consumption of a meal the amplitude of the gastric component increased by about 150%. This increase was assumed to be due to a decreased distance of the electrodes to the distended stomach.

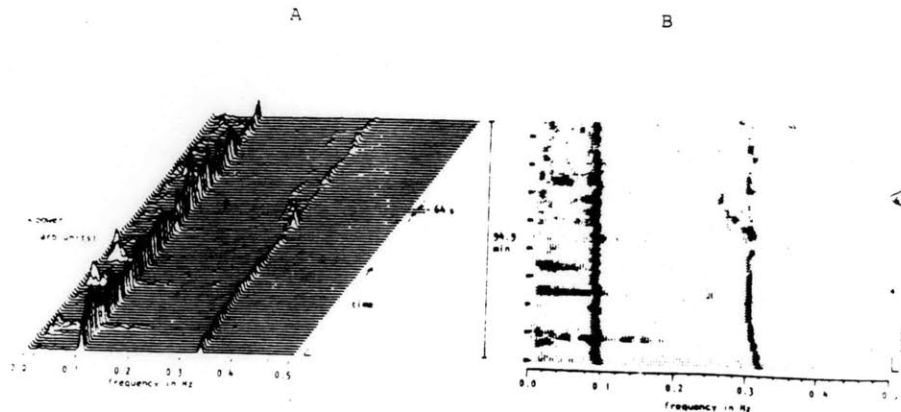
The amplitude of the raw EGG is typically 100-300 μ V. The size of the BER varies with subject, electrode position with respect to the gastric antrum, gastric contractile activity, extent of fasting, and other factors. Because of this small amplitude and the ultra-low frequency range of interest (0-0.5 hz), EGG records are hampered by electrode motion artifact, usually respiratory in origin. Successful recordings usually require that the subject remains relatively still. Also, various bandpass filtering protocols have been utilized to produce better quality recordings for visual inspection[56,70].

Recently, the most comprehensive research of EGG origin, measurement, and analysis has been conducted by a clinical group at Erasmus University in Rotterdam, The Netherlands. The objectives of their work in electrogastrography are geared toward clinical applications, with an emphasis on the diagnostic and noninvasive value of the EGG recording technique. Smout's introductory paper on EGG, "What is measured in Electrogastrography?" details the evidence that gastric myoelectrical activity is, indeed, being reflected in the surface recordings of the EGG[52]. Other human experiments have verified that the BER obtained from cutaneous electrodes is similar in character to the signal recorded directly from the stomach mucosa using mucosal electrodes[1,2,18,21]. In the latter portion of his paper, Smout proposes a dipole model to explain the postprandial amplitude increase of the EGG. Figure 1.2 summarizes the basic idea. Smout also characterized a 'second potential' which is phase-locked to the ECA and indicative of contractile activity in the stomach. This has been designated electrical response activity (ERA). ERA is frequently characterized by spiking activity in the intracellular recordings of stomach tissue. However, Smout warns that "...in the canine stomach ERA does not always consist of spikes."



- A Computer simulation of the potential variations recorded when a series of equally spaced depolarization dipoles travels slowly underneath a remote electrode, as in a mechanically inactive stomach.
- B Computed potential variations when in addition to depolarization dipoles repolarization dipoles are present, as in mechanically active stomach.
 (Distance from electrode to dipoles was 5 cm. For other parameters see Appendix.)

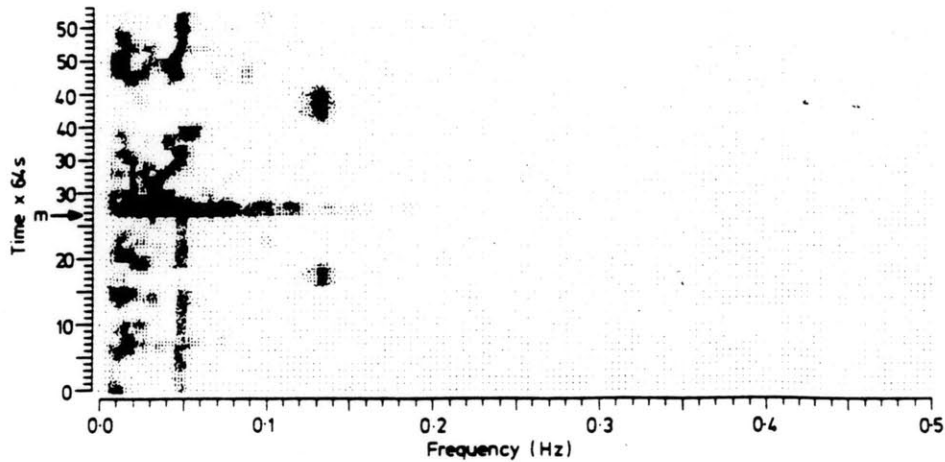
Figure 1.2: Dipole model (from Smout,1980).



Running Spectrum display of 94.9 min of postprandial recording. Cutaneous signal R-L. Overlap 75%. Dog 2. A. Pseudo 3-D display. B. Grey-scale plot.

Figure 1.3: EGG displays (from Van Der Schee,1982).

Fourier analysis of EGG time series is widespread[8,32,50,52,53,65]. Other analysis methods include auto-regressive modelling[33], phase-lock techniques[49], and adaptive filtering[30,72]. The use of Fourier transformations to implement running spectrum analysis (RSA) was introduced by Van Der Schee, et.al.[70]. In RSA, frequency changes in the input signal over time can be derived by taking Fourier transforms of successive overlapping stretches of input data. The resulting information can be displayed as a grey-scale plot, or waterfall plot, both shown in Figure 1.3. Parameters such as sampling rate, length of window, percentage overlap, windowing function, and electrode configuration are proposed by Van Der Schee. A discussion of the methods and rationale behind their recording procedure is also presented. The final conclusion is that "RSA offers the possibility of extracting both qualitative and quantitative information from the electrogastrogram. It can be considered as a significant improvement in the analysis of the EGG, which brings electrogastrography one step closer to (clinical) application."



Grey-scale plot of an electrogastrogram from the patient with tachygastrias both in fasting and postprandial states at about 0.13 Hz. Coinciding with food intake (start marked with 'M') the effect of a motion artefact is visible in the spectrum.

Figure 1.4: Occurrence of tachygastrias (from Geldof, et.al., 1986).

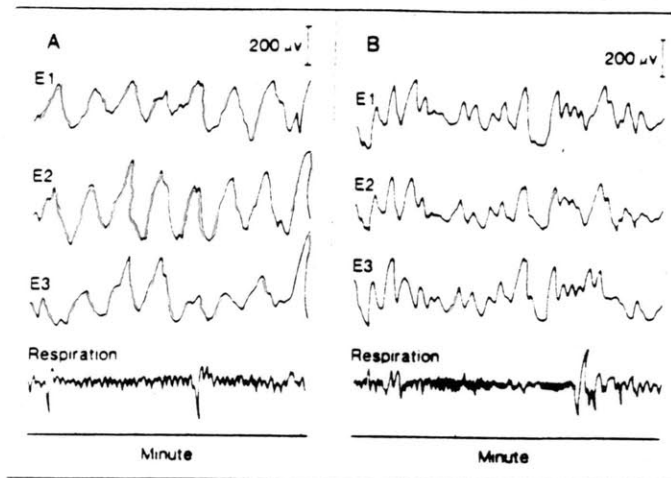
Recent clinical studies of certain selected patients with chronic or unexplained nausea and vomiting have suggested that a disturbance of the frequency of the BER can be found intermittently in these patients [17, 21, 63, 78, 79]. These disturbances are typically characterized by abnormal increases in BER frequency, called tachygastrias. Geldof, et.al., report that tachygastria occurred in 8 of their 48 patients, and that these episodes lasted between 3 and 14 minutes [17]. Figure 1.4 shows evidence of tachygastrias in a grey-scale plot. Hamilton observed in one normal subject a period of 2.5 minutes in which the BER rate "exceeded five per minute." However, the intermittent occurrence of tachygastrias in normal, resting subjects has yet to be validated.

Geldof, et.al., utilized EGG techniques in assessing gastric myoelectrical activity in patients with unexplained nausea and vomiting [17]. They state that their "study shows that with electrogastrography... abnormal myoelectrical behaviour can be discerned." Based on their observations, 48% of the patients exhibited anomalous myoelectrical activity which

was characterized by instability of the BER, tachygastrias in both the fasting and postprandial states, and the absence of the normal amplitude increase in the postprandial electrogastrogram. Thus, Geldof was successful in defining a subgroup of patients exhibiting abnormal myoelectrical activity as indicated by the EGG.

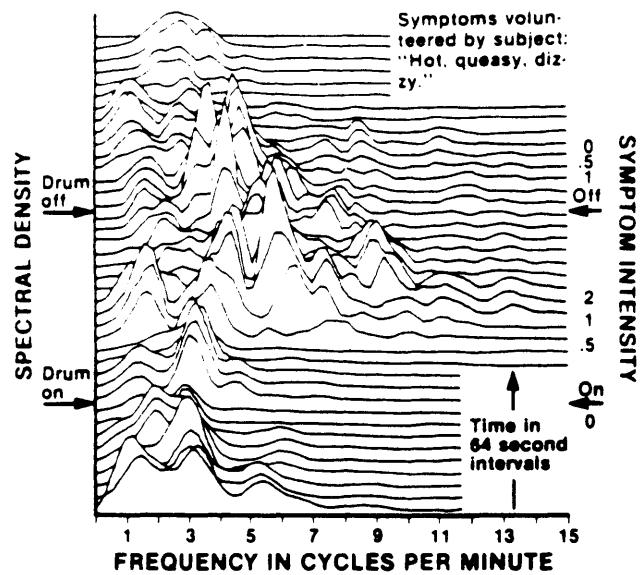
The correlation between clinical nausea and changes in the EGG frequency has, not surprisingly, prompted investigations into the effect of motion sickness on gastric myoelectrical activity. Early investigators reported decreased gastric contractions and tone in subjects experiencing motion sickness[34,77]. In related work, it was demonstrated that labyrinthine stimulation caused decreased antral contractions and delayed gastric emptying of a standard meal[64]. Also, there are anecdotal accounts that abdominal sounds are absent during periods of space sickness stress(Thornton & Linder, personal communication). Most recently, Stern, et.al., have presented evidence of a disappearance of the 3 cpm BER, and increased tachygastric activity in the 4-9 cpm frequency range[56,57].

Initially, Stern and his colleagues visually inspected the EGG time series records of 21 healthy volunteers, 14 of whom exhibited signs of motion sickness. Figure 1.5 shows a record of tachygastric activity in one of Stern's subjects who reported symptoms. Stern states that for each of the 14 motion sick subjects, "the EGG frequency shifted from the normal 3 cpm to 5-8 cpm, tachygastric, an abnormal pattern." Only one of the seven asymptomatic subjects showed any alteration in normal gastric rhythm. Stern concludes that his findings "clearly link tachygastric activity and symptoms of motion sickness induced byvection." Two years later, Stern published a similar paper which utilized running spectrum analysis to indicate and display frequency changes in the EGG. Figure 1.6 shows the results of one of his experiments. Again, Stern claims a "very strong temporal correspondence between onset and resolution of tachygastric activity and increasing and decreasing symptoms." In this set of experiments, 10 of 15 subjects reported symptoms related to motion sickness induced by their circularvection stimulus. All 10 subjects "showed a shift of their dominant gastric



A. EGG activity recorded from upper, middle and lower electrodes (E1-E3) prior to drum rotation (Subject No. 10). The EGG frequency is 3 cpm. B) EGG from the same subject after the start of drum rotation. Note the presence of tachygastric activity (6 cpm). Tachygastric activity began at minute 4. The subject reported nausea at minute 6 and requested that drum rotation be stopped at minute 11.

Figure 1.5: Tachygastric event (from Stern, et al., 1985).



Running spectral analysis of the EGG of subject 8 who reported that during rotation he was sweating, dizzy, and had a queasy stomach. Whereas 3- and 1-cycles/min activity dominate the spectral analysis before drum rotation. 6 min after the onset of rotation spectral density showed a peak at 6 cycles/min with additional density in the tachygastria range (5-9 cycles/min). At approximately this same point in time the subject reported his first symptoms of motion sickness.

Figure 1.6: Tachygastria shown by waterfall plot (from Stern,et.al.,1987).

frequency from 3 cpm to 4-9 cpm." The five subjects who reported no symptoms of motion sickness "showed a continuation of normal 3 cpm activity during drum rotation."

Results from the test sessions presented in this report are compared with those of Stern to verify his findings. Initial comparisons indicate that differences in electrode position, recording procedure, and stimulus protocol may lead to varying conclusions about the behaviour of the EGG during motion sickness. Clearly, the efforts of several investigators will be required to determine the true value and efficacy of the EGG in detection of motion sickness onset.

Chapter 2

Background Issues

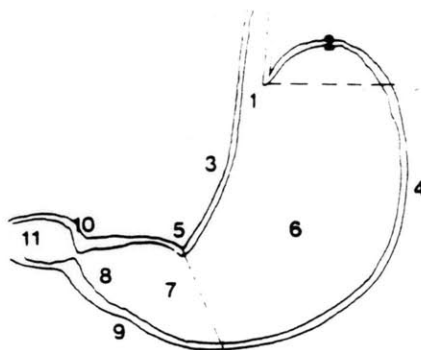
This chapter will provide information about the physiological mechanisms responsible for the generation of the EGG, the time course and development of motion sickness signs and symptoms, and the signal processing theory involved in the measurement and analysis of abdominal biopotentials. These explanations are an attempt to elucidate the motivation behind EGG investigations and to present the problems and trade-offs associated with the experimental design. The topics to be described are important in understanding the procedures and results of the test sessions.

2.1 Electrical and Mechanical Activity of the Stomach

Smout[51] and Van Der Schee[69] both give a clear, detailed account of stomach morphology and physiology in their respective theses. A concise summary of the main points of their work provides the basic information about gastric terminology and function needed to conduct investigations of stomach motility.

2.1.1 Anatomy of the stomach

Figure 2.1 is a schematic diagram of stomach anatomy. The cardiac portion or cardia (1) is that part of the stomach that surrounds the gastroesophageal orifice. The fundus(2)



*Macroscopic anatomy of the stomach.
For explanation of numbers see text.*

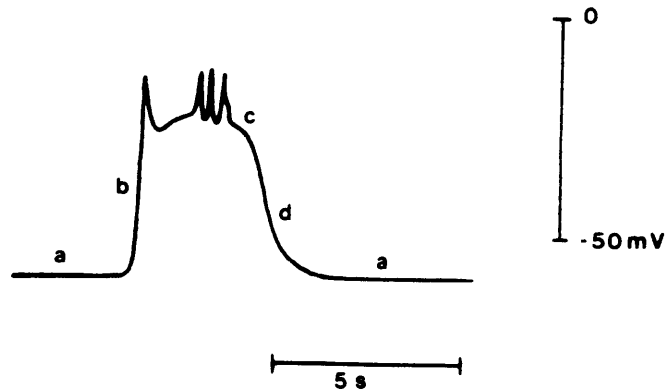
Figure 2.1: Stomach anatomy (from Smout,1980).

is the part oral to the gastroesophageal junction. The concave right border of the stomach is called the lesser curvature(3), and the left border, which is five times as long, is the greater curvature(4). In the lesser curvature a notch is present, the angular incisure(5). The plane through the angular incisure and perpendicular to the longitudinal axis of the stomach separates corpus(6) and pyloric portion(7+8). The pyloric portion is divided into a proximal part, the pyloric antrum(7), and a distal part, the pyloric canal(8). The boundary between these parts is sometimes indicated by a shallow indentation of the larger curvature, the sulcus intermedius(9). In the pyloric canal (length 2 to 3 cm) the circular muscle layer thickens to what has been called an intermediate sphincter.

The junction between stomach and duodenum(11), the pyloric sphincter or pylorus(10), is also characterized by a thickening of the circular muscle layer. The term 'antrum' is often used as a synonym for pyloric portion. 'Terminal antrum' is often used as a synonym for pyloric canal. Both these definitions will apply in this thesis as well.

2.1.2 Gastric action potentials

Intracellular electrode measurements reveal the shape of a typical action potential generated by the smooth muscle tissue of the stomach. Figure 2.2 shows the characteristic



Configuration of the action potential generated by gastric smooth muscle cells.

Figure 2.2: Gastric action potential (from Smout,1980).

waveform as it appears *during a gastric contraction*. The resting membrane potential (phase a) found in circular muscle cells of the canine stomach is about -70 mv. The amplitude of depolarization (phase b) increases from the corpus to the pyloric sphincter (28.5 mv to 73.8 mv). Depolarization rate increases in this anatomical direction as well (.54 V/s to 2.15 V/s)[15]. It should be noted that the proximal third portion of the stomach does not generate these action potentials.

Phase c is typically called a plateau phase, which may or may not bear spikes. Contractile activity has been closely linked to the size and duration of the plateau as shown in Figure 2.3[62]. Stronger contractions are associated with plateaus of higher amplitude and longer duration. Although slower in time, the shape of a gastric action potential during contraction is similar to that generated by cardiac smooth muscle tissue. The likeness is most evident in the contractile related plateau phase. Spiking activity, superimposed on the plateau phase, may or may not occur. As mentioned in Chapter 1, contractions may occur

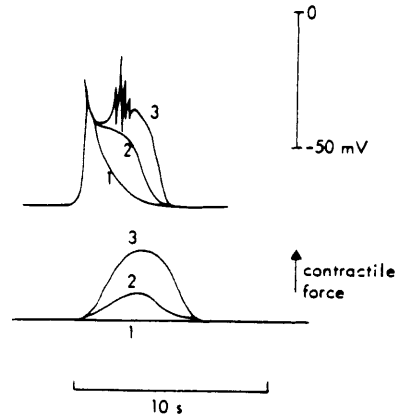


Figure 2.3: Relationship between contractile force and gastric action potential (from Van Der Schee, 1984).

in the absence of these spikes. Phase d is the repolarization phase. A high repolarization rate is directly correlated with a high plateau amplitude. Smout utilizes this fact in his discussion of increased EGG amplitude during gastric contractions shown in Figure 1.2.

2.1.3 Propagation of action potentials

In order to understand the direction of propagation of gastric action potentials, a brief description of stomach smooth muscle orientation is necessary. Figure 2.4 shows the three basic muscle layers that line the outside surface of the stomach.

The *longitudinal layer* is the most superficial muscle layer, situated directly under the serosal surface. A group of fibers is continuous with the longitudinal layer of the esophagus; these fibers run along the curvatures and end in the corpus. A second group of longitudinal fibers originates in the corpus at the greater curvature. Transection experiments of the gastric muscle layers have demonstrated that the BER is generated in this region [29,75]. Thus, like the heart, the stomach may be considered to possess a pacemaker node. However, histological investigations have yet to verify the existence of a group of gastric pacemaker cells. These longitudinal fibers originating in the corpus radiate in all directions, but in particular toward the pylorus. Examination of BER propagation direction has revealed that

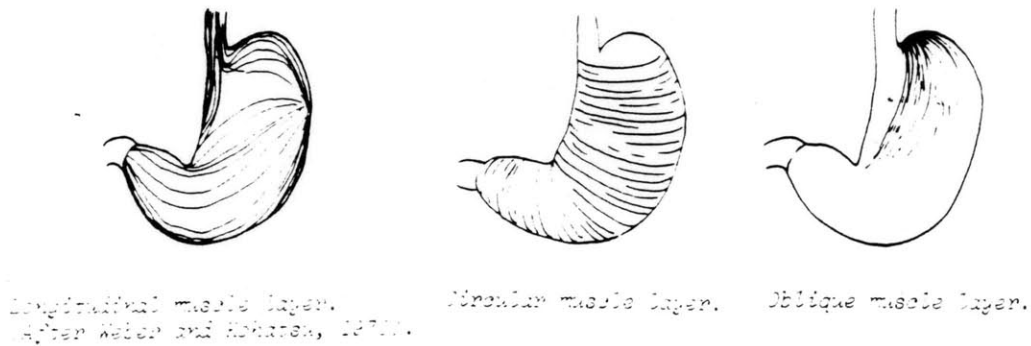


Figure 2.4: Smooth muscle layers in the stomach (from Smout,1980).

it sweeps distally, from its point of origin, along these longitudinal fibers to the pylorus, where it vanishes[29]. Morphologically, a part of the longitudinal fibers passes over the pylorus into the longitudinal muscle layer of the duodenum. Propagation velocity increases towards the pylorus: from 0.1-0.2 cm/sec in the corpus to 1.5-4.0 cm/sec in the distal antrum[10].

The *circular layer*, the middle of the three layers, is continuous with the circular layer of the esophagus. The gastric circular fibers are primarily responsible for the mechanical contractions resulting in gastric emptying. Indeed, the thickness of the circular layer increases in the antrum and especially in the pyloric canal, where gastric emptying occurs. Circular fibers are absent over the fundus and are alleged not to be continuous with the circular fibers of the duodenum.

The *oblique layer*, the innermost layer, has the shape of a horse-shoe hanging over the fundus. On the right side (near the lesser curvature) the borders of this layer are sharply defined. On the the left side and towards the antrum the oblique fibers disappear gradually. The physiological purpose of the oblique fibers has not been determined.

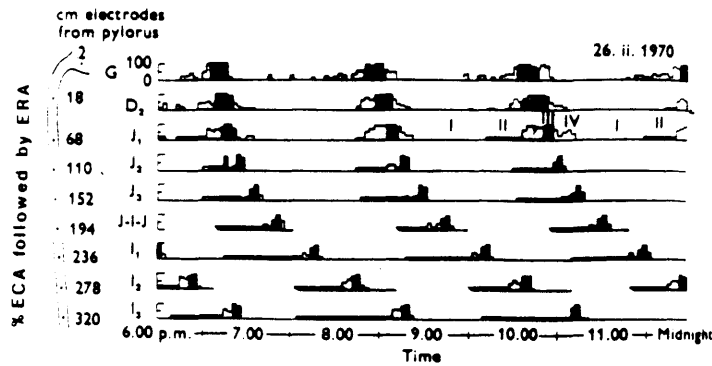


Figure 2.5: Interdigestive migrating complexes (from Code and Martlett,1975).

2.1.4 The interdigestive migrating complex

BER fronts propagate aborally and at regular intervals during motor quiescent periods. In the interdigestive state, the stomach is mechanically inactive most of the time. In fasting dogs, recurring fronts of intense spike activity have been found to migrate slowly down the entire small intestine (approx. 90 minute period)[61]. This so-called interdigestive migrating complex (IMC) has also been found to occur in the canine stomach[9]. Figure 2.5 shows three separate IMC's and their rate of propagation from the gastric region to the terminal ileum.

The quantity measured (%ECA followed by ERA) is directly proportional to the level of contractile activity, which is defined as groups of strong contractions irregularly spaced in time. Code and Marlett have divided the interdigestive pattern into four phases. During phase I there is no ERA ('second potential') or spike activity. Phases II and IV are transition phases. Phase III represents the activity front, which lasts for about 12 minutes in the stomach. Phase III is characterized by groups of strong contractions being alternated by short periods with weak or absent contractions[27]. As shown in Figure 2.5, the propagation rate of the IMC decreases as it moves distally along the lower alimentary canal. When an IMC front reaches the terminal ileum, another one develops in the stomach.

Van Der Schee, et.al., have studied interdigestive gastric contraction-related phenomena in four dogs using running spectrum analysis of EGG's[71]. Their study demonstrated that the presence of frequencies lower than the normal gastric one, in running spectrum representations of EGG's recorded in fasting dogs, is indicative of strong antral contractions and that the mechanism through which this is brought about involves *prolongation of contraction-related BER intervals*. Contractile activity was monitored via strain-gauge force transducers sutured to the serosal surface of the stomach.

Invasive studies with pressure transducers have revealed that IMC patterns in man are less regular with regard to periodicity and to the point of origin than those found in dogs[73]. Not all IMC complexes start in the stomach[16]. Instead, the duodenum was found to be the point of origin, with phase III activity lasting for about 3 to 6 minutes. Results using RSA analysis of EGGs recorded from resting, fasted subjects reveal much variability in the running spectrum during the interdigestive period[69]. In some recordings, a consistent gastric frequency remained during phase III activity. In other running spectra, phase III activity was not accompanied by the 3 cpm rhythm. In another instance, an increase in gastric frequency correlated with the occurrence of phase III activity in the duodenum. Unlike in the dog, the occurrence of low-frequency components in the running spectrum could not be proven to be indicative of an activity front in the human because such frequencies were often observed in cases when there was no contractile activity measured. As a consequence of the above observations, Van Der Schee concluded that "electrogastrography does *not* enable us to detect with certainty that gastric motor activity exists during the IMC in man."

2.1.5 The cutaneous waveform

In Chapter 1, several investigations were cited which verified that surface EGG recordings contained information about gastric electrical activity. The relationship between the

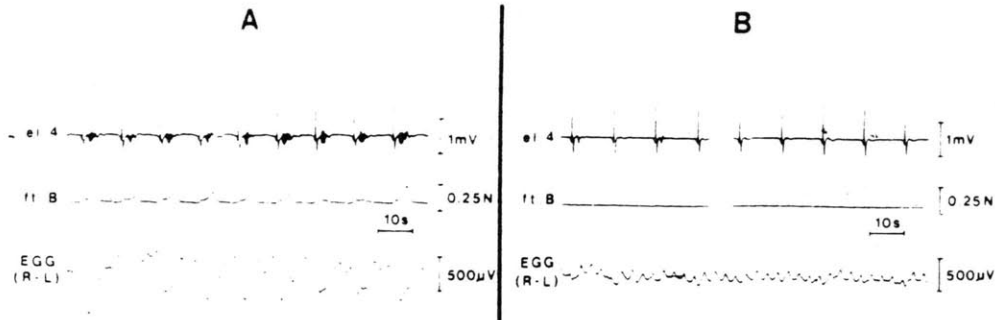


Figure 2.6: Serosal and EGG recordings of gastric activity (from Smout,1980).

biopotentials recorded by serosal electrodes and the cutaneously recorded EGG in the dog is depicted in Figure 2.6. Part A shows a postprandial record and part B was measured during an interdigestive period. Also shown are pressure recordings acquired from a force transducer situated in the antrum. The plots confirm Smout's report of increased EGG amplitude during gastric contractions, as indicated by the existence of the 'second potential'[52].

Beyond amplitude variations, analysis of the EGG waveform is seriously hampered by the generally poor quality and weak amplitude of the gastric signal. Bandpass filtering procedures are typically used to essentially 'clean up' the EGG, but this approach introduces phase distortions of the signal. Van Der Schee, et.al., employed a modified adaptive filtering technique but found that cutaneous signals obtained during the activity front of the IMC "are not suitable for detailed waveform analysis." Another complication is the existence of two or more BER fronts on the stomach at any instant of time. This precludes the identification of an EGG 'epoch' in the raw signal. Compare this to the unequivocal P wave, QRS complex, and T wave that compose the ECG waveform. Also, unlike the ECG, phases of the EGG cycle cannot be directly related to specific gastric physiological activity, mostly because of possible EGG contamination by electrical potentials generated in the small or large intestine. In contrast, the QRS complex of the ECG essentially indicates ventricular depolarization.

Because time domain analysis of the EGG has limited diagnostic value, a more profitable approach is to study the frequency characteristics of the EGG. This leads to the topic of running spectrum analysis, which is treated in more detail in Section 2.3.4.

2.2 Motion Sickness

The advent of new and faster types of transport vehicles has imposed novel stresses on man's physiological motion detection mechanisms that maintain posture and balance in both static and dynamic environments. An unfortunate consequence of these stimuli is the subsequent development of motion sickness, as evidenced by its characteristic signs and symptoms. Since the US Space Shuttle missions commenced in 1981, approximately half the crew members have experienced symptoms during their first 3-5 days in weightlessness which qualitatively resemble those of motion sickness[26]. Results from MIT/Canadian vestibular experiments on Spacelab-1 support the view that space sickness is a motion sickness[41]. In space, information about body position, locomotion, and orientation is initially misinterpreted by the brain because the inertial environment produces radically different sensory inputs than those experienced on the earth. The following discussion presents an overview of the salient topics of motion sickness research to provide a rationale for quantitative assessment of abdominal biopotentials.

2.2.1 Organs for transducing motion

Three semicircular canals, each roughly aligned in three orthogonal planes, are primarily responsible for detecting accelerations induced by head movements. The canals are membranous circular ducts, located in the inner ear, and filled with a fluid called endolymph. Due to inertia of this fluid, rotation of the head produces motion of the endolymph with respect to the membranous wall of the canal. Movement of endolymph in the duct produces distortion of a gelatinous structure called the cupula, which occludes the lumen of the canal in a segment called the ampulla. Essentially, the properties of the endolymph cause it to act like an integrator so that cupula distortion is proportional to head *velocity*. Hair cells located beneath the cupula are the mechano-electrical transducers serving as the interface between the external stimuli and its neural encoding. The dominant time constant of the

entire system is dictated by cupula return (on the order of 12 seconds)[43].

Also located in the labyrinth of the inner ear are fibro-gelatinous otolithic membranes. These structures contain calcium carbonate crystals denser than surrounding endolymph. The membranes overlay hair cells embedded in utricular and saccular maculae. The utricle is roughly aligned in the horizontal plane; the saccule is oriented in the vertical plane. Thus, gravito-inertial accelerations of the head (and, presumably, the body), are transduced by the movement of the otoliths across the maculae. The steady state component of unit response most likely encodes acceleration magnitude, although details of membrane mechanics are not yet known[68].

Other sensory modalities used for motion detection are visual and proprioceptive. A false sensation of motion can be achieved in a stationary subject by exposure to a visual scene moving at a constant velocity and direction. This sensation is commonly referred to asvection. Pressure stimuli on specific parts of the body may be indicative of movements and are detected by receptors in the musculature. A familiar proprioceptive sensation is the "seat of the pants" input one gets during initial take-off of a commercial aircraft. There may be more subtle and refined motion transduction processes employed by highly trained pilots and other persons typically exposed to a moving environment, but the ones described above are the primary channels used to interpret a novel inertial input.

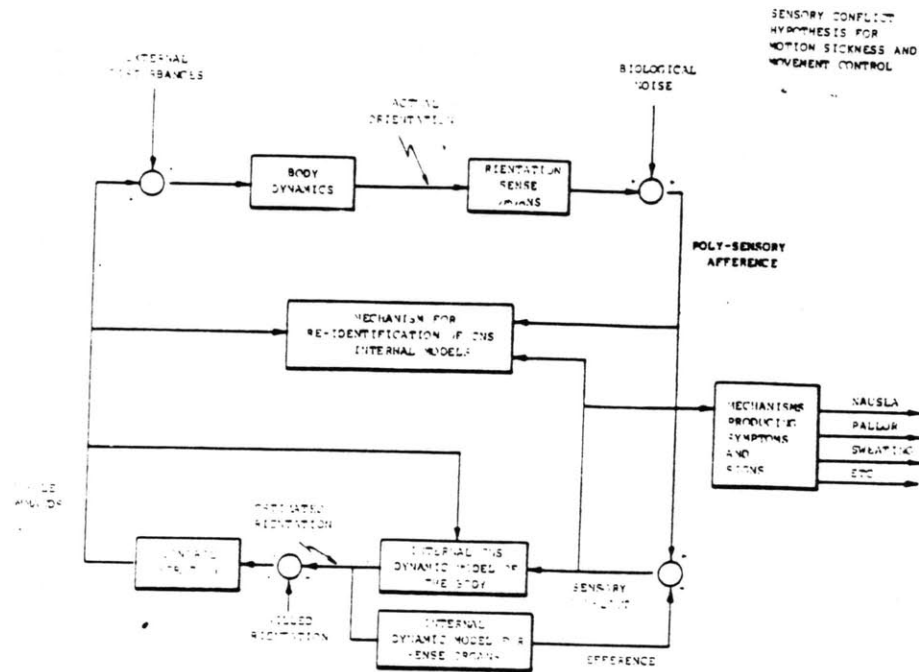
2.2.2 Etiology of motion sickness

Some of the symptoms elicited by motion sickness are typically stomach discomfort, nausea, vomiting or retching, pallor, cold sweating, salivation, drowsiness, and warmth[47]. Although our physiological understanding of motion sickness is incomplete, behavioral evidence has led to the development of various "sensory conflict" hypotheses[38,47]. Sickness has been noted to occur in situations where man is passively exposed to certain real or apparent motion stimuli, or to conditions of "sensory rearrangement." Reason states the

sensory rearrangement theory in the form of two premises[48]. "The first is that all situations which provoke motion sickness are characterized by a condition of sensory rearrangement in which the motion signals transmitted by the eyes, the vestibular system and the nonvestibular proprioceptors are at variance one with another, and hence with what is *expected* on the basis of previous transactions with the spatial environment. The second...is that irrespective of what other spatial senses are part to these conflicts, the vestibular system must be implicated, either directly or indirectly (as in visually-induced sickness), for motion sickness reactions to ensue." An important point is that the idea of "sensory conflict" does not refer to an inter-modality conflict, but to a disparity between present sensory information and that retained from past experiences.

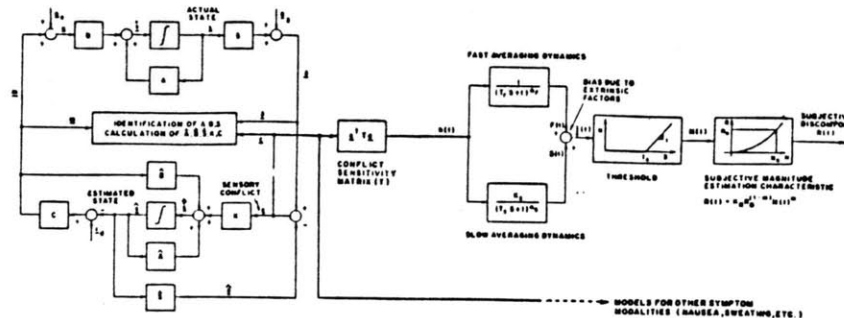
The issue of how the central nervous system might actually "compute" the conflict between previous sensory-motor experience and the present environment has led to the "neural mismatch model", proposed initially by Held[25]. Reason, extrapolating from Held's work, argued that as motor actions are commanded, the CNS probably continuously predicts the corresponding sensory inputs to be expected, based on a "neural store" of sensory/motor experience. The "sensory conflict" signal would result from a continuing comparison between actual and expected sensory inputs. Oman explains rearrangement adaptation as sensory/motor learning which would make predicted sensory inputs more concordant with those actually experienced, thereby reducing sensory conflict[42].

Oman identified some significant shortcomings in the "neural mismatch" model[40]. Specifically, the model is only qualitative, with structural elements like "neural store" and "memory traces(engrams)" being intuitively defined. No conflict neuron has been identified. Oman states that "the model accounts for many known facts concerning motion sickness, but its predictive value is very limited." Oman's "sensory-motor conflict" model[38] is shown in Figure 2.7. It was developed from a formal control theory consideration of the information processing task faced by the central nervous system as it actively controls



Sensory-Motor Conflict Model for Motion Sickness and Movement Control. Internal models consist of differential equations describing body and sense organ dynamics. Based on current muscle commands, equations provide "estimated orientation" state vector, used to determine new muscle commands. Simultaneously, "estimated orientation" drives differential equations for sense organs to compute "efference copy" vector. If internal models are correct, and there are no system external disturbances, efference copy vector nearly cancels poly-sensory afference. If not, the difference - a "sensory conflict" vector - can be used to steer the model predictions towards reality, trigger corrective muscle commands, and indicate a need for re-identification of the internal model differential equations and steering factors. Conflict vector couples also to symptom production mechanisms. Adaptation via re-identification takes place by analysis of the new relationship between muscle commands and poly-sensory afference, and model updating.

Figure 2.7: Sensory-motor conflict model (from Oman,1982).



Mathematical formulation of model shown in Fig. 1. Left side represents body movement control loop. A, B, and S are matrices of differential equation coefficients describing body and sense organ dynamic characteristics, expressed in state variable notation. A, B, and S represent CNS internal model estimates of these matrices, and correspond to the "Neural Store" of Reason's (1978) model. Right side of figure shows conflict coupling and preliminary dynamic model for symptom response, aspects not specifically represented in earlier models.

Figure 2.8: Mathematical formulation of Oman model (from Oman,1982).

body movement using a limited set of noisy sensory signals. The mathematical version of the model is shown in Figure 2.8. Note in the figure the coupling of conflict signals to the autonomic/emetic pathways. The linkage shown here implies that conflict signals are *continuously* functionally "averaged" by mechanisms which determine the intrinsic dynamics (latency, avalanching tendency, recovery time, etc.) of symptoms and signs.

Although the sensory conflict theory is now the generally accepted explanation for motion sickness in its many forms on earth, it does not provide a comprehensive scientific definition of motion sickness in physiological terms. A more precise identification of the neural-humoral mechanisms responsible for the onset of motion sickness symptoms is clearly a priority.

2.2.3 Coriolis cross-coupled stimulation

Various stimuli can be used to elicit sensory conflict, and at sufficiently high levels to provoke motion sickness. Seasickness is brought on by the visual-vestibular rearrangement of watching waves over the side of the vessel. Making head movements while wearing prism goggles (optical devices which reverse left-right vision) has a strong disorienting and nauseogenic response. A commonly used stimulus utilized by motion sickness researchers equipped with a rotating chair is the Coriolis cross-coupling effect. This refers to the vestibular effect of tilting the head during whole-body rotation.

The disorienting sensation felt by the subject experiencing Coriolis stimulation is best described using an example. A subject is seated in a rotating chair apparatus as in Figure 2.9. The subject is rotated for a few minutes in a counter-clockwise direction at a constant velocity. The subject then makes a rolling head movement to the right, which is accompanied by a sensation of pitching forward and accelerating slightly to the right. This provocative sensation conflicts with the otolith signal, which, because of the head movement, registers a change in the direction of gravity relative to the head. The net effect is a disorienting and potentially nauseogenic stimulus based on the incompatible signals detected by the canals and otolith.

As implied in the above description, rotating one's head in one axis, the ω_2 axis, while rotating about another axis, the ω_1 axis, produces an instantaneous stimulus about a third axis. The term "cross-coupled" is therefore used to describe this effect because the resulting stimulus can be calculated from vector algebra as the vector cross product of the ω_1 and ω_2 velocity vectors.

Guedry and Benson present a study which distinguishes conditions in which Coriolis cross-coupling effects are disorienting and nauseogenic from conditions in which they are neither[20]. The basic purpose was to present angular accelerations or decelerations of whole body rotation immediately preceding the head movement. The result was that dis-

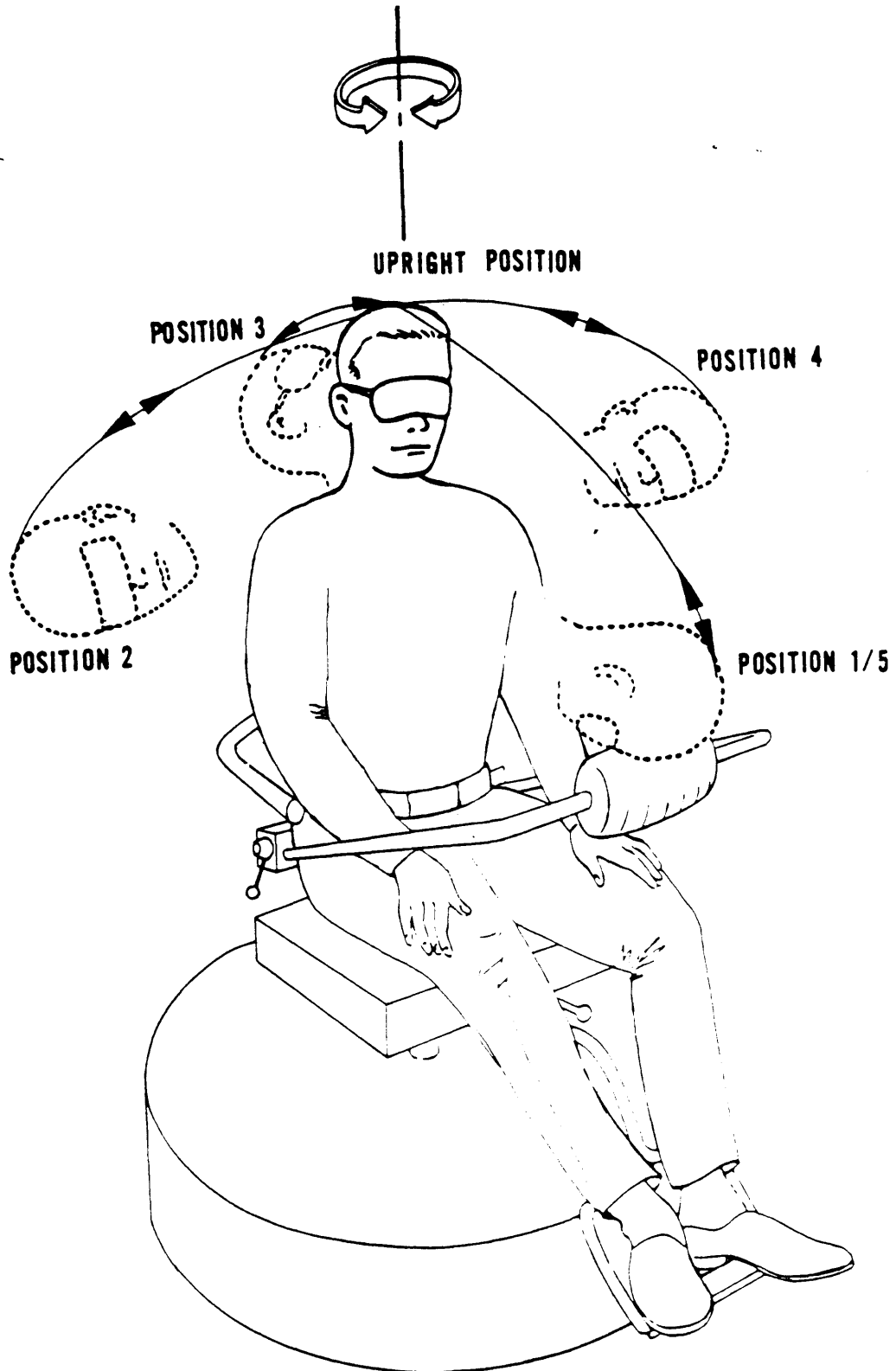
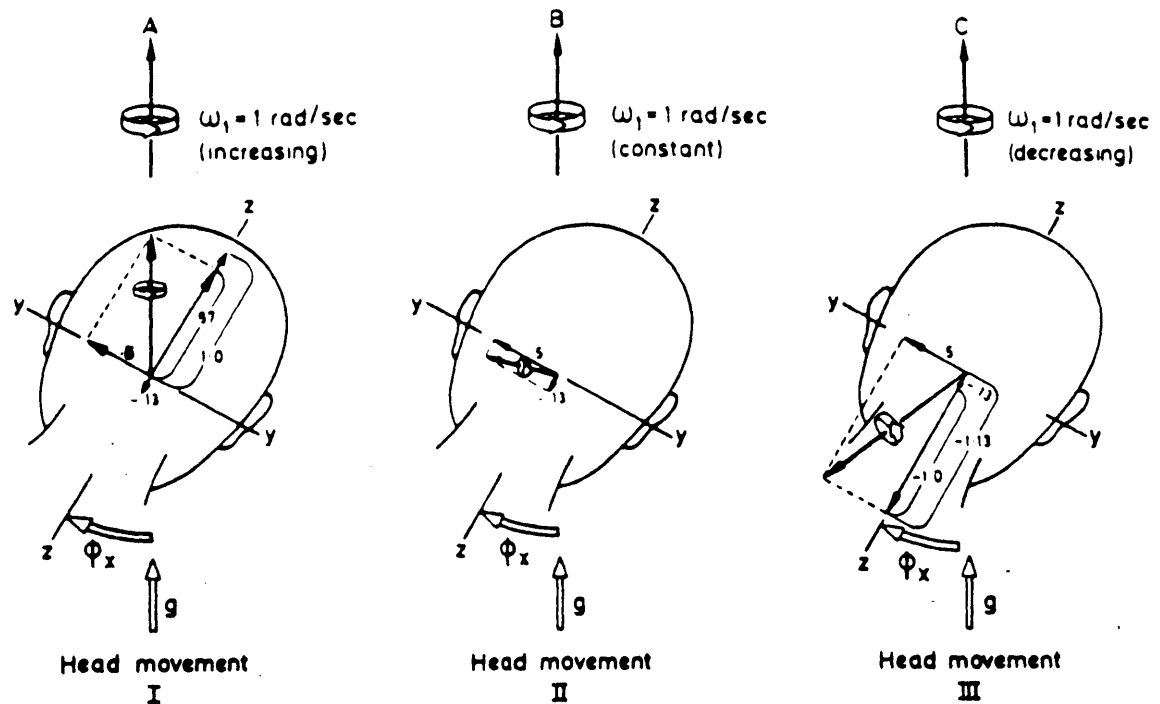


Figure 2.9: Rotating apparatus with diagrammed head movements (from Miller and Graybiel, 1969).

orienting or disturbing effects reported by the 12 subjects tested were either cancelled, as when accelerating from rest, or exacerbated, as when decelerating from a constant velocity. The three situations are illustrated in Figure 2.10. Note in the figure the different alignments of the resultant angular impulse of the semicircular canals. These resultant vectors are compared with the inputs from the otoliths (g-vector) to produce either agreeable or disorienting sensations.

A key point in Guedry's analysis was that "the temporal characteristics of the angular acceleration and deceleration in starting and stopping the quick head rotation in roll about the X-axis of the head are well within the dynamic response of the canals transducing the motion so that there is no erroneous signal from an idealized roll-axis 'canal' on termination of the head tilt." In other words, cupula dynamics are such that a rapid head roll to the right yields essentially no input sensation from the roll axis canals. Thus, the cross-coupling occurs in the Y-plane and Z-plane only, as shown in Figure 2.10.

Also, Guedry explains that the stimulus intensity does not depend on the *angular velocity* of the head movement in the roll axis (as implied by the cross-coupling formula), but on the amplitude of the head *angular displacement*. With this rightward head movement in the roll axis, the pitch canal is being rotated into the plane of chair rotation and the yaw canal is being rotated out of the plane of chair rotation. As a result, angular velocity steps, whose magnitudes depend directly on the angle of displacement, are being input to the canals. These angular velocity steps are depicted as vectors along the Y and Z axes in Figure 2.10. More generally, the velocity change ($\Delta\omega_y$) which occurs when a canal is moved from an initial position (ϕ_i) to a final position (ϕ_f) is $\omega_1 (\sin \phi_f - \sin \phi_i)$, where ω_1 is the angular velocity of the rotating chair, and ϕ is referenced to the positive z-axis. Under the situation of a rightward head roll in a counter-clockwise rotating environment at constant velocity, the pitch canals would receive a positive angular velocity step input while the yaw canals would receive a negative step input. This is depicted in Head Movement



(A) The resultant angular impulse to the semicircular canals at completion of the first head movement, considering both the effects of angular acceleration of the turntable and the Coriolis cross-coupling effects. The resultant vector would be located relative to the skull by inputs from all six semicircular canals so that it remains aligned with the axis of the rotation device which, in turn, is aligned with gravity. (B) The resultant angular impulse to the semicircular canals at completion of the second head movement. This resultant Coriolis cross-coupled stimulus is the same as that which occurred in the first head movement, but absence of effects of angular acceleration of the rotation device leaves the resultant vector displaced by about 75° from gravity. (C) The resultant angular impulse to the semicircular canals at completion of the third head movement. The Coriolis cross-coupled stimulus resolved with the effects of angular deceleration of the device yields a stimulus vector of $1.24 \Delta\omega_1$. This is much greater than the $0.52 \Delta\omega_1$ stimulus vector from the second head movement, but it is displaced from gravity by about 54°, less than the angular displacement of the stimulus vector in the second head movement.

Figure 2.10: Effects of whole-body accelerations preceding head movements during Coriolis cross-coupled stimulation (from Guedry and Benson, 1978).

II of Figure 2.10 in which a 30 degree rightward head movement was made from resting position. As stressed in Guedry's paper, a detailed analysis of the Coriolis cross-coupling effect on the vestibular system is required to determine the true nauseogenic or disorienting impact on a rotated subject.

2.2.4 Symptom scoring and magnitude estimation

As stated above, some of the more common symptoms of motion sickness are stomach discomfort, nausea, vomiting or retching, pallor, sweating, and salivation. Other observable signs include belching, and yawning. Tests of motion sickness susceptibility, beyond a simple pass-fail criteria, would require a standardization and quantitative definition of symptoms that are reliably diagnostic of a specific level of motion sickness. Another prerequisite is a stimulus that is effective for the majority of normal subjects and can be generated by conventional apparatus. The Coriolis cross-coupled sensations induced by making head movements during whole body rotation is generally accepted to be a quantifiable, controllable, easily executed, and effective stimulus. The major problem is devising a symptom or discomfort rating scale that would permit *comparison* of individual susceptibilities to motion sickness.

In 1968, Graybiel, et.al., proposed a rating scale that essentially translated the subject's symptom reports into a numerical score that is believed to provide a measure of relative sickness severity[19]. In this procedure commonly known as the Pensacola Diagnostic Rating Scale, the presence and/or strength of epigastric awareness and discomfort, nausea, drowsiness, salivation, headache, dizziness, and warmth are subjectively assessed by the subject, working with a trained observer who also subjectively evaluates the extent of pallor and cold sweating. A weighted sum of individual symptom reports yields a score which formally classifies the tested subject as being at a specific level of severity, indicated by the lower section of Figure 2.11. Graybiel claims that one of the advantages of this rating

Diagnostic Categorization of Different Levels of Severity of Acute Motion Sickness

Category	Pathognomonic 16 points	Major 8 points	Minor 4 points	Minimal 2 points	AQS* 1 point
Nausea syndrome	Vomiting or retching	Nausea II, III	Nausea I	Epigastric discomfort	Epigastric awareness
Skin		Pallor III	Pallor II	Pallor I	Flushing/Subjective warmth ≥ I
Cold sweating		III	II	I	
Increased salivation		III	II	I	
Drowsiness		III	II	I	
Pain					Headache ≥ II
Central nervous system					Dizziness Eyes closed ≥ II Eyes open III

Levels of Severity Identified by Total Points Scored				
Frank Sickness (S)	Severe Malaise (M III)	Moderate Malaise A (M IIA)	Moderate Malaise B (M IIB)	Slight Malaise (M I)
≥ 16 points	8 - 15 points	5 - 7 points	3 - 4 points	1 - 2 points

*AQS - Additional qualifying symptoms. + III - severe or marked, II - moderate, I - slight.

Figure 2.11: Pensacola rating scale as proposed by Graybiel (from Graybiel, 1969).

scale is that test session endpoints can be based on symptomatology manifested prior to the more severe signs of nausea or vomiting. Graybiel's evaluation of his proposed rating scale uses a Malaise III (M III) endpoint[35].

In that study, Graybiel was able to evoke the M III endpoint in 98.8% of 250 normal subjects. His subjects were rotated in a chair at a constant velocity subjectively predetermined using information given in a motion sickness questionnaire. While rotating, the subject would execute a standardized sequence of 90° head movements, inducing the Coriolis cross-coupled accelerations: front,up; right,up; back,up; left,up; front,up. Each set of 10 head movements would require 10 seconds, leaving 20 seconds for symptom reports. Thus, a set of 5 down-up head movements was performed every 30 seconds. Graybiel proposed a quantitative susceptibility score scaled by the magnitude of the stressor effect (E factor), defined as the vestibular stress experienced by the subject when making a head movement at a given chair angular velocity. This definition presupposes that the subject is being spun at a rate fast enough to evoke the M III endpoint, and Graybiel cautions that head movements in the four specified directions are *not* equally stressful. Graybiel and Miller have shown that "the E factor...varies directly and, in log-log terms, is linear with rotational velocity." This means that head movements at successively higher rotational velocities are exponentially more stressful(Figure 2.12).

The susceptibility score, called the Coriolis Sickness Susceptibility Index (CSSI) was calculated simply by multiplying the appropriate E factor for the RPM used in the test by the number of down-up head movements required to elicit M III. CSSI values of the normal subjects were markedly right skewed on an arbitrary scale of 0 to 100 points as shown in Figure 2.13. High test-retest reliability was found for both CSSI scores and pattern of symptomatology. The correlation coefficient, as shown in Figure 2.14, was $\rho=0.89$.

Kohl extended CSSI score evaluations to include step increases in chair velocity during the test session, a procedure called the Staircase Profile Test[31]. By approximating the

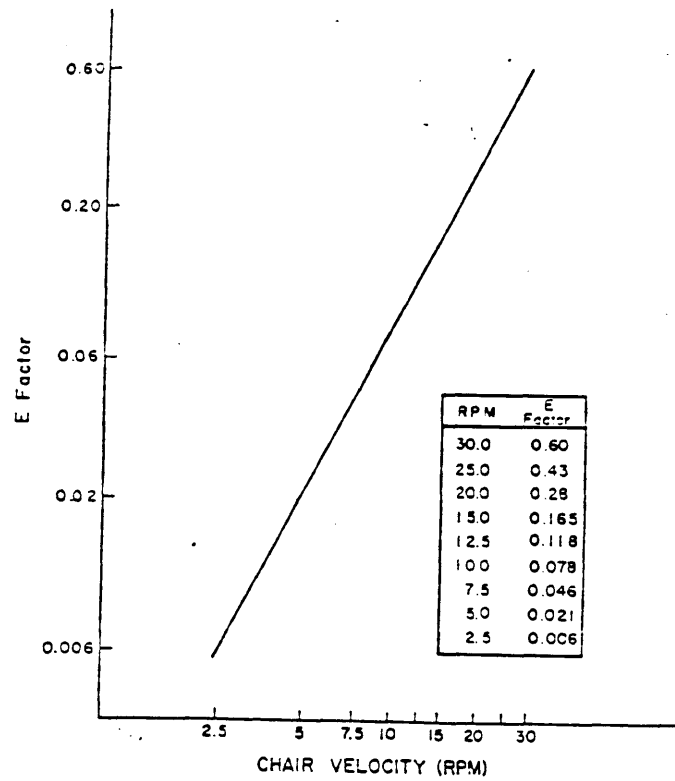


Figure 2.12: Relationship between E factor of a single head movement and rotational velocity (from Graybiel, 1969).

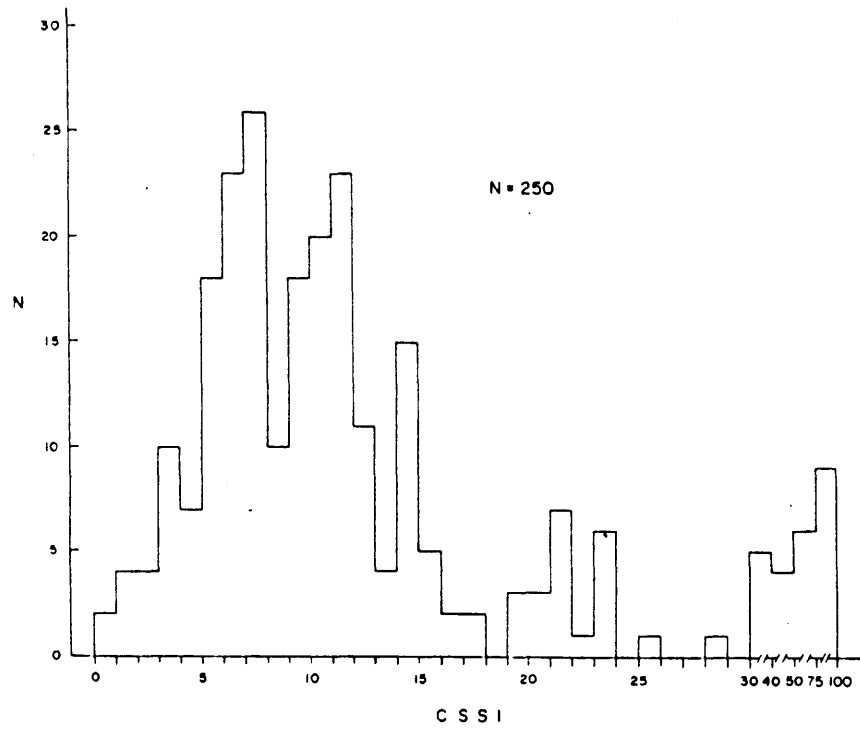


Figure 2.13: Distribution of CSSI score among 250 normal subjects (from Graybiel,1969).

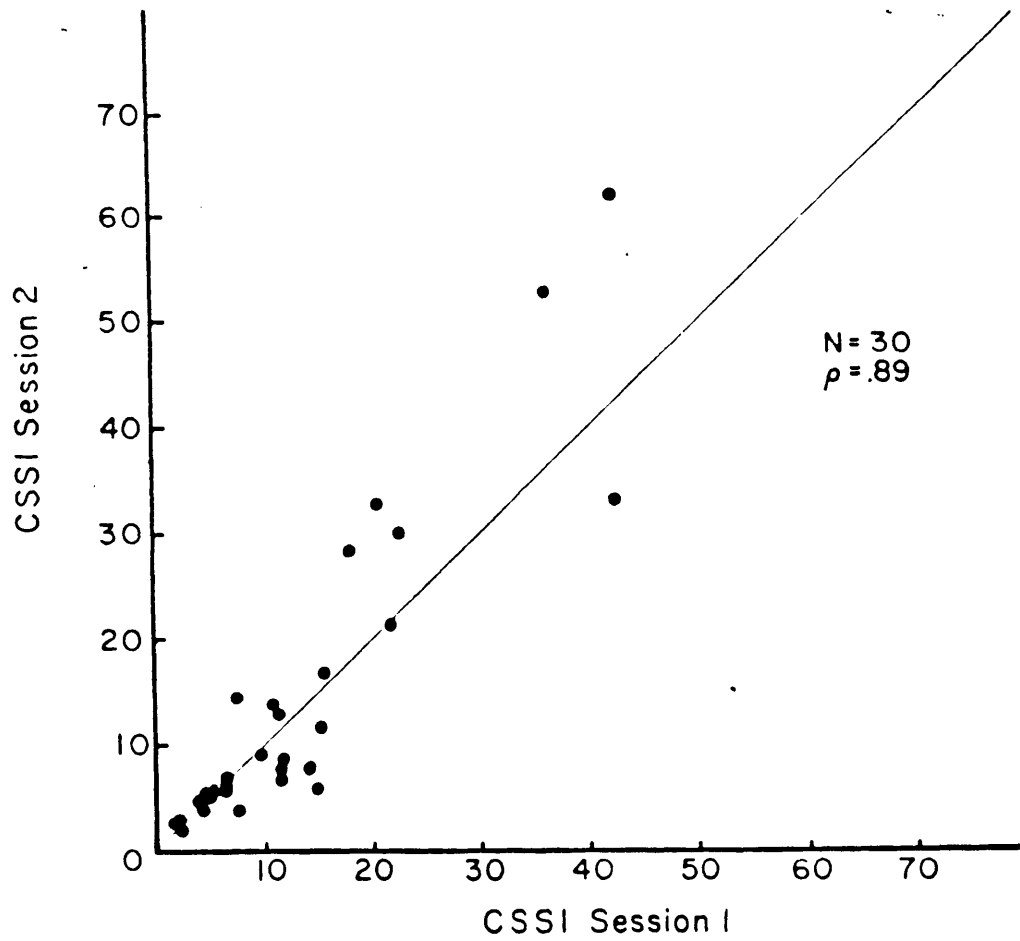


Figure 2.14: Test vs. Retest of CSSI scores for 30 normal subjects (from Graybiel, 1969).

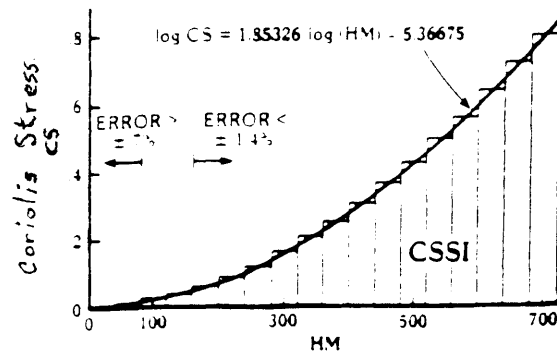


Figure 2.15: Exponential function depicting relationship between coriolis stress (E factor) and angular velocity (from Kohl,1987).

cumulative stress endured by making 40 head movements at each odd RPM, Kohl calculated CSSI scores for two separate endpoints, M III and frank sickness. The M III endpoint calculations are shown in Figure 2.15. To standardize CSSI scores across different endpoints, the E factor must be appropriately scaled upward for less severe endpoints since it should take fewer head movements to achieve a smaller number and degree of symptoms. Generally it may be concluded from past and present research that stimulus intensity or conflict increases approximately as the square of chair rotation velocity (expressed in RPM).

The Pensacola Diagnostic Scale is useful in determining a standardized motion sickness endpoint based on subjective reports of signs and symptoms. However, it's usefulness in assessing the magnitude of the subject's overall discomfort level is suspect. For example, there is no reason to believe that the sensation reported as nausea level II is twice as great as nausea level I, or that an overall score of 12 points (M III) is subjectively twice as uncomfortable as a 6 point score (M IIa). Also, symptom definition is not yet standardized

between laboratories and research groups. Further complicating the interpretation of the Pensacola score is that subjective reports originate not only from the subject but also from the observer, making symptom evaluation highly dependent on the previous experience of two individuals. This approach countermands the basic tenets of magnitude estimation, in which only the subject's judgement of a stimulus should be involved.

Stevens and co-workers demonstrated that observers can reliably make numerical estimates of subjective sensations resulting from a wide variety of sensory stimuli (e.g. loudness, vibration, electric shock) using "ratio scaling" techniques[58,59,60]. Essentially, magnitude estimation is a form of ratio scaling in which the subject is required to assign numbers to a series of stimuli under the instruction to make the numbers *proportional* to the apparent magnitudes of the sensation produced. Reason and Graybiel proposed an ordinal "well being" scale, but the instructions given to the subjects did not indicate that a doubling of the score should correspond to a doubling of subjective sensation[46]. In magnitude estimation, the experimenter may prescribe a standard sensation ("modulus") by presenting a control stimulus and instructing the subject to call the resulting sensation some particular value, or the subject may be free to choose his own modulus. Using cross-modality testing and sensation matching techniques, Stevens argued that subjects were actually able to make consistent, veridical estimates of the relative strength of their sensations.

Bock and Oman developed a simple technique for reporting overall subjective discomfort (or, alternatively, nausea) based on Stevens' magnitude estimation rules[7]. Subjects are instructed to choose a sensation magnitude of overall discomfort in the middle of the "moderate range" and to rate all subsequent sensations with respect to it. This complies with Steven's request that only one reference point near the center of the range of magnitudes to be estimated should anchor the scale. After a practice period to establish a consistent modulus, a subject's reports appear internally consistent. However, the discomfort experienced at the reference level most likely varies between subjects, so the numerical

scores of different subjects cannot be equated. This method is well suited to studies in which time course of symptoms must be quickly assessed. Bock and Oman, using results from magnitude estimation reports by subjects wearing prism goggles, found that subjective discomfort exhibits a profile characterized by both fast and slow response components. Magnitude estimation serves as a useful complement to the Pensacola Diagnostic Scale.

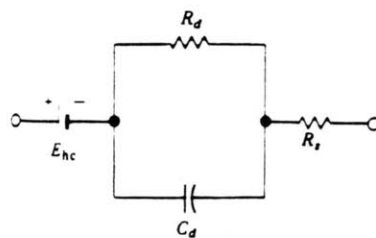
2.3 EGG Processing and Analysis

In electrogastrography, as in any other 'EXG' technique, surface electrodes must be attached to the skin. The signal generated from the gastric smooth muscle tissue is small (100-500 μ V) and typically contaminated by various kinds of noise (electrode-to-skin interface potentials; electrical contributions from the heart, respiration muscles, and duodenum; motion artifacts). Therefore, the EGG signal picked up by the electrodes must be appropriately amplified and filtered. Straightforward waveform analysis of the cutaneously recorded signal is complicated by the existence of two or more BER fronts on the stomach at any instant of time. The roughly sinusoidal shape of the EGG, coupled with its characteristic periodicity (3 cpm) in a normal resting subject, makes frequency analysis a viable alternative to time series investigation. This section provides the theoretical framework and practical limitations of the EGG recording and analysis procedure.

2.3.1 Electrodes and electrode placement

In order to measure and record potentials and, hence, currents in the body, it is necessary to provide some interface between the body and the electronic measuring apparatus. Biopotential electrodes serve this purpose mainly as electrochemical transducers between the closed-line action currents generated by specific body organs and the electrical currents required by the recording set-up. A half-cell potential is generated when putting a metal in contact with a solution (electrolyte) containing ions of that metal. This potential is determined by the metal involved, the concentration of its ions in solution, the temperature and other second order factors. Essentially, neutrality of charge is not maintained at the electrode-electrolyte interface producing the half-cell potential. A double layer of charge evolves at the interface as well.

In electrode circuit models, this half-cell potential is represented as a battery, and the characteristics of the double layer of charge are lumped together as a capacitor. A resistor



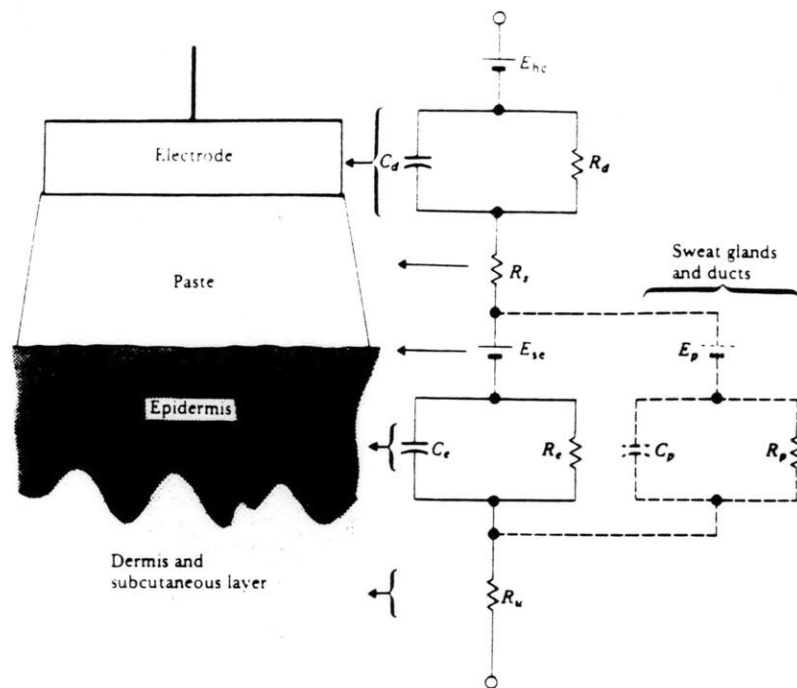
Equivalent circuit for a biopotential electrode in contact with an electrolyte. E_{hc} is the half-cell potential. R_d and C_d make up the impedance associated with electrode-electrolyte interface and polarization effects, and R_s is the total series resistance in the circuit due to resistance in electrolyte and electrode lead wire.

Figure 2.16: Electrode circuit model (from Webster, 1978).

is introduced to represent the total series resistance in the circuit due to the resistance in the electrolyte and electrode lead wire. A widely accepted circuit model for the electrode, a battery in series with a resistor and capacitor, breaks down at the lower frequencies where this model would suggest an impedance going to infinity at dc. A more complete model would incorporate a parallel RC circuit in place of the capacitor, as shown in Figure 2.16. Thus, the electrode has a purely resistive impedance at very low frequencies.

Smout studied the total impedance of Hewlett-Packard 14245A Ag/AgCl ECG electrodes as a function of frequency [51]. At frequencies below 10 Hz, the electrode impedance appeared to be frequency independent, confirming the modified circuit model described above. At these low frequencies, the impedance of one electrode-electrolyte interface appeared to be a constant value of approximately 100 ohms. Hewlett-Packard 14445A disposable cutaneous electrodes were used in this study and can be expected to exhibit similar impedance characteristics as the electrodes tested by Smout.

When the electrode is placed on the skin, the electrical impedance characteristics of the epidermis add more components to the equivalent circuit model, as shown in Figure 2.17. The outer surface of the epidermis, the stratum corneum, is composed of dead material whose electrical equivalent is a parallel RC circuit. The semipermeable quality of this



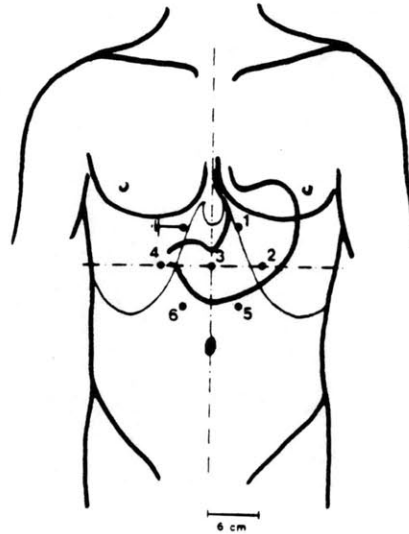
Body-surface electrode placed against skin, showing total electrical equivalent circuit obtained in this situation. Each circuit element on the right is at approximately the same level at which the physical process that it represents would be in the left-hand diagram.

Figure 2.17: Electrical equivalent circuit of electrode-skin interface (from Webster, 1978).

outer membrane also creates a difference in ionic concentration on either side, producing a potential difference represented by E_{se} in Figure 2.17. Sweat glands and ducts introduce similar electrical elements to the circuit model, but these components are often neglected in considering biopotential electrodes that are not used to measure a galvanic skin response. Clearly, if the effect of the stratum corneum can be reduced, a more stable electrode will result. Smout found that the total impedance between a pair of electrodes placed on opposite sides of the human leg could be reduced by 90% by thorough abrasion of the site underneath the electrode. By effectively removing the skin's outer protective layer, signal stability is enhanced. In this study, the subject's skin beneath the electrode was lightly scratched with a sterile hypodermic needle.

Motion artifact is primarily the result of mechanical disturbances of the distribution of charge at the electrode-electrolyte interface. These capacitive effects are more noticeable in a polarizable electrode, where the primary interface current is a displacement current. In nonpolarizable electrodes, current passes freely across the electrode-electrolyte interface, requiring no energy to make the transition. Ag/AgCl electrodes closely approximate nonpolarizable electrodes, and thus minimize the effect of mechanical disturbances. Accordingly, HP Ag/AgCl ECG electrodes were used in this study.

Electrode positioning and recording configuration have been carefully studied by Smout, Van Der Schee, and Webster[22,51,69]. The unanimous conclusion was that EGG signals bipolarly obtained from electrodes placed at the epigastric region were superior in terms of signal-to-noise ratio as compared to extremity leads, commonly used in electrocardiography, and to monopolar recordings. Each bipolar lead would be referenced to an indifferent electrode placed somewhere on the body. A disadvantage of the use of bipolar leads is that the configuration of the EGG signal cannot be analyzed because it is impossible to determine which potential variation occurred at which electrode in bipolar recordings. Therefore, Smout recommends both monopolar and bipolar EGG recordings. Smout obtains his bipo-



Positions of abdominal electrodes used in our electrogastrographic studies in man.

The electrodes 2, 3 and 4 are situated on Addison's line; this is a transverse line halfway between the lower end of the sternum and the navel (transpyloric line). Electrode 3 is placed at the intersection of the line of Addison and the median plane. The distance between all other electrodes and electrode 3 is 3 cm. The seventh electrode depicted is an earth electrode.

Figure 2.18: Electrode positions used by Smout (from Smout,1980).

lar measurements by electronically subtracting the monopolar signals. Because this study is primarily concerned with the EGG repetition frequency, not with signal configuration, only bipolar recordings were used.

Because the quality of the recorded signals appears to vary from subject to subject, and even within subjects, an 'optimum' electrode position cannot be defined. Van Der Schee and Smout routinely recorded from a few leads and, through visual inspection, selected the best signal. Standard electrode positions used by the Rotterdam group are shown in Figure 2.18. Using visual analysis to grade EGG time series records on a three point scale,

Smout found the best bipolar signals in the fasting state to be 1-3, 1-6, and 2-3. Van Der Schee states that "visual examination of the recorded EGG's revealed that in most subjects the bipolar signal obtained from electrode 1 minus 4 was suitable" [70].

Electrode positions used in this study were based on Van Der Schee's above recommendation. However, his suggestions were based on recordings of supine subjects. The stomach frequently repositions itself with respect to the abdominal surface, depending on body position and volume of stomach contents. A caudad shift in electrode position (1 cm) was made to compensate for any downward movement of the subject's stomach while seated. (In retrospect, it may have been wiser to make a cephalad compensation since the subjects in this study had fasted prior to testing, and the relatively empty stomach may have been buoyed upward by air bubbles instead. Also, preliminary recordings showed that an orientation almost perpendicular to the 1-4 electrode alignment yielded a signal about 50 times greater in amplitude. These electrode positions will be described in Chapter 3.)

Volkers, et.al., applied a coherent averaging technique to canine EGG waveforms to determine whether the waveforms depended on the position of the cutaneous electrodes [74]. They concluded that differently positioned surface electrodes 'see' different electrically active parts of the stomach, but in all electrodes the electrical activity of the terminal antrum was reflected. Some electrodes placed to the left of the midline reveal the activity from the orad corpus, but also contained antral components. This observation is consistent with the increase in depolarization amplitude of BER's as they move distally towards the pylorus. The strength of the electrical signal in the highly active pyloric region, where gastric emptying occurs, is detected by all abdominal electrodes.

2.3.2 Fourier Analysis and windowing

Theoretically, any random signal can be decomposed into a sum of sinusoids (sines and cosines). The method of transforming a time series signal into a representation of weighted

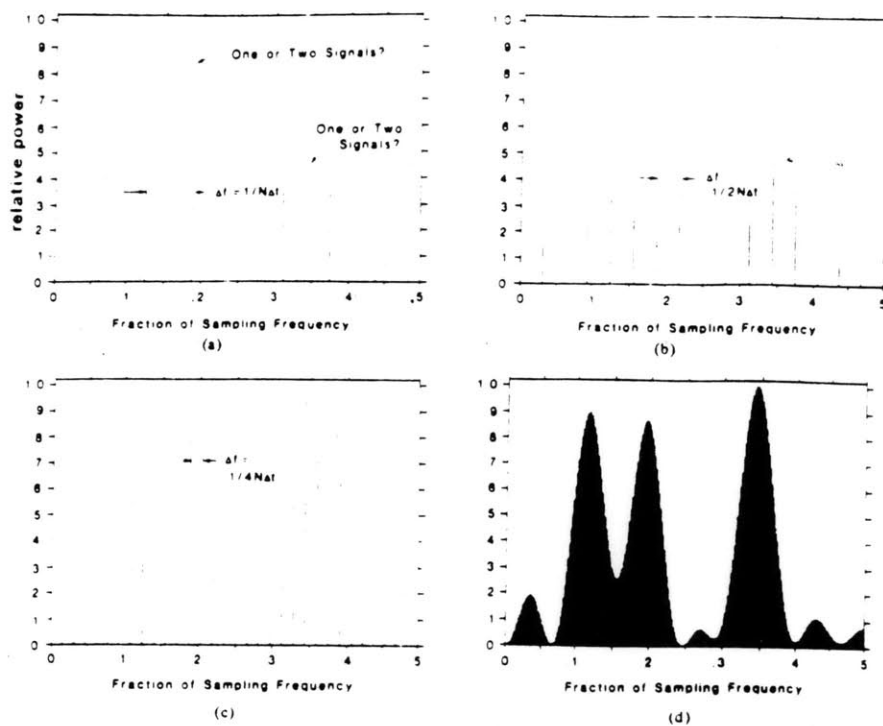
frequency components is called Fourier analysis, and the mathematical basis for this procedure is the Fourier transform. In digital signal processing, the time domain signal is sampled at discrete intervals and is assumed to be periodic, which gives rise to the Discrete Fourier Transform (DFT) pair:

$$X(k) = \sum_{n=0}^{N-1} x(n)e^{j2\pi kn/N}, \quad 0 \leq k \leq N-1 \quad (2.1)$$

$$x(n) = \frac{1}{N} \sum_{k=0}^{N-1} X(k)e^{-j2\pi kn/N}, \quad 0 \leq n \leq N-1 \quad (2.2)$$

Equation 2.1 represents the analysis transform, and equation 2.2 represents the synthesis transform. Various computer algorithms have been implemented which perform rapid evaluation of the above equations. Fast Fourier transform (FFT) algorithms are based upon the principle of decomposing the computation of the discrete Fourier transform of a sequence of length N into successively smaller discrete Fourier transforms. For a more detailed explanation of the DFT and FFT methods, please refer to Oppenheim & Schaffer[44].

The frequency domain representation of a time series, as computed by the DFT, is by definition discrete and periodic. The period (in frequency units) is the sampling rate(f_s). This periodicity imposes a well known restriction on f_s as defined by *Shannon's Sampling Theorem*, which states that a band-limited signal must be sampled at a rate at least as high as twice the highest frequency contained in the input signal. This rule avoids aliasing, or overlap of periodic spectra, in the frequency domain. A disadvantage of representing the spectrum of an input signal by discrete samples in the frequency domain is the 'picket fence' effect, illustrated in Figure 2.19. The amount of spectral information that can be 'seen' using the DFT depends on the number of samples acquired in the time domain. The common practice is to zero pad the input data to effectively increase the number of samples, thereby smoothing the appearance of the spectrum via interpolation. This method resolves potential ambiguities and reduces the error in estimating the frequencies of spectral peaks. However, the *resolution* of the spectrum estimate is not improved by zero padding;



Consequences of zero padding. All spectra were calculated using the same 16 samples of a process consisting of three sinusoids of fractional sampling frequencies 0.1335, 0.1875 and 0.3375 respectively.

- (a) No zero padding; ambiguities are present.
- (b) Double padding; ambiguities resolved.
- (c) Quadruple padding; smoothed spectrum seen.
- (d) 32-times padding; envelope is approximation to continuous Fourier transform.

(From Kay and Marple, 1981)

Figure 2.19: Picket fence limitation of Discrete Fourier Transform (from Kay and Marple, 1981).

resolution depends solely on the number of actual data samples taken, i.e., the duration of the sampled time series.

The magnitude of the Fourier transform estimate at a specific frequency is directly related to the amplitude of the frequency, and the length of time that the frequency exists in the sampled time series. This implies that a spectral estimate of a frequency sampled for, say, 12 seconds, is 6 times as great as a that of any frequency sampled for 2 seconds. This is shown for two pure cosines sampled N times:

Given an input signal

$$x(n) = \cos \frac{2\pi n}{N} + \cos \frac{6\pi n}{N}$$

where N is the number of samples, and $0 \leq n \leq N - 1$, $x(n)$ can be decomposed into a sum of exponentials

$$x(n) = \frac{1}{2}e^{j\frac{2\pi n}{N}} + \frac{1}{2}e^{-j\frac{2\pi n}{N}} + \frac{1}{2}e^{j\frac{6\pi n}{N}} + \frac{1}{2}e^{-j\frac{6\pi n}{N}}$$

Multiplying the second and fourth terms above by

$$e^{j\frac{2\pi Nn}{N}} = 1$$

yields

$$x(n) = \frac{1}{2}e^{j\frac{2\pi n}{N}} + \frac{1}{2}e^{j\frac{2\pi(N-1)n}{N}} + \tag{2.3}$$

$$\frac{1}{2}e^{j\frac{2\pi 3n}{N}} + \frac{1}{2}e^{j\frac{2\pi(N-3)n}{N}} \tag{2.4}$$

Comparing eqn. 2.4 with eqn. 2.2 results in evaluation of the discrete spectral estimates

$$\frac{1}{N}X(1) = \frac{1}{2}, \quad \frac{1}{N}X(3) = \frac{1}{2}, \quad \frac{1}{N}X(N-1) = \frac{1}{2}, \quad \frac{1}{N}X(N-3) = \frac{1}{2}$$

or

$$X(1), X(3), X(N-1), X(N-3) = \frac{N}{2} \tag{2.5}$$

Equation 2.5 shows that the magnitude of spectral estimates depends on the length of data window N .

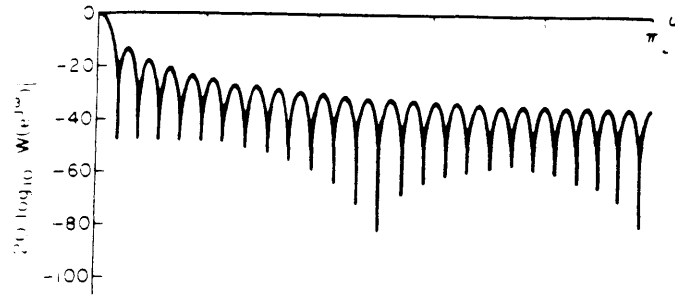


Figure 2.20: Magnitude response of Fourier transform of rectangular window (from Oppenheim and Schaffer, 1975).

A second limitation of the FFT is due to the implicit rectangular windowing of the data. In the frequency domain each computed spectral data point is convolved with the Fourier transform of the time window, given that

$$x_1(t) \cdot x_2(t) \Leftrightarrow X_1(f) * X_2(f)$$

Multiplication in the time domain is equivalent to convolution in the frequency domain. The transform of the rectangular window is the well-known *sinc* function, whose magnitude response is shown in Figure 2.20. The half-width of the main lobe and full width of side lobes is $1/N$ where N is the number of samples. Ideally, a time window of infinite length should be used in Fourier analysis, since as N increases the *sinc* curve begins to approach the impulse function. As revealed in Figure 2.20, convolving a spectral component with the Fourier transform of a rectangular window results in a smoothing or 'leakage' of the energy of the main component into adjacent spectral estimates, thereby distorting the overall spectrum. Clearly, reduction in the amplitude of the side-lobes of the windowing function will decrease the 'leakage' effect, but always at the expense of broadening the main lobe. This compromise between side-lobe reduction and main-lobe width is addressed in many digital signal processing texts and papers [6,13,24,37,44,45,55].

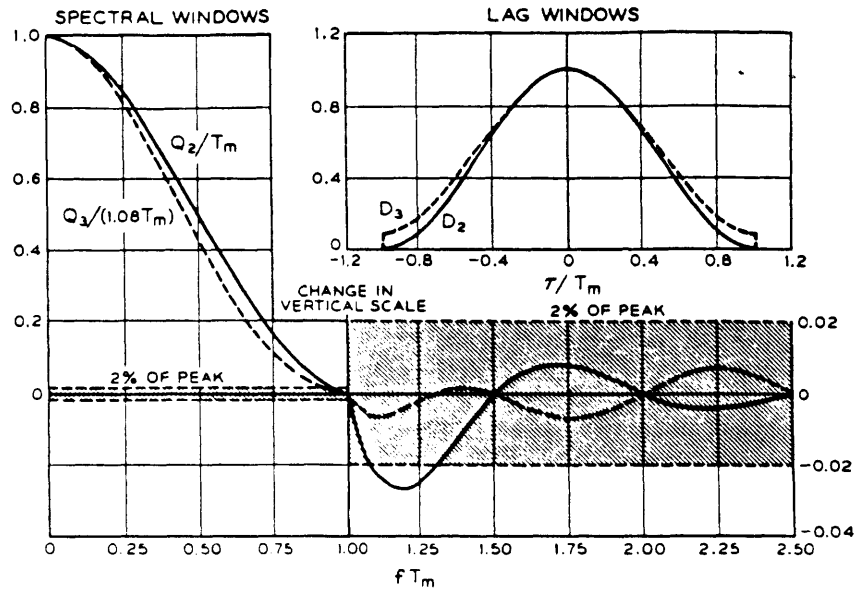


Figure 2.21: Comparison of Hamming(D_3) and Hanning(D_2) windows in both time and frequency domains(from Blackman & Tukey,1968).

Blackman & Tukey summarize the problem: “We would like to concentrate the main lobe keeping the side lobes as low as feasible. In order to concentrate the main lobe we have to make the window flat and blocky. To reduce the side lobes, however, we have to make the window smooth and gently changing. Since the window must vanish beyond the time interval of interest, we must compromise. So far, cut-and-try inquiry has been more powerful in finding good compromises than has any particular theory.” In essence, no optimum window has been determined from the several possibilities proposed since the mid-60’s. Blackman & Tukey compare two commonly used windows illustrated in Figure 2.21. The Hamming window is defined as:

$$0.54 + 0.46 \cos\left(\frac{2\pi n}{N}\right), \quad 0 \leq n \leq N - 1$$

The Hanning window is defined as:

$$0.5 + 0.5 \cos\left(\frac{2\pi n}{N}\right), \quad 0 \leq n \leq N - 1$$

The two most important differences between the Hamming and Hanning windows are (a) the highest side lobe for the Hamming spectral window is about $\frac{1}{3}$ the height of the highest side lobe for the Hanning window and (b) the heights of the side lobes for the Hanning window fall off more rapidly than do those for the Hamming window. One difference (a) favors the Hamming window, while the other difference (b) favors the Hanning window. This study employs the Hamming window.

Durrani and Nightingale list two detrimental effects of windowing on spectral estimates of a time series using the FFT[13]. First, data windows taper the amplitude of the sequence of observations, attenuating the estimates in the frequency domain. This point is more clearly made by recognizing that the area under a modified window is always less than the area under a rectangular window, thus some amplitude information is lost due to windowing. To correct for this, a compensating factor, U , has been derived which scales the spectral estimates accordingly. This scaling factor depends only on the window used and is defined as

$$U = \frac{1}{N} \sum_{n=0}^{N-1} w^2(n)$$

where $w(n)$ is the window and N is the length of the window. Since $U < 1$, rescaling is achieved by *dividing* the spectral estimate by U .

Associated with each window is an effective duration (T_{eff}) which can be referenced to the rectangular window ($T_{eff}=1$). For the Hamming window, $T_{eff}=0.571$. An analogous measure in the frequency domain is the effective bandwidth β_{eff} . The Hamming window value for $\beta_{eff}=1.75$. Other values for various windows are shown in Figure 2.22. The figure shows that T_{eff} and β_{eff} are inversely proportional quantities in all cases. This is expected since increasing window length in the time domain will effectively decrease the width of the

Data window	Uniformly weighted	Triangular ¹³ $\alpha = 1$	Parabolic ¹³ $\alpha = 2$	Cubic $\alpha = 3$	Quartic $\alpha = 4$	Hanning ² $q = 1$	Hamming cosine bell	Minimum bandwidth taper
Halfpower bandwidth	0.887	1.28	1.16	1.082	1.045	1.440	1.305	1.075
Dispersion factor η	1.0	1.333	1.20	1.142	1.111	1.500	1.363	1.125
Variance compensation factor Q	1.0	0.333	0.533	0.643	0.712	0.375	0.40	0.50
Effective bandwidth β_{eff}	1.0	1.680	1.414	1.30	1.225	2.0	1.75	1.255
Information-theoretic bandwidth β_{inf}	1.0	1.54	1.305	1.213	1.1625	1.719	1.586	1.250
Effective duration T_{eff}	1.0	0.595	0.709	0.769	0.816	0.50	0.571	0.796
Power content of major lobe, %	90.28	99.705	99.208	98.057	97.04	99.948	99.963	99.00
$\Delta h, \%$	4.72	0.222	0.744	1.80	2.212	0.07122	0.00406	0.173
Δw_1	0.5	0.5	0.349	0.429	0.466	0.25	0.206	0.50
Δw_2	1.0	2.0	1.4166	1.290	1.2166	2.0	2.0	1.4166
ΔBW	1.0	1.430	1.295	1.220	1.178	1.628	1.470	1.212

Figure 2.22: Spectral-window parameters for general data windows (from Durrani and Nightingale, 1972).

main lobe in the frequency domain.

The second detrimental effect of windowing is that some loss in the statistical stability of spectral estimates occurs because of smoothing in the frequency domain. For raw data sequences (rectangular window), the probability-density function of the power spectral estimator, obtained by taking the squared modulus of the finite Fourier transform of the data, is a chi-square distribution with two degrees of freedom. This value of degrees of freedom is effectively reduced by smoothing in the frequency domain, thereby making adjacent samples in the frequency domain statistically dependent. Durrani suggests that this loss of statistical independence among samples may be compensated for by increasing the data window length by a factor equal to β_{eff} .

2.3.3 Power spectrum estimation

The power spectrum estimator was briefly mentioned above. The most widely used estimator is the *periodogram*, $I_N(\omega)$, defined as the Fourier transform of the biased auto-correlation estimate $c_{zz}(m)$. That is,

$$I_N(\omega) = \sum_{m=-(N-1)}^{N-1} c_{zz}(m) e^{-j\omega m} \quad (2.6)$$

where

$$c_{zz}(m) = \frac{1}{N} \sum_{n=0}^{N-|m|-1} x(n)x(n+m), \quad |m| \leq N-1 \quad (2.7)$$

The periodogram, $I_N(\omega)$, can be expressed in terms of the Fourier transform $X(e^{j\omega})$ of the real finite-length sequence $x(n)$, $0 \leq n \leq N-1$, as

$$I_N(\omega) = \frac{1}{N} |X(e^{j\omega})|^2 \quad (2.8)$$

In terms of the real and imaginary parts of the Fourier transform

$$I_N(\omega) = \frac{1}{N} (X(e^{j\omega})X^*(e^{j\omega})) = \frac{1}{N} (X_R^2 + X_I^2) \quad (2.9)$$

Thus, computing a spectrum estimate via the periodogram approach is straightforward when an FFT algorithm is used. The steps are:

1. Compute the Fourier Transform of the N-point data sequence using an FFT.
2. Sum the squares of the real and imaginary parts of the FFT results at each sampled frequency.
3. Divide the sum by the number of points, N.

What results is an approximation of the true power spectrum, albeit a rough one.

In general, the periodogram is not a consistent estimate of the power spectrum. As N increases, the variance of the periodogram approaches the square of the true value of the power spectrum. In a consistent estimate, the variance would become zero as N increases. Various methods have been applied to the periodogram to achieve a consistent estimate. Three of the more common techniques are (a) averaging periodograms determined over successive nonoverlapping segments of the data sequence $x(n)$, (b) averaging adjacent periodograms, and (c) windowing the spectrum estimate to smooth the wildly fluctuating behavior of the periodogram estimates with increasing N. Each improvement has individual advantages and disadvantages which are explained in detail in Oppenheim and Schaffer[44].

The issue of terminology must be addressed at this point. Generally, the result $|X(e^{j\omega})|^2$ is referred to as the *energy* at a given frequency ω , and the collection of these estimates represent the *energy density spectrum*. The periodogram, $\frac{1}{N}|X(e^{j\omega})|^2$, represents, alternatively, an estimate of the *power* contribution of a given frequency component. The difference between the two estimates is clearly the $\frac{1}{N}$ term. It follows mathematically that dividing the energy estimate by the time index N will result in a power estimate, yet very often $|X(e^{j\omega})|^2$ is referred to as part of a power density spectrum. Digital signal processing texts are careful to point out this disparity [23,44,55], but many software analysis packages and

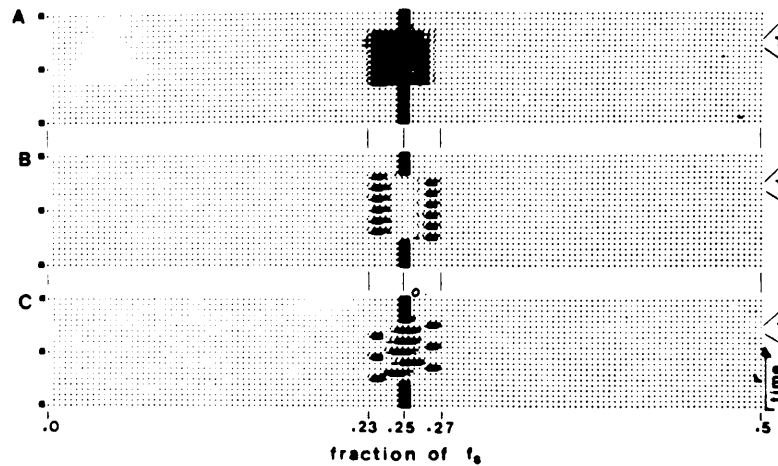


Figure 2.23: Running spectrum display without overlap (from Van Der Schee, 1984).

cursorly treatments of power spectrum estimation are content to define the power spectrum as Durrani does above, i.e., “the squared modulus of the finite Fourier transform.” Since the difference is a scaling constant, relative measurements between spectrum estimates are not affected, but the terminology must still be made clear.

2.3.4 Running spectrum analysis

In principle the procedure of running spectrum analysis (RSA) is simple: every Δt seconds a spectrum is computed from the preceding T seconds of signal and each spectrum computed is individually displayed, for example as a grey-scale plot or in a waterfall format as discussed in Chapter 1. Depending on the signal characteristics and the frequencies of interest, values of Δt and T may be chosen so that adequate resolution for observing changes in the spectrum over time can be preserved.

To clarify the previous statement, Figure 2.23 shows the result of executing running spectrum analysis on contiguous segments of data (no overlap). The input signal frequency is itself being modulated sinusoidally with period P . In part A of Figure 2.23, the time

window length equals P , the period of modulation. In part B, the time window length equals $\frac{1}{2}P$, and in part C, the time window length equals $\frac{1}{4}P$. As shown in the figure, the details of the modulation scheme are borne out as the window length decreases. If we consider one window length to be equivalent to one 'sample' of the modulation sinusoid, then 4 'samples' were acquired in part C of Figure 2.23. Applying Shannon's sampling theorem in an analogous way to running spectral analysis would result in the rule that each period of the modulator has to be 'sampled' at least two times for accurate recovery of frequency information (no aliasing).

Part C of the figure shows a rather discretized representation of the changes in frequency over time. By introducing overlap between consecutive data segments, the RSA equivalent of 'interpolation' results, yielding the smoother, more recognizable patterns in Figure 2.24. The overlap in all three parts of Figure 2.24 is 75%, with window length corresponding to those given for Figure 2.23. Part C shows clearly the modulation scheme applied to the input signal. In effect, overlap in RSA has the same 'interpolative' effect as zero-padding does in the time series domain. In both cases, no new information is gained but a clearer picture results.

When applying RSA, decisions must be made about length of window, type of window, and percent overlap. The trade-offs are made explicit when considering the window length while assuming a fixed sampling rate. In the extreme case, the window would be as long as the data sequence. This would give superb spectrum information, but the changes in frequency over time would be lost. The opposite situation is a very short window, in which frequency changes would be carefully tracked but frequency resolution would suffer. Thus, good temporal resolution requires a short window while good frequency resolution calls for a long window.

The choice of window shape recalls the issues addressed above about leakage of spectral estimates in the frequency domain. Percent overlap is more of a space problem in that the

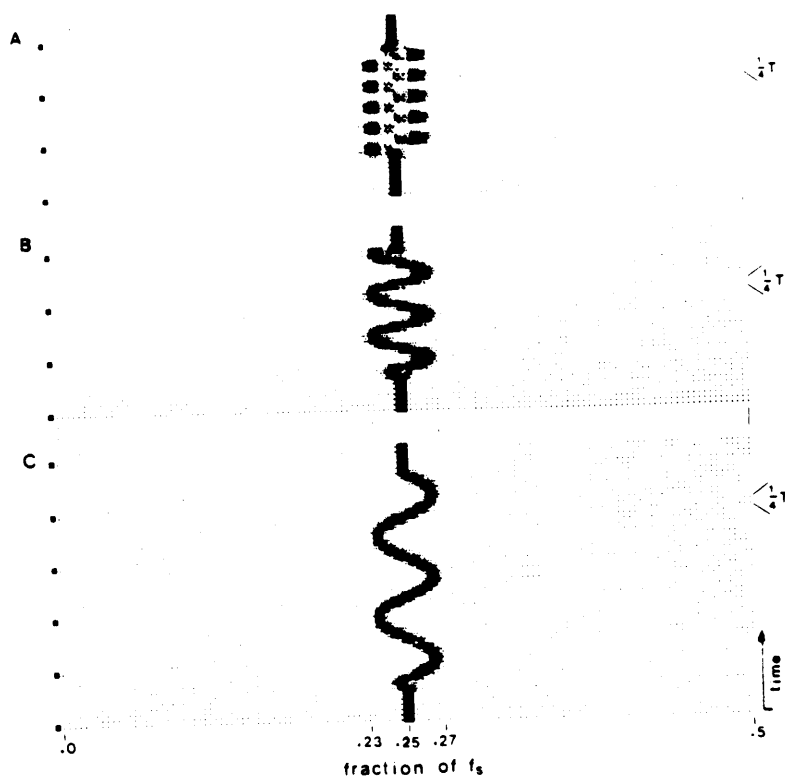


Figure 2.24: Running spectrum analysis with overlap (from Van Der Schee, 1984).

choice of the number of interpolated spectra boils down to a trade-off between how distinctly the frequency changes are illustrated and how often the computer software/hardware set-up can handle a new spectrum display.

Another important point about RSA is the inherent time delay in detecting changes in the frequency of the input signal. The window shape plays a large role here because of the tapering of time domain information on either end of the data segment. For example, the effective duration of a Hamming window was stated above as .571 of the width of a rectangular window. The Hamming window shape shown as curve D_3 in Figure 2.21 tends to emphasize samples towards the middle of the data segment while attenuating those towards the end. Thus, frequency changes of interest must lie towards the center of the data window before being detected in the spectrum.

Figure 2.25 illustrates the progression of a 64 second long doubling of the baseline frequency (.05 hz) in an RSA scheme in which a Hamming window is used, sampling rate is 1 hz, $T=512$ seconds, and $\Delta t=64$ seconds(87.5% overlap). Adjacent to each time record is the corresponding energy spectrum. Visual examination reveals that the specific increase in frequency, which appears initially in time segment #12, is apparent by no earlier than spectrum #14. Thus, an effective detection delay of roughly 128 seconds occurs. A slight, but recognizable decrease in the .05 hz baseline component occurs with the initial appearance of the 64 second .10 hz rhythm (compare spectrum #'s 11 and 12). The conclusion from this first glance at RSA time delay is that spectral analysis of changes in dominant rhythm components lead to earlier detection of frequency disturbances in the input data than does analysis of changes of other frequency components.

Van Der Schee concluded that "running spectrum analysis offers the possibility of extracting both qualitative and quantitative information" from the electrogastragram[70]. The value of a real-time RSA processing instrument for monitoring gastric disturbances has yet to be determined because of the unknown clinical diagnostic significance of the

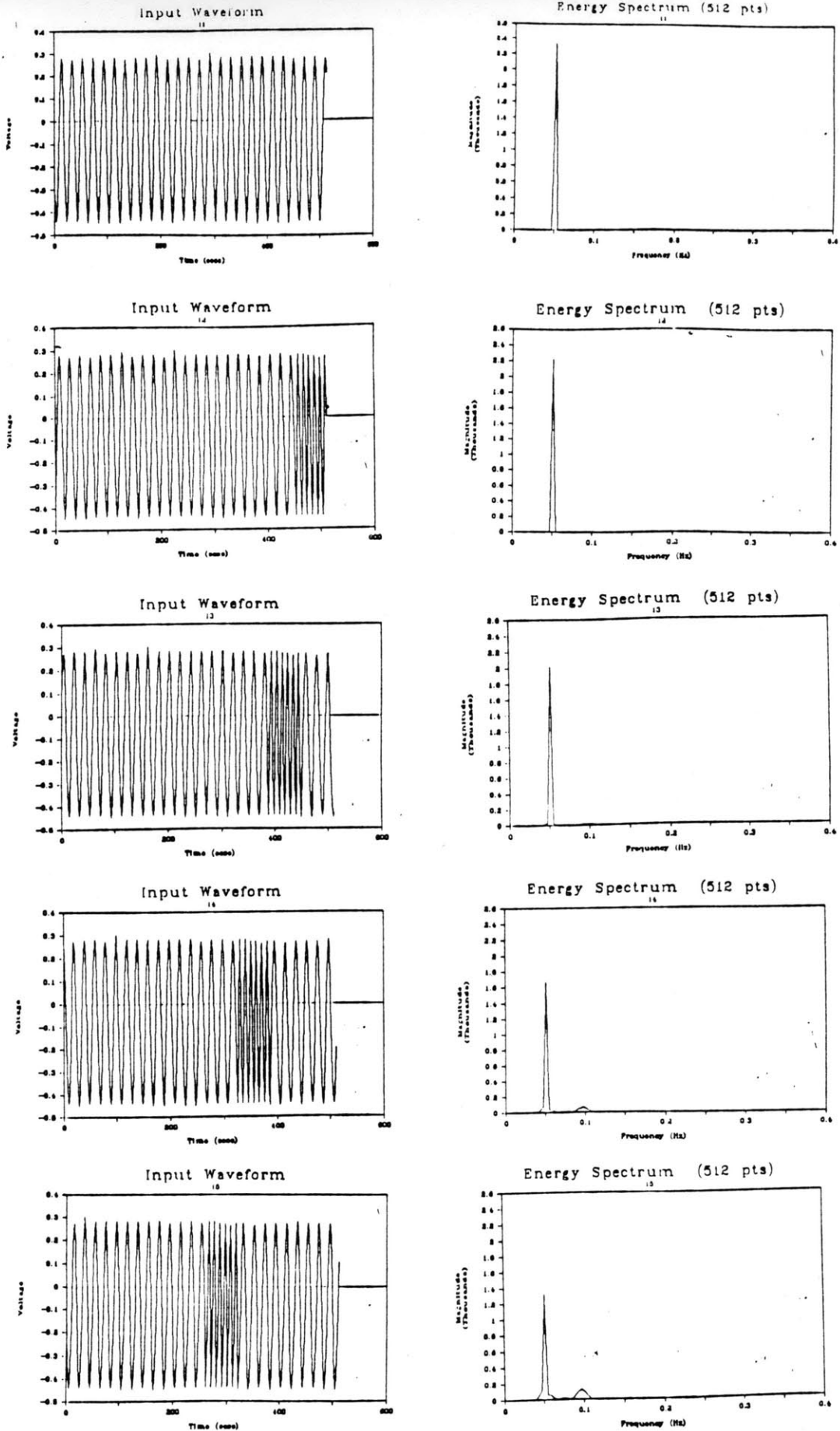


Figure 2.25: Time delay of running spectrum analysis.

EGG. However, preliminary use has indicated that anomalies in electrical rhythms can be detected using RSA analysis[17]. In this study, RSA analysis has proved useful in revealing gross changes in the frequency content of the EGG of a subject experiencing motion sickness.

Chapter 3

Materials and Methods

3.1 Subjects

Six paid college student volunteers each participated in one pilot session and four test sessions. The subjects included three men and three women, five of whom are between 21-23 years old, while the sixth is 27 years old. Each subject exhibited a prominent 3 cpm BER based on pilot EGG sessions. Each subject was asked to fill out a Motion Sickness Questionnaire designed to find out (a) if there are any factors in the subject's medical history which may affect the results, (b) a brief survey of the subject's history of motion sickness susceptibility, and (c) the kinds of motion that the subject feels have been most effective in causing motion sickness. None of the subjects had a prior history of chronic gastrointestinal complaints.

In addition, prior to each test session, the subject was asked to fill out a Pre-Session Questionnaire used to determine the subject's overall state of physical fitness; any recent consumption of alcohol, tobacco, or drinks containing caffeine; any recent use of medication; the number of hours of sleep the previous night; the number of hours of fasting; and any existence of abdominal discomfort, or nausea. Replies to the questionnaire that were noticeably different from the subject's answers in previous experiments or otherwise indicative of an unrested or unwell subject necessitated the disqualification of the subject

and the cancellation of that trial. Also, each of the subjects was required to read a short introduction/tutorial on the magnitude estimation technique of rating overall discomfort. As explained in section 3.4, this method was used to determine a "halfway to vomiting" sickness endpoint for the test sessions.

The study was approved by the MIT Committee on the Use of Humans as Experimental Subjects (COUHES), and each subject signed an informed written consent form prior to each test session. (The Motion Sickness Questionnaire, Pre-Session Questionnaire, Magnitude Estimation instructions, and Informed Consent Statement are all listed in Appendix A.)

3.2 EGG Recording

To record EGG, disposable cutaneous Ag/AgCl electrodes (Hewlett-Packard 14445A) were applied to the abdomen. To enhance signal stability, the skin beneath the electrode was lightly scratched with the tip of a sterile hypodermic needle (Yale, 20g). Figure 3.1 shows electrode positions for bipolar recordings. A point half the distance along the vertical midline from the umbilicus to the xiphoid was located. From this position, the first electrode was placed 1 cm caudad and 6 cm to the subject's left, and the second electrode was placed 2 cm cephalad and 5 cm to the subject's right. The reference electrode placement was on the left side of the subject's lower back.

Electrodes were connected to a computer data acquisition system through a DC amplifier (Denver Research Institute NASA/LSLE EOG pre-amp; 0-30 hz; input impedance 50 M Ω). Total system gain for the EGG signal was 4000 (1000 through DRI amp, 4 in software). No high-pass filtering was required because the amplifier contained step autobalancing circuitry. Any combination of signal plus DC bias plus noise which causes the output signal to reach a threshold of ± 2.4 volts will cause a DC restoring signal 'step' to be added to the input signal. This reset of ± 2.4 volts was detected and compensated electronically

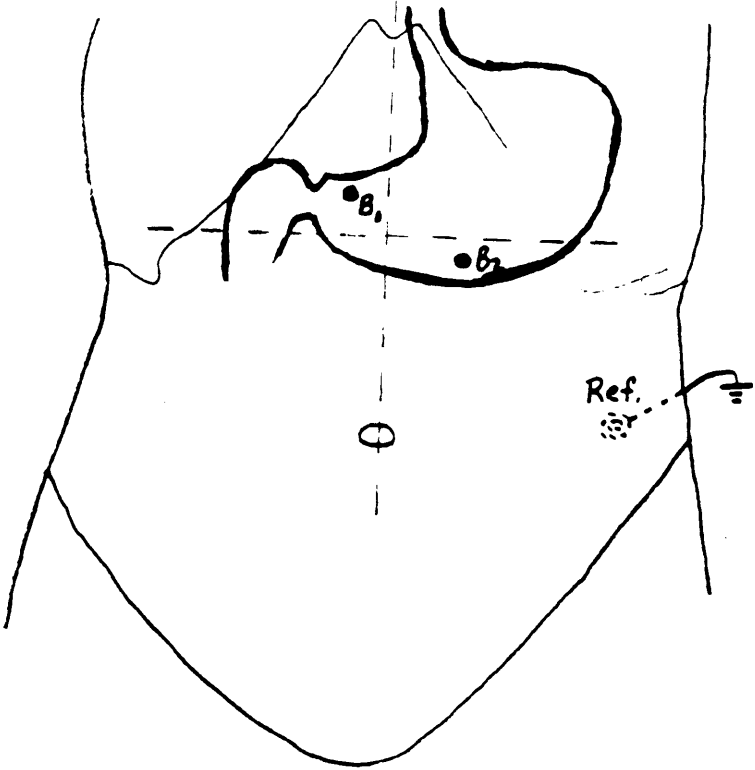


Figure 3.1: Electrode positions used in this study.

in software before signal analysis. Prior to sampling at 1 hz, the analog EGG output from the amplifier was anti-aliased via a low-pass filter (Krohn-Hite; 8-pole Butterworth; $\omega_c = .35$ hz). Filter response is shown Figure 3.2.

Respiration was monitored using a nostril thermistor incorporated as one leg of a bridge circuit, as shown in Figure 3.3. Another equivalent thermistor is inserted on the opposite side of the bridge to compensate for changes in ambient room temperature. The thermistor was placed just below the subject's nostril and held there using regular transparent tape. Respiration input was anti-aliased by a Krohn-Hite low-pass filter with identical specifications as the one described above. Total system gain for respiration signal was unity.

3.3 Signal Analysis and System Overview

Both EGG and respiration signals were sampled at 1 hz using a personal computer (PC Limited AT) equipped with a Metrabyte Dash 16 data acquisition and control board (see below). Running power spectrum analysis software written in Lattice-C performed real-time processing and grey-scale display of the EGG input. (See Appendix C for description and listing of programs.)

Running spectra were computed every 64 seconds from the preceding 512 samples (512 seconds), resulting in an overlap of 87.5% (448 secs). A Hamming window was applied to reduce leakage effects. Using this method, *independent* frequency samples exhibit a resolution of .0039 hz (see Section 2.3.2). Since the magnitude of the EGG signal was expected to vary between subjects and between runs, we defined a dimensionless index reflecting the relative height of the most prominent spectral peaks. This index is defined as the magnitude of the highest peak (P_1), within the frequency range from 2.5 to 9.0 cpm, divided by the geometric mean of the three next highest peaks (P_2, P_3, P_4) in that range, or

$$\text{Spectral Peak Index} = \frac{P_1}{\sqrt[3]{P_2 P_3 P_4}}$$

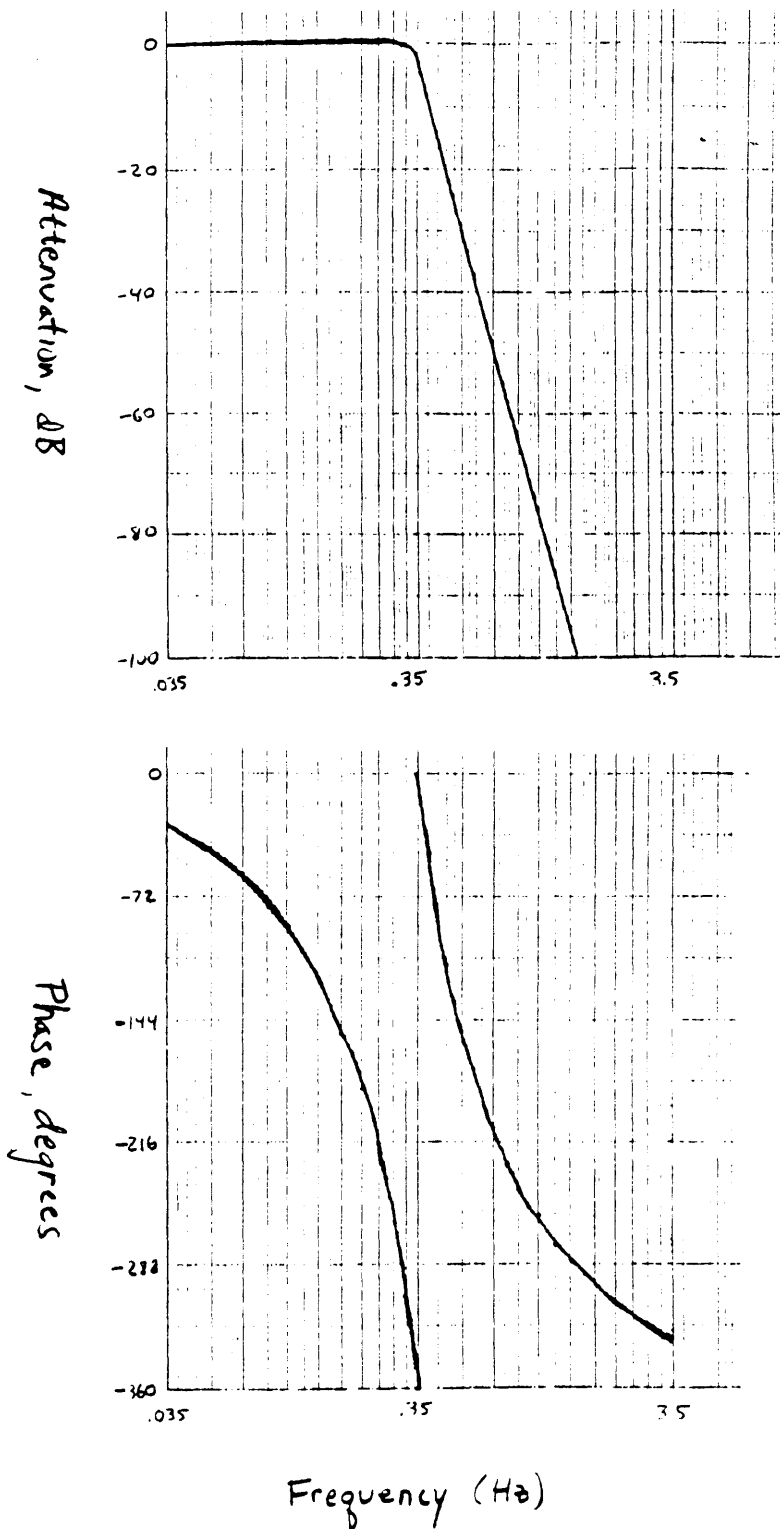


Figure 3.2: Amplitude and phase response of 8-pole Butterworth low-pass filter used in this investigation.

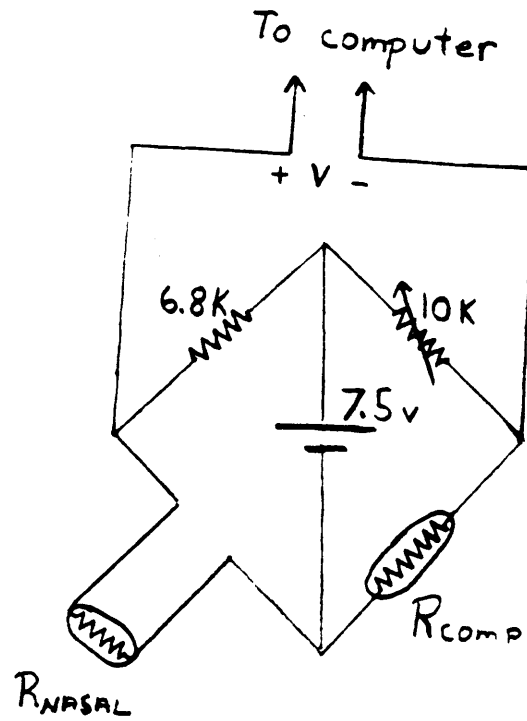


Figure 3.3: Nasal thermistor and bridge circuit used to monitor respiration. Nominal room temperature resistance for R_{nasal} and $R_{comp} \approx 7 \text{ K}\Omega$.

The highest spectral peak in a normal, unstimulated subject in these experiments is the BER. Frequencies above 9 cpm were excluded to avoid any influence of possible respiration artifacts.

Figure 3.4 is a block diagram of the complete EGG measurement and processing system. The core of the system is a PC Limited AT microcomputer (virtually identical to the IBM version), equipped with a multifunction analog/digital I/O expansion board (Metrabyte Dash-16), and IBM monochrome graphics adapter. The I/O board is capable of analog-to-digital data acquisition at very low rates (1 hz in this application), and can simultaneously sample either 16 single ended channels or 8 differential channels. The DASH-16 board uses an industry standard (AD574A) 12 bit successive approximation converter with a 25 μ sec conversion time. Bipolar analog input ranges of $\pm 0.5v$, $\pm 1v$, $\pm 2.5v$, $\pm 5v$, or $\pm 10v$ are available. (The $\pm 5v$ range was used for this investigation.) A menu-driven software package, *LabTech Notebook*, was used to control the functions provided by the Dash-16 board.

As indicated in Figure 3.4, seven channels of input data were monitored: 1 channel each for chair RPM, EGG, and respiration; 2 channels each for different measurements of pallor and skin temperature. *LabTech Notebook* performed real-time display and storage of chair RPM, pallor, skin temperature, and respiration signals. The EGG input was analyzed by specialized software written for real-time processing, which in the figure includes all the blocks to the right of the dotted line. As explained above, the EGG data is windowed, then transformed into frequency components using a standard 512 point FFT842 routine. The real and imaginary results are used to compute the *energy* spectrum estimates, $|X_N(f)|^2$. Results from both the FFT and squaring routines are stored in separate data files.

To calibrate the real-time grey-scale plot, the peak BER spectral magnitude (BER_{peak}) acquired during the first 15 minutes of EGG monitoring is determined. The range between 0 and BER_{peak} is subsequently divided into six equal intervals. These intervals, plus the

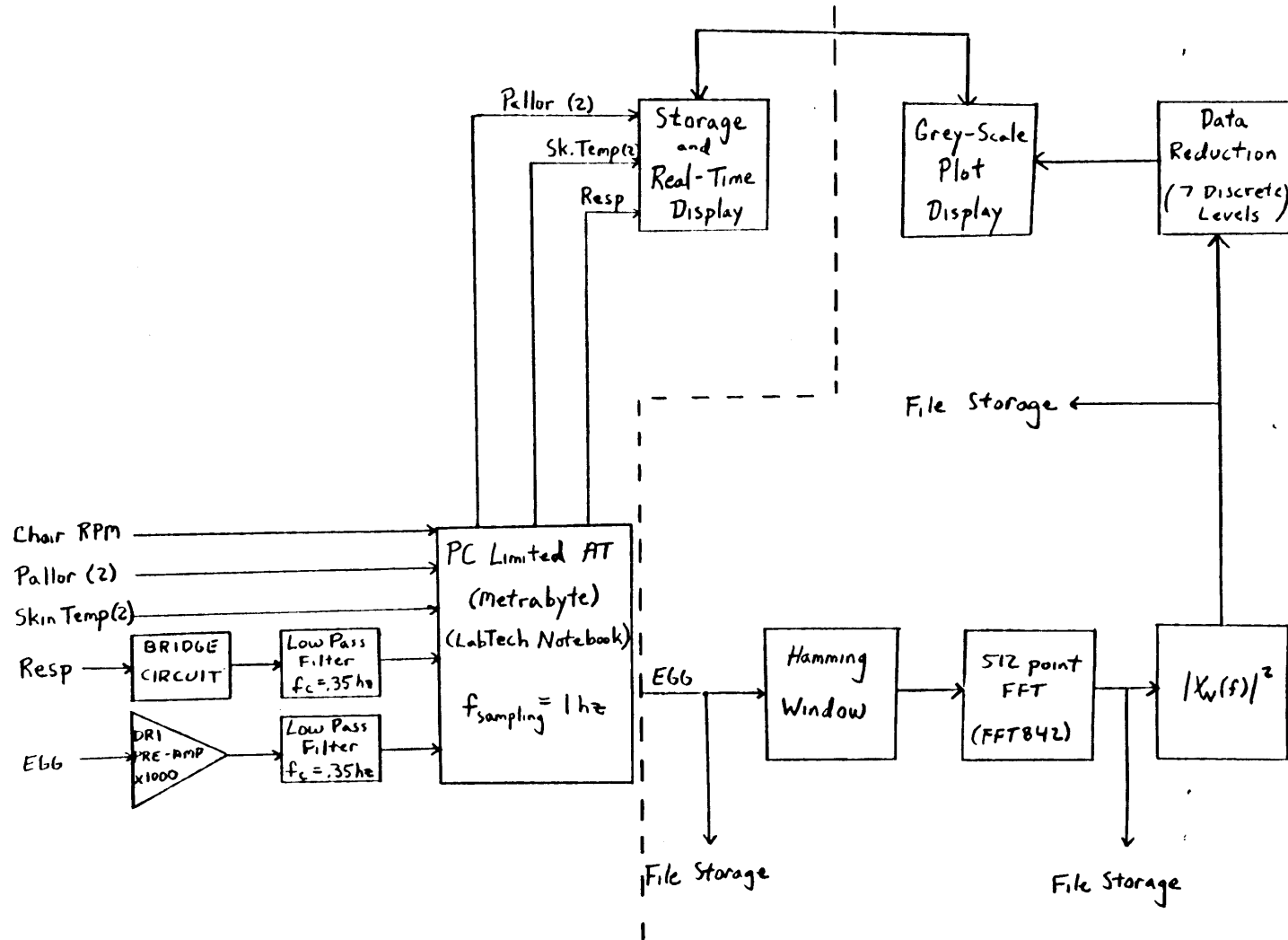


Figure 3.4: EGG system overview.

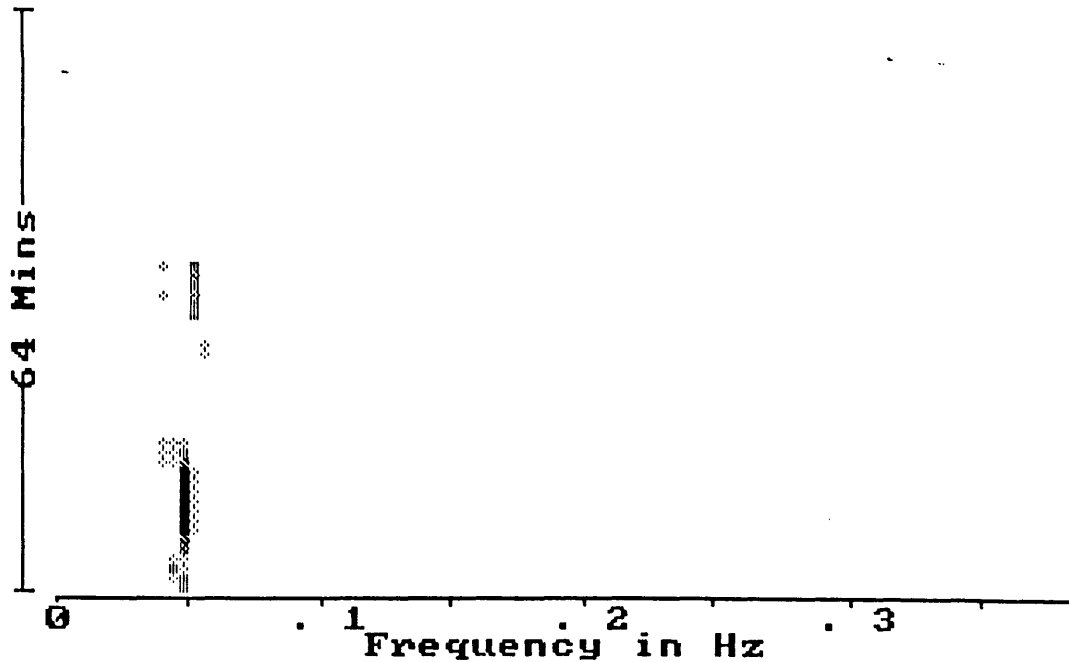


Figure 3.5: Typical grey-scale plot generated by software.

range above BER_{peak} , result in seven discrete levels, each represented by a specific pixel brightness in the grey-scale plot. Thus, each component of the energy spectrum is placed in one of these seven ranges, and is indicated on the grey-scale plot as a specific pixel intensity (see Figure 3.5). In this way, frequency changes in the EGG over time may be carefully monitored. The double arrow in the upper part of Figure 3.4 shows that one may exit the EGG processing and display software to return to the time domain graphics of *LabTech Notebook*. The Real Time Access feature of *LabTech* provides this communication interface between programs written by the user and those of *LabTech*.

3.4 Procedure

All subjects fasted at least 6 hours before the session. Three subjects performed all their experiments in mid-morning; the other three performed all their experiments in mid-afternoon. Hours of sleep and amount of exercise prior to the session were monitored closely to maintain consistency between trials within an individual subject. The subjects were seated in a rotating chair (see Figure 2.9), EGG electrodes and nasal respiration thermistor were applied, and baseline EGG spectra were monitored for 15 minutes prior to chair rotation. Real-time software analysis indicated the magnitude and frequency of the highest peak in power spectra computed over this resting period. The trial was discontinued if the subject did not exhibit a prominent resting BER.

After this 15 minute baseline period, motion sickness was induced in the subject via a modification of the Coriolis Velocity Staircase method (see section 2.2.4.) This approach was used to insure that significant symptoms were elicited in all sessions. The subject was rotated, eyes open, about an earth vertical axis (Z-axis) while executing 45° head movements in pitch (Y-axis) and roll (X-axis). The subject made 10 head movements in five specific directions (front, up, right, up, back, up, left, up, front, up) to a 1 hz cadence for ten seconds. The subject was asked to keep the upper body as stationary as possible during execution of head movements to avoid motion artifact contamination of the recorded EGG signal. After completing 10 head movements, the subject was allowed 20 seconds to report symptoms, and then began the next set of head movements. Initial chair rotation rate was either 7, 9, or 11 RPM, based on the susceptibilities of the individual subjects. The initial RPM was kept constant for all the sessions of an individual subject. Rotation rate was incremented by 2 RPM after every 4 minutes (80 head movements). Once a moderate sickness level was achieved, chair RPM was maintained constant. If symptoms subsequently stabilized, the 2 RPM staircase was resumed. When the subject reached

his symptom endpoint (see below), chair rotation was gradually stopped over a 3 minute period, in order to avoid further exacerbation of symptoms. EGG monitoring continued during the recovery period, usually for about 10 minutes.

The pilot session served a two-fold purpose: 1) to familiarize the subject with his own range of symptoms, and 2) to establish a "halfway to vomiting" subjective sickness endpoint for subsequent experiments using the overall discomfort magnitude estimation method of Bock and Oman (see section 2.2.4). As mentioned above, pilot sessions were also used to select only those subjects who exhibited a prominent 3 cpm BER rhythm. The subject's symptoms were simultaneously scored according to the Pensacola Diagnostic method (see section 2.2.4). Symptom definitions were those presented in a report issued by Oman, Rege, and Rague in January 1987, *Standard Definitions for Scoring Acute Motion Sickness using the Pensacola Diagnostic Index Method* (see Appendix B).

Chapter 4

Results

EGG recordings from all 24 trials showed a strong BER rhythm during all or part of the resting period prior to chair rotation. The BER is defined as any dominant spectral peak within the range .04-.06 hz. Only one test session (Subject B, Expt. 3) was postponed because of the absence of a prominent BER rhythm. Figure 4.1 is a histogram of the experiment duration times for all 24 sessions. The duration time is specified as the total time that the subject is exposed to the stimulus (rotating chair) in an individual session. The top half of Figure 4.2 shows a typical time series EGG of a normal, resting subject. Average BER magnitude during the resting period was approximately $300 \mu V^2$ (microvolts²) across all sessions, with a range of $80 \mu V^2$ - $1600 \mu V^2$. Appendix D contains results from all 24 sessions, presented in various formats. Some of these figures may be referenced to facilitate explanations.

The RPM staircase stimulus successfully elicited moderate to severe motion sickness symptoms in all sessions. A minimum Nausea I level was reached in all trials, and two different subjects experienced brief vomiting or retching in an individual session, clearly exceeding the nominal endpoint. The BER magnitude decreased in all trials by an average of 85% (range 50%-96%) during severe symptom onset as reported by the subject. The spectrum peak index similarly fell from an average value of 12 (range 4-40) to below 3

Experiment Duration Time Distribution
(n = 24)

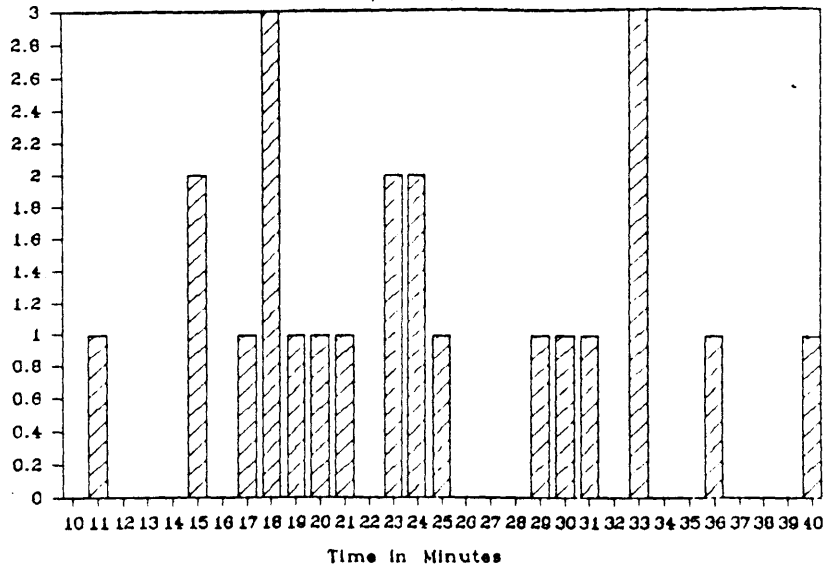


Figure 4.1: Histogram of the total time that the subject is exposed to the stimulus in an individual session.

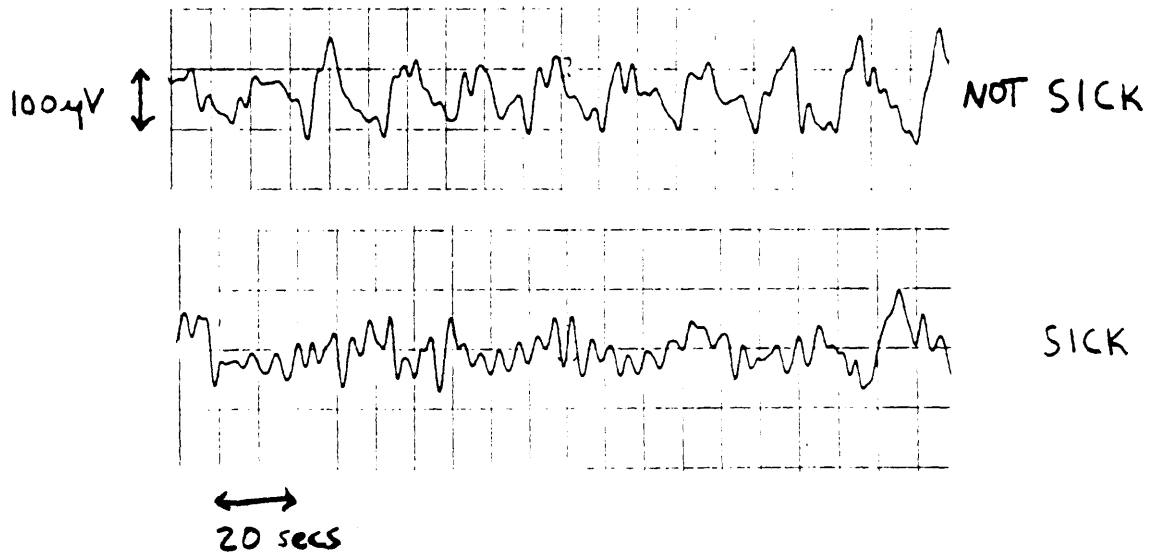


Figure 4.2: Time series EGG.

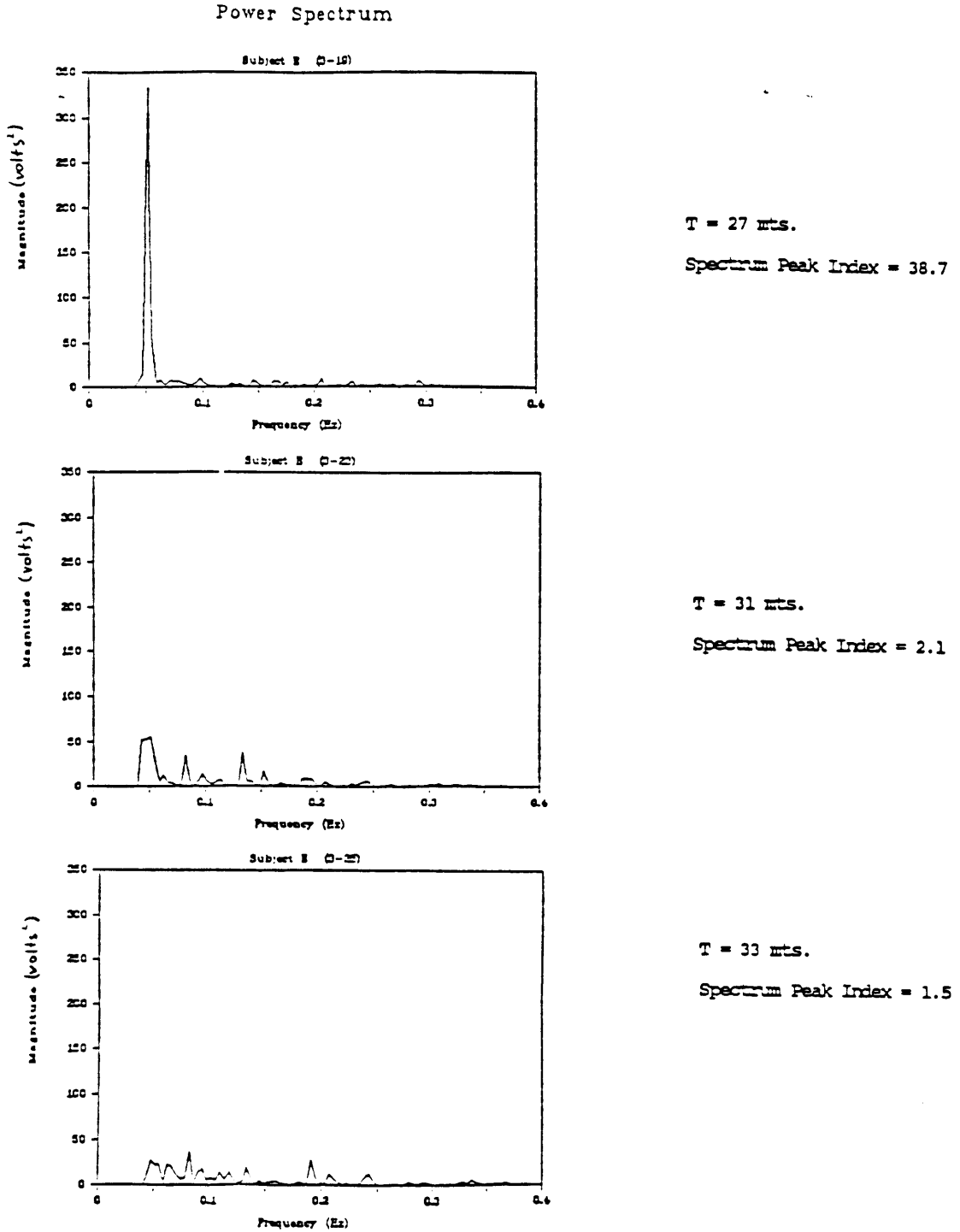


Figure 4.3: Typical change in EGG Energy Spectrum during Motion Sickness.

during the same period (see Figure 4.3). A portion of a recorded EGG signal during a period of motion sickness is illustrated in the bottom half of Figure 4.2.

In 14 sessions, periods of moderate or severe motion sickness were accompanied by an increase in frequency 'activity' in the interval from just above the BER through the respiration range (.06 hz-.30 hz). Based on visual inspection of waterfall and grey-scale plots, these episodes of 'tachygastria' can be divided into two distinct groups: those in which any of the spectral magnitudes within this .06 hz to .30 hz range increase to values at least 50% of the resting BER magnitude (high-level tachygastrias; see Figure 4.4), and those in which any increases in this range measure between 10 and 50% of the resting BER magnitude (low-level tachygastrias; see Figure 4.5).

High-level tachygastrias appeared in half of the 14 sessions, and were distributed across 3 of the 6 subjects: all 4 trials from subject D, 2 trials from subject C, and 1 trial from Subject E. Subject D consistently reached the same level of motion sickness in each trial. Subject C exhibited high-level tachygastric activity during a brief period of retching. (See Appendix D, Subject C, Expt. 2). During episodes of high-level tachygastrias, subjects C and E had clearly reached a more severe level of motion sickness as compared to their other trials and had probably gone beyond their nominal endpoint.

In the other 7 sessions, low-level tachygastrias occurred and were distributed across 4 of the 6 subjects: 3 trials from subject B, 2 trials from subject F, 1 trial each from subjects C and E. Subject B showed low-level tachygastric activity during a period of slight vomiting (See Appendix D, Subject B, Expt. 1). Subject A revealed no visually discernible tachygastric events in any of the four test sessions, but a decrease in BER magnitude and spectrum peak index prior to the sickness endpoint consistently occurred in all trials (see Figure 4.6). (In the figure, spectrum peak index, ratio index, and sickness index are all equivalent.)

Subject E's sickness endpoint decreased in intensity from session 1 to session 4. Relative

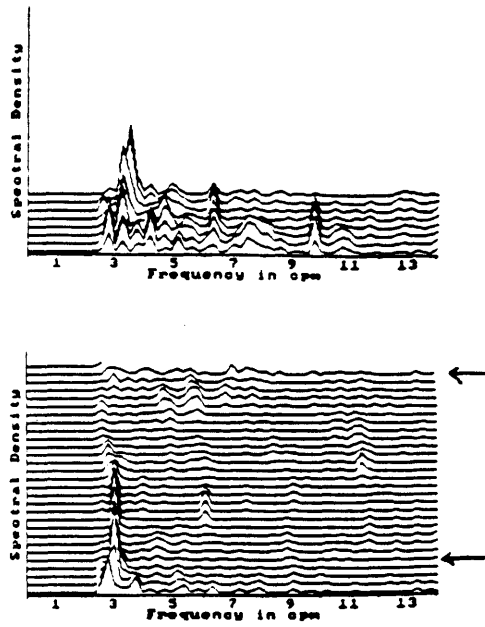


Figure 4.4: Waterfall plot of increased frequency activity in range above BER during motion sickness. In all waterfall plots, arrows indicate start and end of the stimulus.

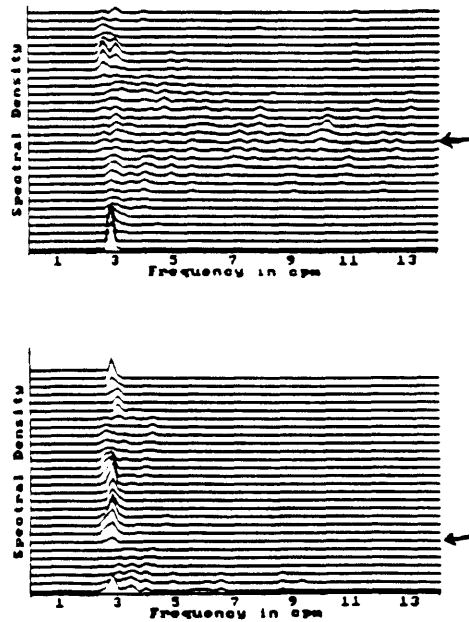


Figure 4.5: Waterfall plot of low level increase in frequency activity in range above BER during motion sickness.

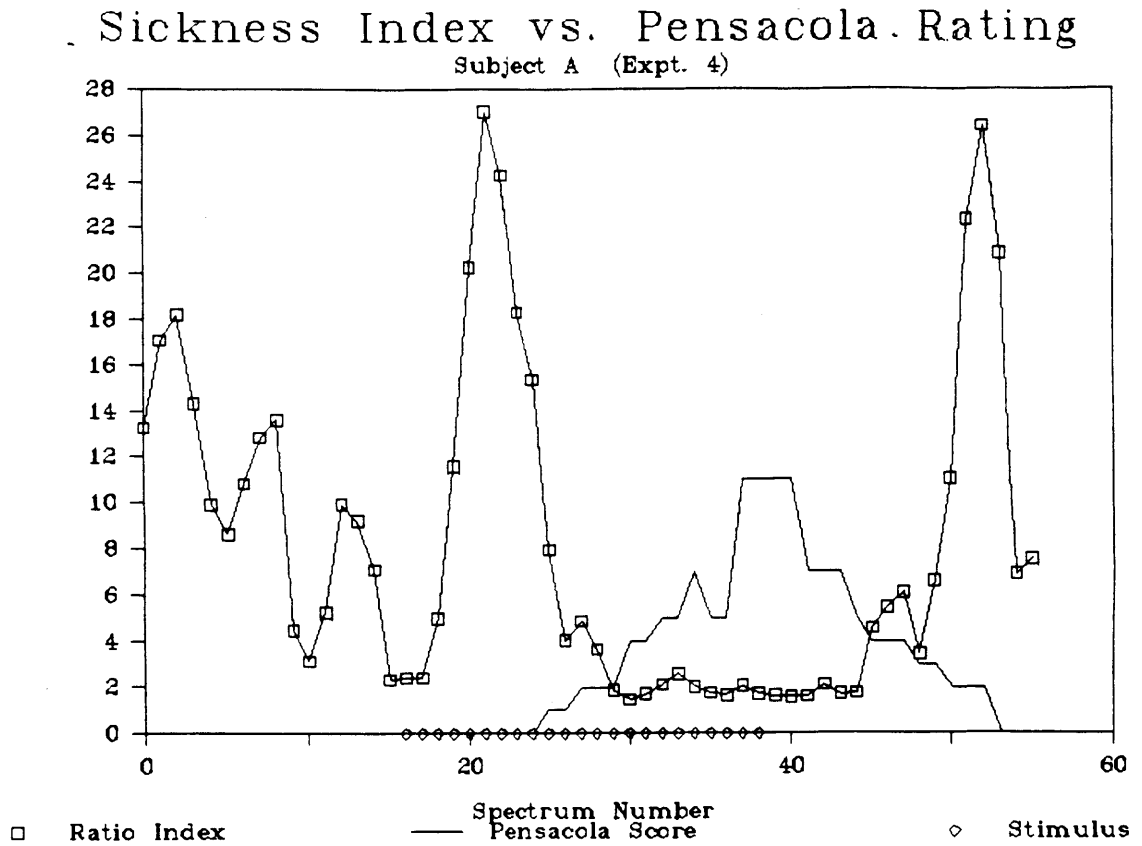


Figure 4.6: Decrease in spectrum peak index during motion sickness period. Subject A, Expt. 4. Sickness Index = Ratio Index = Spectrum Peak Index.

to this trend, high-level tachygastric episodes occurred in session 1, low-level tachygastric episodes occurred in session 2, and no discernible tachygastrics occurred in sessions 3 and 4. Subject C's sickness endpoint was also noticeably moderated for the final trial, the only session in which the subject did not exhibit a tachygastric episode.

The intermittency, or periodic disappearance and reappearance, of the BER rhythm was difficult to establish because of the relatively short 15 min preliminary recording period. However, Subject B showed an intermittent baseline frequency during reports of mild symptoms (see Appendix D, Subject B, Expt. 1). Subject F exhibited BER intermittency during moderate and severe motion sickness reports (Expt. 3). The symptoms stabilized during periods when the BER was present, and gradually worsened after the BER disappeared.

During motion sickness, distinct shifts of the dominant BER from 3 cpm to frequencies at or above 4 cpm occur only in two individual sessions with Subject D (Expts. 3 and 4). The duration of both these BER shifts was about 4 mins. Subject F shows a clear BER change from 3 cpm to 5 cpm for ~3 mins during mild symptom reports (Expt. 4). Peaks at 11 cpm and 12 cpm occur during symptom reports in 7 of the 24 trials, but these could not be positively correlated with respiration frequencies. Respiration artifacts are present but are typically insignificant as shown by Figure 4.7. During the recovery period in three of the four sessions with Subject A, the BER frequency settled at a value slightly higher than the original resting BER frequency. Figure 4.8 shows the increase in BER frequency following a test session.

For Subject B, the existence of a BER appeared highly dependent on the amount of sleep the subject had the previous night. The one trial that was postponed was attempted when Subject B had only 1 hour of sleep the night before. Session 4 was done when the subject had only 5 hours of sleep the night before (see Appendix D). All other sessions were done when the subject had a normal night's sleep (7 hours). The obvious difference between the spectral plots of session 4 and those of the other sessions might be due to a sleep dependent process regulating the EGG.

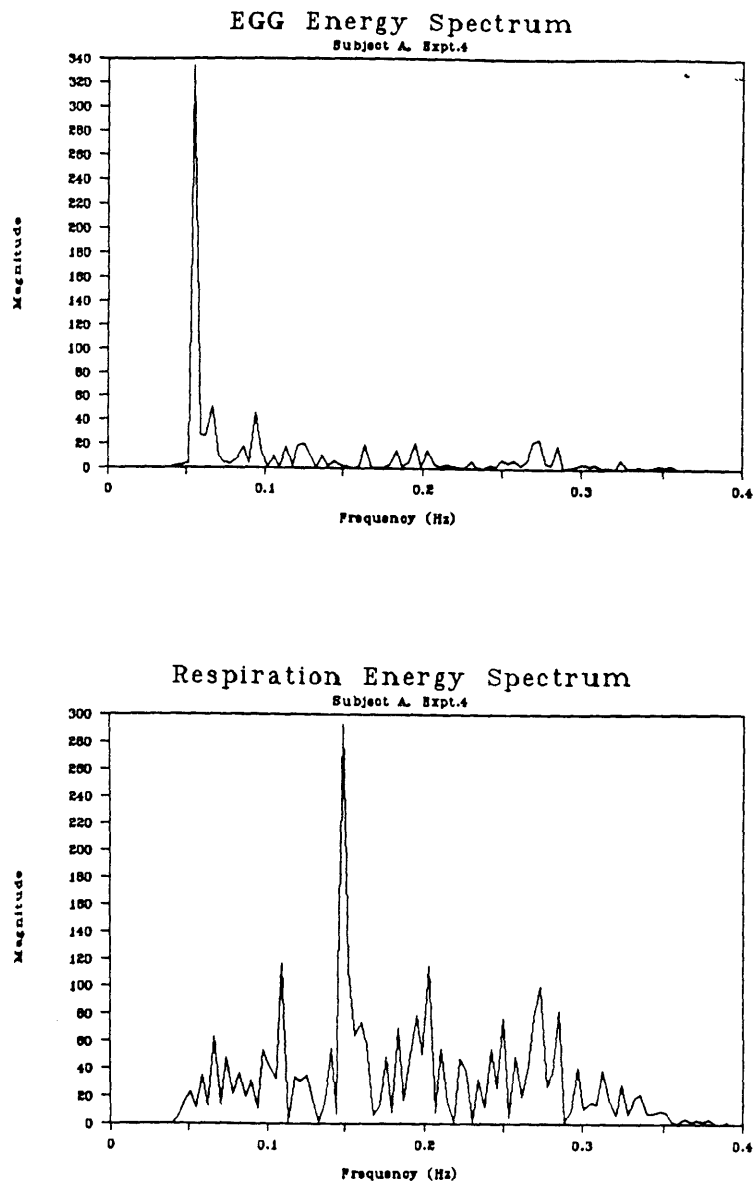


Figure 4.7: Influence of respiration artifacts on energy spectrum.

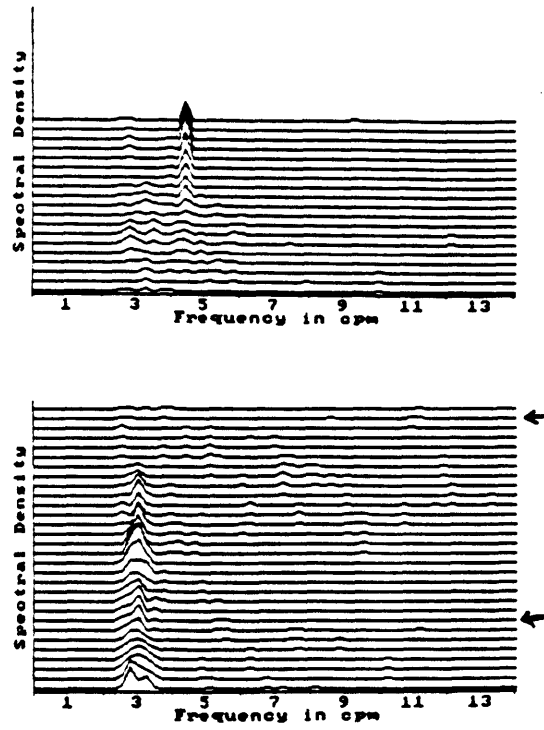


Figure 4.8: Recovery BER for Subject A, Expt. 2.

Chapter 5

Analysis and Discussion

5.1 Spectrum Peak Index

The experimental results show that a *prolonged* reduction in the BER component present at the start of stimulation, with or without tachygastric episodes, is indicative of motion sickness. The time domain EGG signal during motion sickness may best be described as broadband noise in the absence of a regular 3 cpm rhythm. Spectra computed during these periods more likely will show magnitude increases in frequency components in the tachygastric range rather than a specific shift in BER frequency.

The spectrum peak index is defined in Chapter 3:

$$\text{Spectrum Peak Index} = \frac{P_1}{\sqrt[3]{P_2 P_3 P_4}}$$

where P_n is the n th largest peak in the range between 2.5 cpm and 9 cpm. In a normal, unstimulated subject, P_1 is the magnitude of the BER. Thus the peak index will decrease if (1) the BER decreases or (2) several frequency components in the tachygastric range increase. A more reliable indicator of broad-band frequency activity results when using the geometric mean, $g_m = \sqrt[3]{P_2 P_3 P_4}$, rather than the arithmetic mean, $a_m = \frac{P_2 + P_3 + P_4}{3}$, in the denominator of the peak index. To illustrate this point, consider the case when $P_1 \approx P_2$, and both P_3 and P_4 are insignificantly small. As a rule, g_m will always be less than a_m .

For larger values of P_2 , $g_m \ll a_m$. Thus, a peak index incorporating the geometric mean will be less sensitive to the appearance of one large, isolated spectral peak while the BER is simultaneously present. For a significant decrease to occur in the above index, a more broadband response is required, i.e., a minimum of three peaks with magnitudes comparable to that of the BER must be present. Increasingly robust indices of frequency 'activity' can be achieved by taking the geometric mean of more and more peaks below the dominant one, P_1 . Both high-level and low-level tachygastric episodes, which exhibit broad-band behavior during motion sickness, will be reflected as a decrease in the spectrum peak index. BER shifts to higher frequency values will not be tracked by the above index. However, the experimental results show that this kind of response was rare and occurred only for a short period of time. Because EGG magnitude varies between subjects and between runs, the spectrum peak index provides a collective standardized measure of magnitude changes in frequency components during motion sickness. Because the index is a ratio, the minimum value is 1. Information about the relative amplitude of the BER is preserved because in EGG recordings during resting periods the peak index typically follows fluctuations in the BER magnitude (Figure 5.1).

Figure 5.2 shows a change in the spectrum peak index when a window length of 256 points is used in running spectrum analysis. Two major differences surface: (a) the 256 point peak index is generally lower and (b) the 256 point peak index fluctuates more than the 512 point peak index. Difference (a) is due to the issue of independence between adjacent frequency samples. In both cases, the computation of the peak index involved spectra with frequency samples spaced apart by .0039 hz. However, because of the smaller Hamming window in the 256 point case, a smoothing effect occurred across the frequency samples, tending to pull the maximum and minimum values closer together. As a result, lower spectrum peak index values occur when the window length is 256 points. This decrease can be corrected by including only every other frequency value when computing the index.

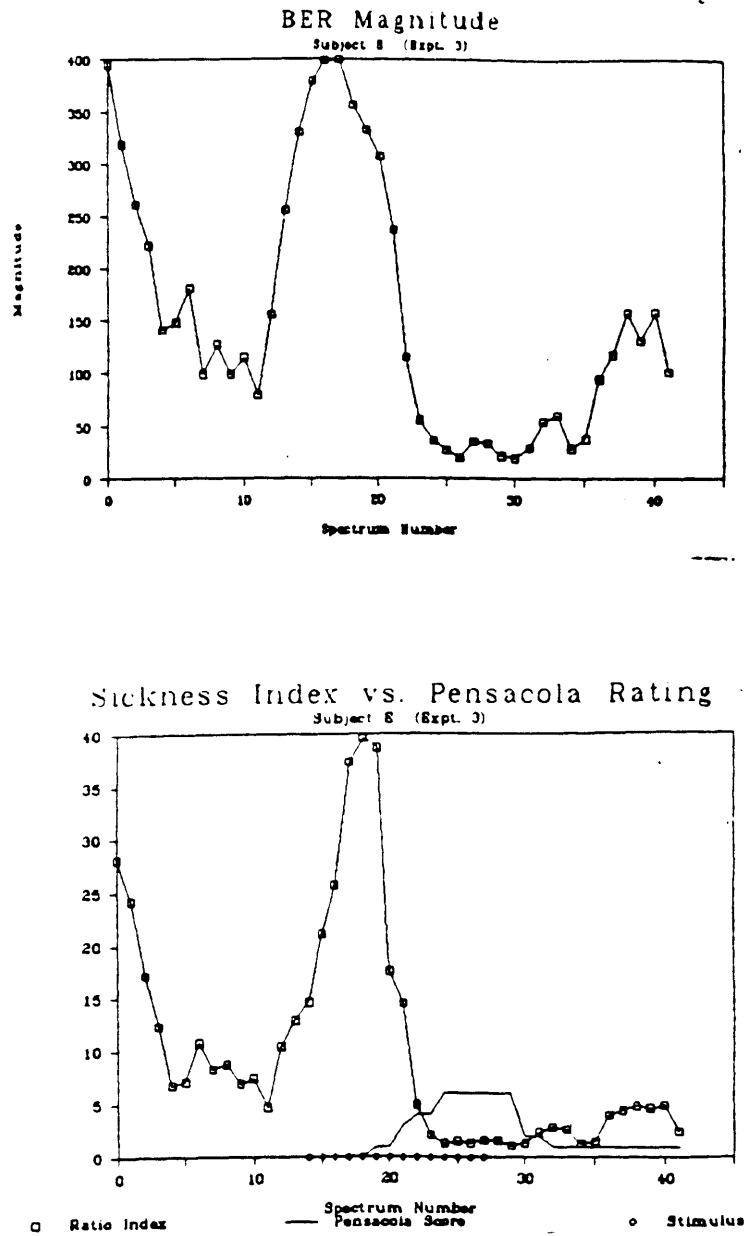


Figure 5.1: Correlation between BER and spectrum peak index.

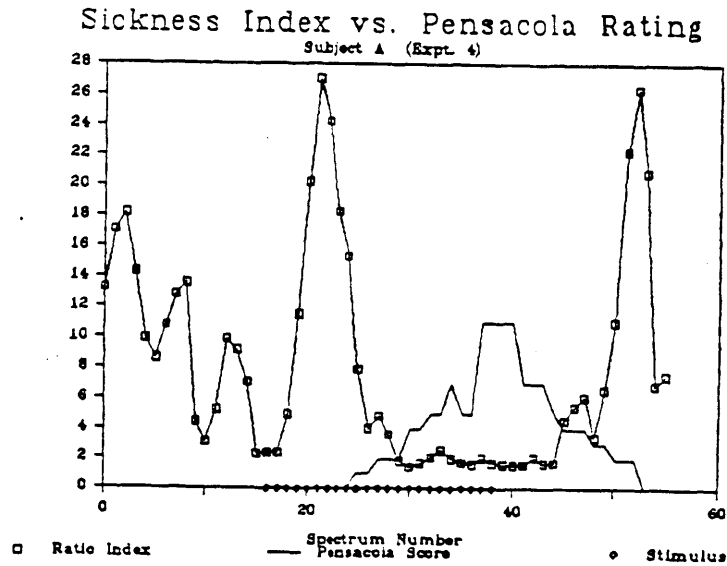
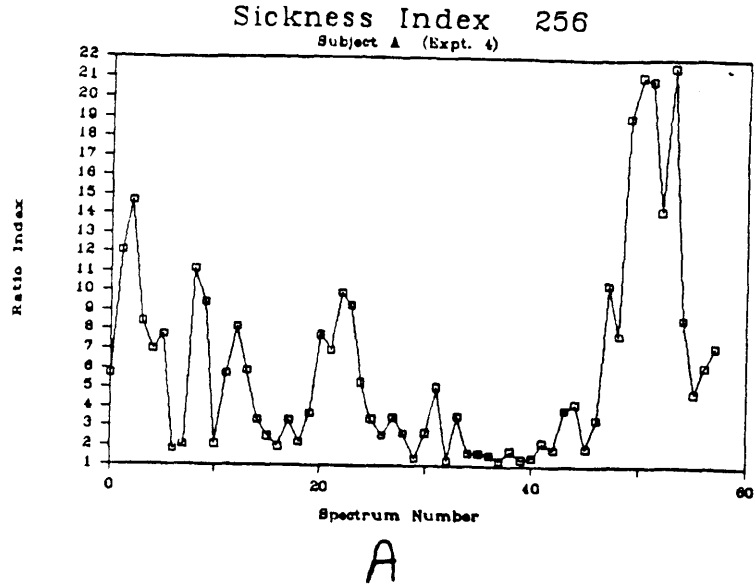


Figure 5.2: Spectrum peak index of same data set using different window length. A: 256 points (256 seconds). B: 512 points (512 seconds). $\Delta t=64$ seconds for both A and B. Spectrum numbers are equivalent in that the window centers on the same time value for both A and B.

However, this essentially cuts the frequency resolution in half (.0078 hz), and doubles the 'picket-fence effect' described in section 2.3.2. Difference (b) can also be explained by the disparity in window length. As discussed in section 2.3.4, a 512 point window with a 64 point increment between successive windows will have twice the interpolative effect as a 256 point window with the same increment. As a result, the change in magnitude of a specific frequency component from one spectrum to the next will be more gradual in the 512 point case. This will naturally yield a more smoothly fluctuating index measure.

Figure 5.3 shows the distribution of spectrum peak index values computed in all 24 experiments as the stomach sensation threshold is increased. The distributions in all cases are roughly Poisson. Notice that as the sensation cutoff approaches NSA II, less of the higher numbered indices remain. The mean spectrum peak index computed during reports of any symptoms (Part A of Figure 5.3) is 4.2. The mean steadily decreases to a value of 2.1 for reports of Nausea II or worse (Part E of Figure 5.3). This trend shows that a low index is indicative of motion sickness. Figure 5.4 shows the distribution of indices in resting, unstimulated subjects. Values appear more evenly distributed (mean = 10.1), but 23.4% of the indices are at 3 and below.

5.2 Running Average Method Applied to the Spectrum Peak Index

The "signature" of the sick state appeared to be when the spectrum peak index decreased and remained low. During motion sickness, the spectrum peak index will typically settle at a low value (1-3) and deviate only slightly from that value for a protracted length of time (at least 3 mins). To distinguish between any occasional drops in the peak index in resting individuals and the more important *prolonged* decreases that occur in motion sick subjects, a *running average* can be taken of the spectrum peak index over time. As indicated in Figure 5.5, a running average measurement will reflect decreases in the spec-

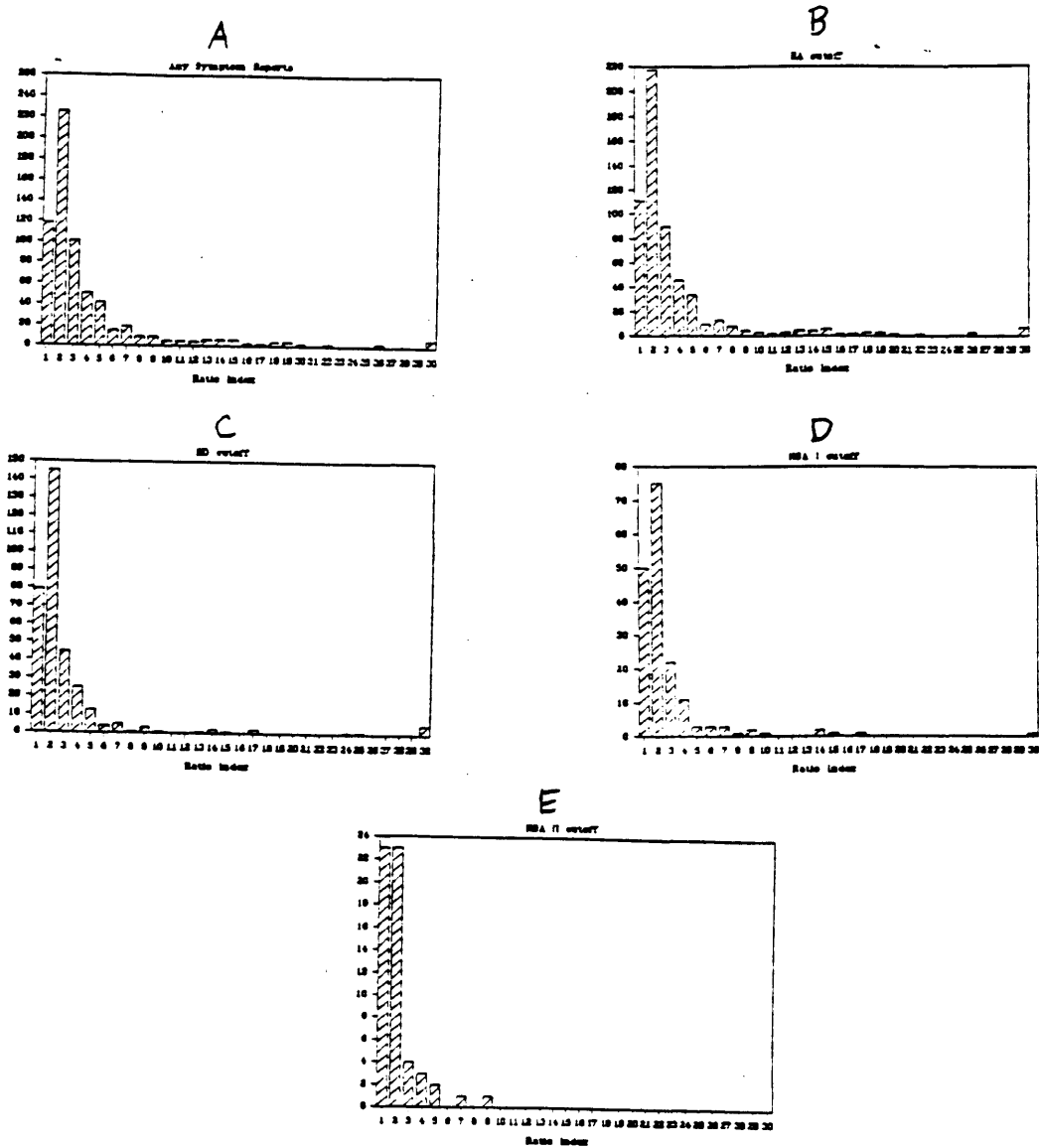


Figure 5.3: Spectrum peak index distribution for different levels of stomach sensation. A: Any symptom reports. B: Epigastric Awareness or worse. C: Epigastric Discomfort or worse. D: Nausea I or worse. E: Nausea II.

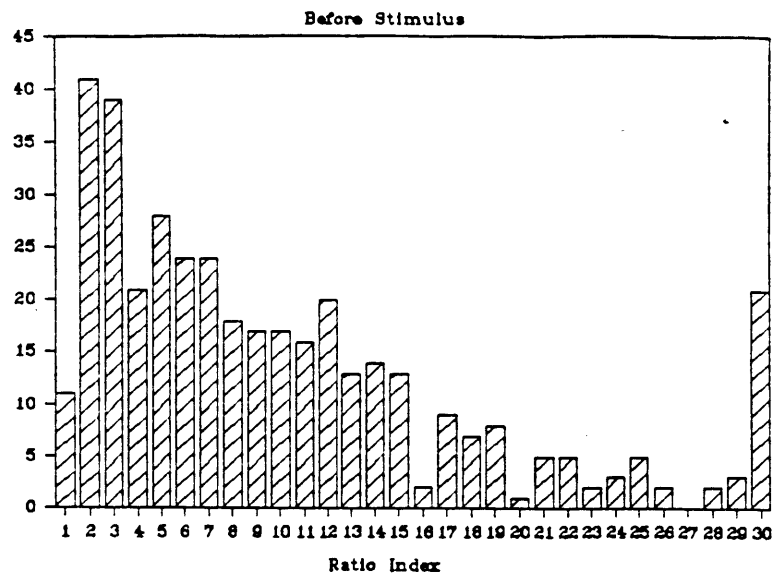


Figure 5.4: Distribution of spectrum peak index in resting subjects.

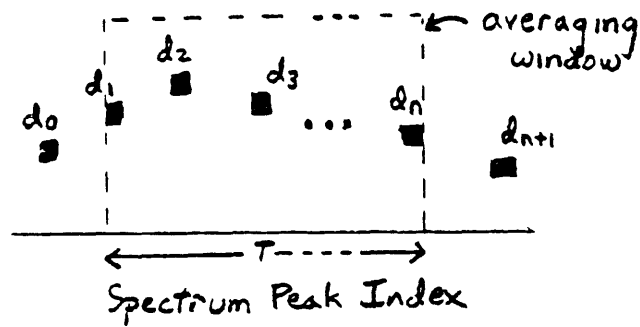
trum peak index, the time duration of the decrease, and the stability of the decrease. The figure also shows that each of these three attributes are directly associated with a specific parameter (m , T , v) used in the running average method.

Using these three parameters described in the figure, the goal was to develop simple threshold criteria applied to the running average which, when satisfied, would indicate a strong possibility that the subject was sick. Thus, the resulting detection procedure is straightforward:

- Compute the average and variance of T successive indices (the present one and the $T-1$ which came immediately before).
- If the average is below m and the variance is below v , then a 'sick' state is predicted.

A more linear measurement than v is the standard deviation (sd), simply the square root of v . Since a spectrum and, subsequently, a peak index, is computed approximately every minute, T may refer to time in minutes or, alternatively, number of spectrum peak indices.

Running Average of Spectrum Peak Index



Parameter	Description	Primarily Measures
T	Length of Averaging window	Duration of decrease in spectrum peak index
$m = \frac{d_1 + d_2 + \dots + d_n}{n}$	Mean of data points within averaging window	Decrease in spectrum peak index
$v = \frac{1}{n} \sum_{k=1}^n (d_k - m)^2$	Variance of data points within averaging window	Stability of decrease in spectrum peak index

Figure 5.5: Important parameters of running averaging method and what they measure.

Thus, three running average parameters must be determined:

1. Averaging length T .
2. Mean threshold m .
3. Standard deviation threshold sd .

The parameters T , m , and sd were optimized to fit the results of these experiments. The optimization approach was based primarily on the trade-off between detection time prior to sickness endpoint and false positives, (false indications of a symptomatic state). Clearly, a minimum number of false positives is desired, but not at the expense of late detection of the sickness endpoint. The effect of the above parameters on the two optimizing criteria are as follows: (1) increasing the number of indices averaged, T , will increase the resulting mean and variance, leading to fewer false positives but also decreased detection time prior to sickness endpoint; (2) lowering the thresholds m and sd will have the same effect as in part (1). Note also that as the number of indices averaged increases, the amount of delay introduced into the detection time goes up. False negatives (not indicating 'sick' when the subject is sick) are inversely related to false positives and are essentially included in detection time considerations since an early detection time implies that a large portion of the subject's 'sick' time was, indeed, indicated as such.

Figure 5.6 graphically illustrates the compromises involved when optimizing the parameters. Experiment 4, Subject B was not included in the analysis because of the unique general instability of the peak index in that particular session. The abscissa (Cum. Detection Time) is the sum total of all the individual detection times for each of the 23 trials, where detection time is the number of elapsed minutes between the moment when a 'sick' state is indicated and the actual occurrence of the sickness, or experimental, endpoint (represented by '0' on the x-axis. Figure 5.6 shows that as m and sd are decreased, both false positives and detection time decreases. Note that changes in sd threshold have

Comparison of Averaging Times

(n = 23)

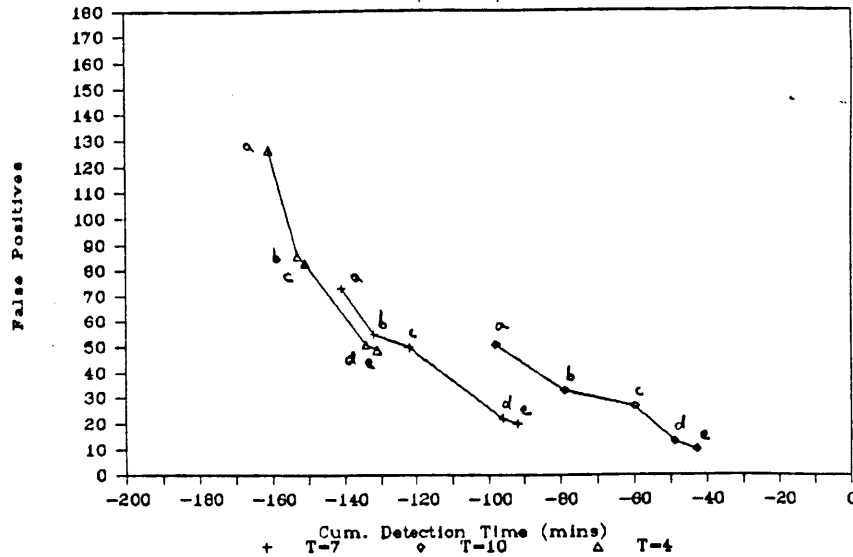


Figure 5.6: Cumulative Detection Time vs. Number of False Positives for varying averaging length T , mean threshold (m), and standard deviation threshold (sd). (a) $m=5, sd=3$; (b) $m=4, sd=3$; (c) $m=4, sd=2$; (d) $m=3, sd=2$; (e) $m=3, sd=1.5$.

less influence on performance as T goes from 10 to 4. This is because the variance of the calculated variance decreases as the number of points averaged decreases. Threshold values significantly above or below those listed in the figure are not considered because, for low thresholds, some episodes of motion sickness are completely missed, and for high thresholds, the sequence of peak indices for the entire experimental run are interpreted as a 'sick' state. Figure 5.7 shows a similar graph for $T=3$ and $T=4$.

Figure 5.8 illustrates the loss in performance as T is decreased to values below 3. Specifically, changes in sd have absolutely no impact on performance, and the number of false positives becomes inordinately high for a given threshold m . Clearly, optimum parameter values will exist at points toward the lower left corner of the graphs in the three previous figures. In this section, cumulative detection time is maximized and number of false positives minimized. If an 'optimization area' is specified in these graphs, the square region

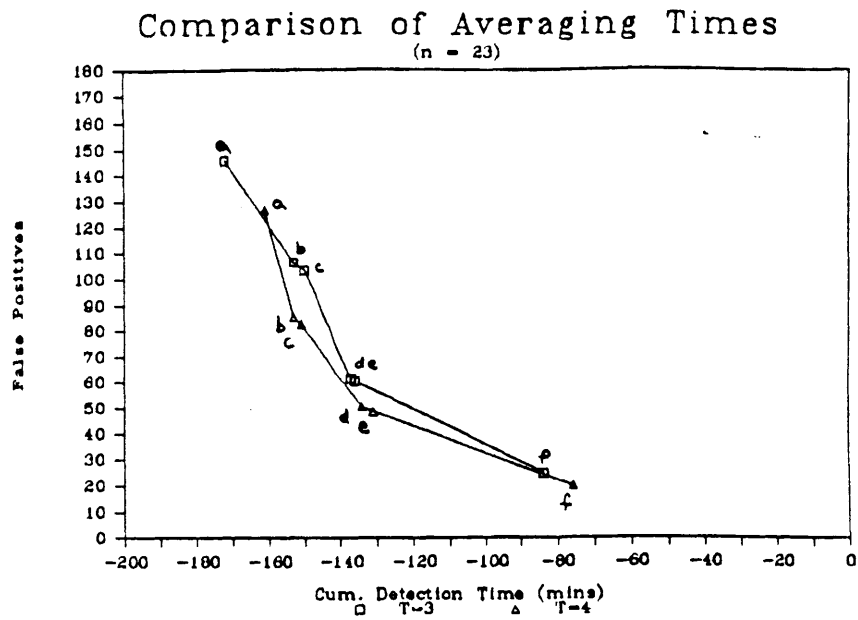


Figure 5.7: Similar letter codes as in previous Figure except that for (f) $m=2, sd=1.5$.

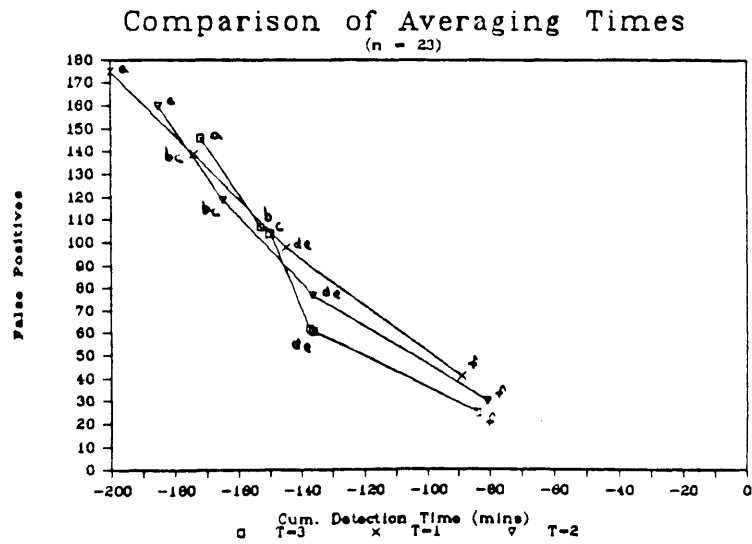


Figure 5.8: Same letter codes as in previous two Figures.

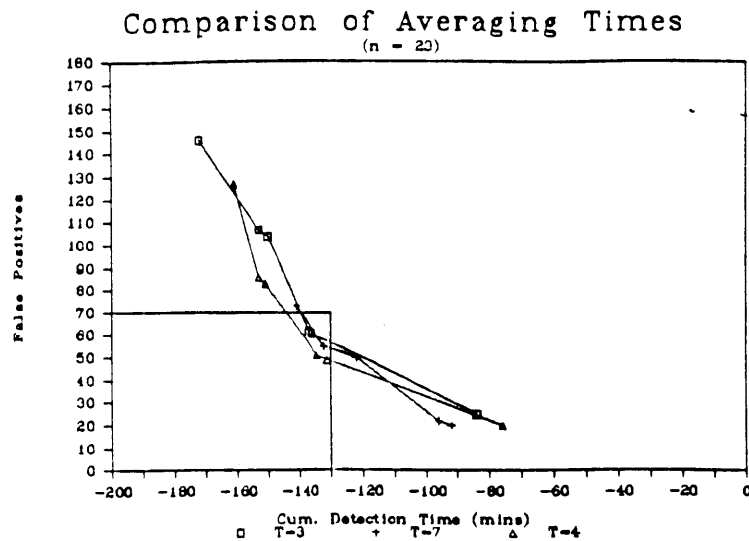


Figure 5.9: Graph showing 'optimization area' for various averaging times, mean and standard deviation thresholds.

indicated in Figure 5.9 results. Comparison of the parameters associated with the points in this square region has led to a more detailed look at the detection times and occurrence of false positives for each specific trial. The table in Figure 5.10 shows results from an analysis of 23 trials. The left column shows the specified parameter values. The center column is the total number of trials in which at least one false positive occurred, and the right column is the total number of trials in which the detection time was either 1 minute before the sickness endpoint or later.

Figure 5.11 graphs the tabular data for the parameter values $m=3$ and $sd=1.5$. If heavy emphasis is placed on the early detection of sick subjects, simple visual analysis Figures 5.10 and 5.11 reveals that 'optimum' parameters would be $T=4$, $m=3$, $sd=1.5$. Under these conditions, the minimum number of trials, 2, with detection times at -1 mins or greater is achieved. (0 mins = sickness endpoint.) Figure 5.11 shows that of the three possible parameter conditions which attain this minimum value of 2, the $T=4$ situation

Parameter Values			Total Number of Trials with...	
T	m	sd	False Positives	Detection Time ≥ 1
7	4	2	12	6
2	3	1.5	14	2
3	3	1.5	13	2
4	3	1.5	11	2
5	3	1.5	10	4
6	3	1.5	8	5
7	3	1.5	7	7
10	3	1.5	4	13
3	2	1.5	6	5
4	2	1.5	4	7

Figure 5.10: Table showing effect of various values of T , m , and sd on False Positives and Detection Time.

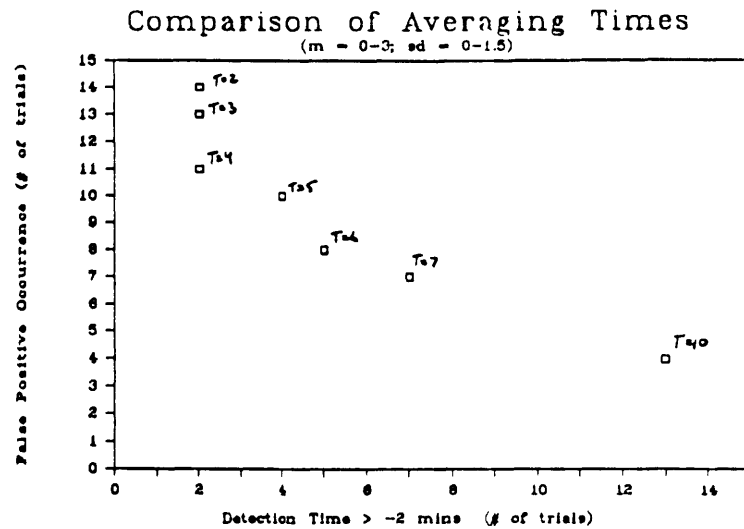


Figure 5.11: Graphical representation of data presented in Table 1 for $m = 3$ and $sd = 1.5$.

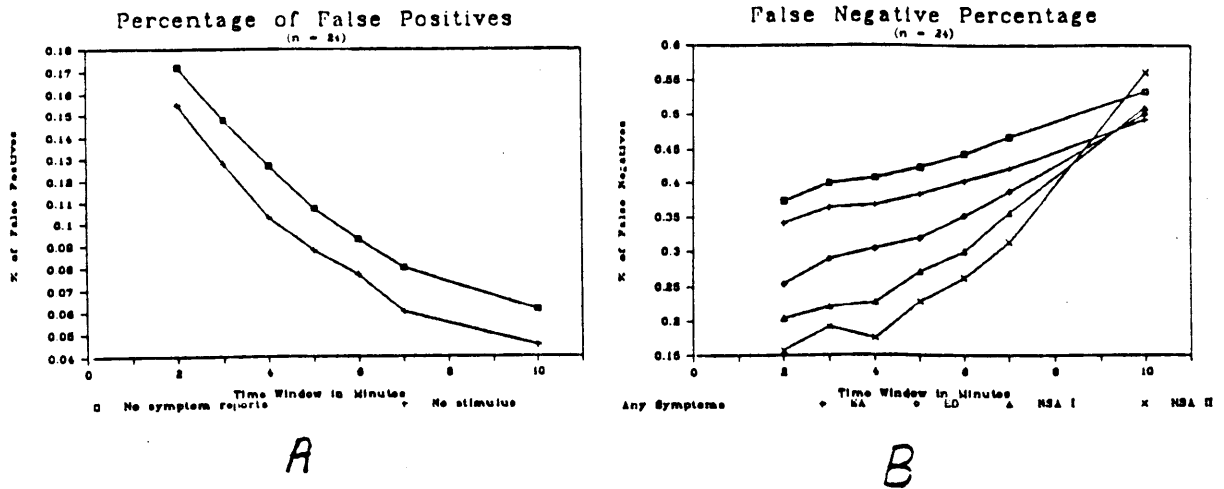


Figure 5.12: Percentage of False Positives and False Negatives where $m=3$, $sd=1.5$. A: Percentage of False Positives. B: Percentage of False Negatives. EA: Epigastric Awareness, ED: Epigastric Distress, NSA I: Nausea I, NSA II: Nausea II

results in the fewest number of trials, 11, in which at least one false positive is detected. It must be stressed that the optimal parameter values mentioned above were deduced by detailed analysis of data from 23 experimental trials. Clearly, more results need to be acquired to either confirm or refute the optimality of these parameter values.

A comprehensive look at the percentages of false positives and false negatives for varying time averaging lengths is provided in Figure 5.12. The parameters $m=3$, $sd=1.5$, remain constant as T varies from 2 to 10. As expected, false positives decrease as averaging time increases and the inverse occurs for false negatives. As stated above, the larger averaging length yields a more conservative decision because the resultant mean and variance for a set

length yields a more conservative decision because the resultant mean and variance for a set of 10 points is typically greater than that for a set of fewer points. The lower curve in the graph for False Positives involves only those peak indices computed during the preliminary resting period (no stimulus). The upper curve shows the increases involved when adding in those indices measured from a subject experiencing chair rotation but reporting *no* symptoms. False negatives occur when the running average algorithm indicates 'not sick' while the subject is actually reporting symptoms. Thus, false negatives can be classified according to the severity of the symptom reports. Figure 5.12 shows the behavior of false negatives as the criterion levels of stomach symptoms are worsened. By $T=10$, the percentage of false negatives has converged to about 50%. It should be mentioned that the total number of peak indices used in the percentage calculations necessarily decrease as the severity of the symptoms increases. As expected, the subjects spent a small amount of time at the Nausea II level as compared to an epigastric awareness (EA) level or worse. For these data, however, the graph shows that fewer false negatives or misses do occur in more extreme cases of motion sickness stress, emphasizing the reliability of a marked decrease in spectrum peak index by the subject's sickness endpoint.

Figure 5.13 displays the results of applying the running average technique to the spectrum peak indices of four separate sessions using the optimizing parameters $T=4$, $m=3$, $sd=1.5$. As shown in Parts A, B, and C, the detecting algorithm works rather well in indicating a 'sick' state prior to the subject's experimental endpoint. Note that, since $T=4$, the running average does not begin until spectrum number 3 is computed. Part D shows the detection scheme as it processes the information acquired in Expt. 4 of Subject B, which was excluded in the above analysis because of poor quality. This trial was the possible 'sleep dependent' response discussed in the last paragraph of Chapter 4. Clearly, the binary detecting algorithm indicates a 'sick' state most of the time. Thus, the running average method may also aid in diagnosing irregular or abnormal behavior in the input

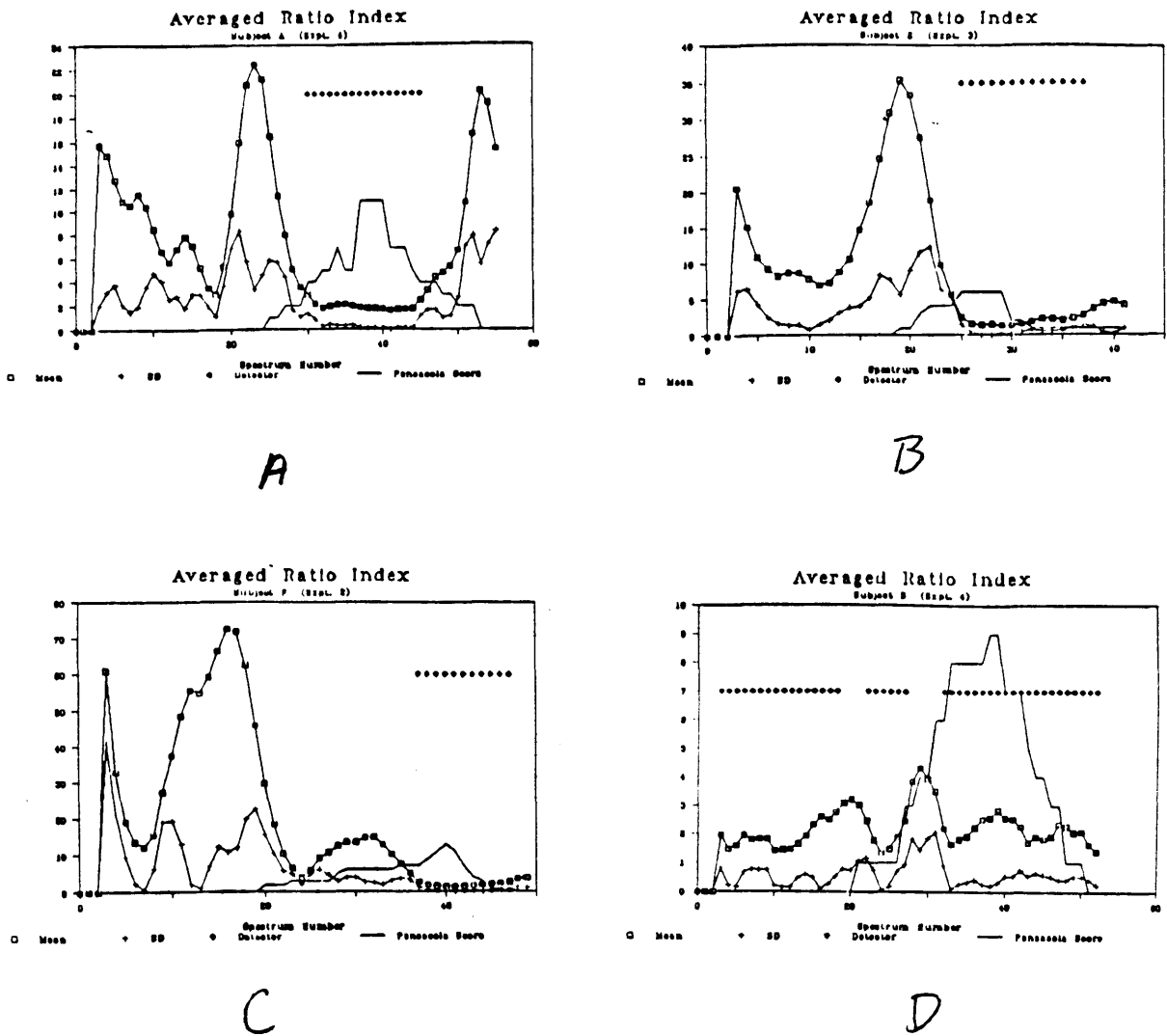


Figure 5.13: Result of detection algorithm on four experimental sessions. A: Subject A (Expt.4). B: Subject E (Expt.3). C: Subject F (Expt.2). D: Subject B (Expt.4).

EKG signal.

5.3 - The Usefulness of Tachygastrias in Motion Sickness Diagnosis

In 1985, Stern, Koch, et.al. recorded EKG's from 21 healthy volunteers exposed to a rotating drum stimulus designed to elicit motion sickness symptoms via illusory self-motion or circularvection[56]. Visual analysis of the resulting data showed a shift of the EKG frequency from 3 cpm to 5-8 cpm in all 14 subjects who developed symptoms. In 6 of 7 asymptomatic subjects, the 3 cpm EKG pattern was unchanged duringvection. In conclusion, Stern states that their "findings clearly link tachygastria and symptoms of motion sickness induced byvection." In 1987, Stern, et.al. performed a group of similar experiments on 15 subjects and analyzed the EKG's using running spectrum analysis[57]. Again, it was found that 10 subjects who reported motion sickness symptoms showed a shift of their dominant frequency from 3 cpm to 4-9 cpm. The 5 subjects who reported no symptoms showed a continuation of normal 3 cpm activity. The hypothesis was upheld that "a close correspondence" exists over time between tachygastria and reports of symptoms of motion sickness. Stern claims that his 1987 study "confirms and extends" the previous 1985 results "linking tachygastria and symptoms of motion sickness."

In both papers, no statement is made as to the strength or reliability of this link. Do tachygastrias occur invariably during motion sickness reports? With one exception, Stern's results seem to imply that they do. Is there any relationship between the *severity* of symptom reports and frequency activity of the EKG? Are the magnitude or appearance of tachygastrias affected by different electrode placements, recording procedures, or running spectral analysis parameters? In essence, what is this "link" between the information perceived by the experimenter and the underlying myoelectric activity of gastric smooth muscle?

To unequivocally define this link, standardization is needed in two areas of EGG research: (1) recording procedure, and (2) terminology. Stern, et.al., have made a first step in area (2) by offering a rough definition of tachygastric activity in 1987: "Tachygastric activity was operationally defined as activity between 4 and 9 cycles/min in the absence of 3 cycles/min activity." However, this definition, somewhat tailored to the specific experimental results observed by Stern, raises more terminological debate. Namely, does "absence of 3 cpm activity" imply absolute zero magnitude at that particular frequency component in the power spectrum? The questions posed here and above are truly rhetorical in that clear answers have yet to be discovered, but they do stress the need for a common frame of reference from which to communicate results of EGG related work.

The data presented here show that different EGG methods *do* yield different results. Essentially, all subjects in all trials reported signs of moderate or severe motion sickness based on magnitude estimations of overall discomfort. During only 7 motion sick periods in the 24 trials, spectral components in the 4-11 cpm frequency range reached magnitude levels which could be visually described as comparable to that of the resting EGG. In another seven trials, frequency component magnitudes in this "tachygastric" range were small in comparison with that of the resting EGG. In 9 trials, moderate or severe motion sickness was accompanied solely by a decrease in magnitude of the 3 cpm BER. The remaining trial was unproductive possibly because of a sleep modulated autonomic effect on the stability of the EGG. Just as in the work of Stern, et.al., results from these experiments constrained the classification of frequency activity during motion sickness. We used the same definition for tachygastric activity as that applied by Stern (excluding "absence of 3 cpm activity"), but in this study, it was useful to define two types, low-level and high-level. Tachygastric activity did not always occur when motion sickness symptoms were reported; however, they did seem to be correlated with more severe forms of motion sickness in two subjects, and as a typical response characteristic for one subject.

What proved to be a constant response in all trials (including a somewhat marginal response in the “sleep” influenced record) was the decrease in magnitude of the BER. This component rarely disappeared, however. The BER, defined as the dominant spectral peak in the range .04 hz-.06 hz, remained at its pre-stimulus magnitude level during 6 of the 7 high-level tachygastrias. Otherwise, during motion sickness the BER magnitude remained low as compared to the resting level magnitude. The issue was then to clearly define quantitative criteria by which a reasonably confident assessment could be made that the BER was indeed “low” for a certain period of time. The result is the *Spectrum Peak Index* defined above. Although the Peak Index detects broad-band tachygastric activity, it is primarily sensitive to changes in the BER magnitude. Also, by the reasoning presented in Section 2.3.4, analysis of spectral magnitude changes in *dominant* rhythm components leads to earlier detection of frequency disturbances in the input signal than does numerical analysis of amplitude changes at the other frequencies. The results of these experiments indicate that the consistent response is the decrease in BER, and a more diagnostic measure of the gastric electrical response during motion sickness is derived from information about BER behavior rather than tachygastric activity.

5.4 EGG Recording and Processing Methods

A standardized EGG recording procedure may have alleviated the differences between the results obtained by Stern, et.al., and the observations of this study. The interface between the cellular activity of the stomach and the statistical analyses of the experimenter (what he “sees”) is the specific hardware and software that is imposed on the input data. That the results from different EGG studies do not agree is not surprising. References to Stern’s set-up are used to illustrate some of the more important processing issues.

Electrode position will affect the magnitude of the frequency components. As discussed in Volkers study in canines[74], it appears that all electrode configurations will ‘see’ the

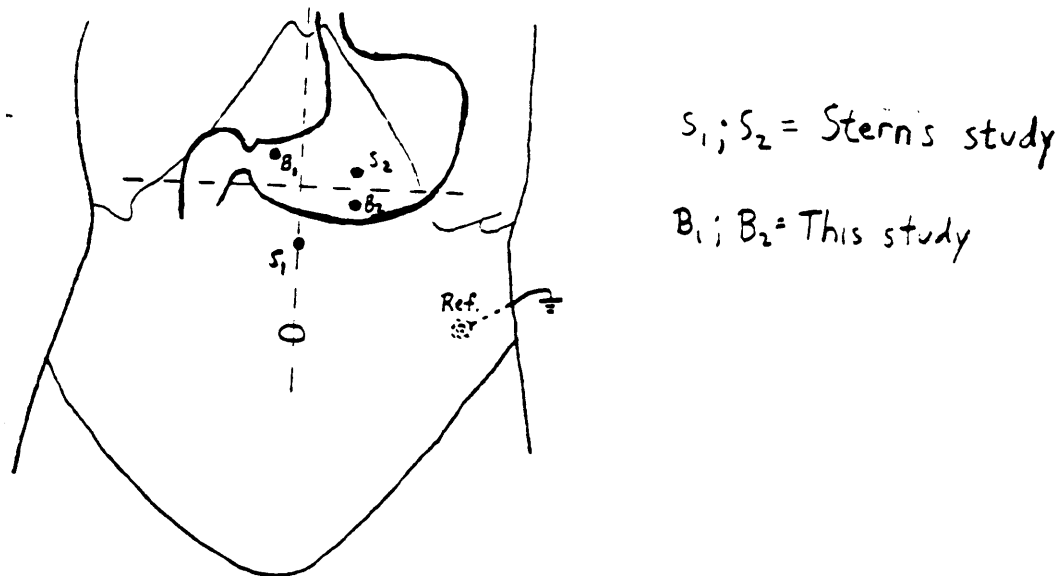


Figure 5.14: Electrode positions in Stern's study and this study.

activity of the antrum, where gastric emptying occurs. However, the amplitude of the EGG varies with the configuration. Recordings of abdominal potentials from humans show that a "best" electrode configuration can be determined for a given individual by visual inspection[70]. Figure 5.14 shows the difference between Stern's electrode positions and those used in this study. Until a model of stomach activity is more succinctly defined, the effect of specific electrode positions on the recorded EGG cannot be explicitly quantified.

The stimulus used to induce motion sickness is also different in the two studies. The Coriolis cross-coupled effect in a rotating environment has been verified as a potent stimulus in motion sickness experiments. Circularvection is a less effective stimulus in that theoretically, after a few time constants related to cupula return, there exists no real visual-vestibular mismatch as claimed in Stern's 1985 paper. Symptom onset may be due more to the flip-flopping between the perceptions of self-rotation and surround-rotation. That Stern was able to induce only slight to moderate symptoms in only $\frac{2}{3}$ of his subjects is

consistent with the mild nature of the imposed stimulus. In this study, head movements executed on a rotating chair were sufficient to elicit moderate or severe sickness in all trials. Stern claims that the advantage of a rotating drum stimulus is that the subject remains stationary throughout the experiment, minimizing the effect of motion artifact and injury to the subject. Preliminary analysis of the effect of head movements on the EGG showed that, as long as the center of rotation of the head was constrained to the neck area, motion artifact in the simultaneously recorded EGG was insignificant.

In the literature, the effect of band-pass filtering on the input EGG is typically overlooked. In his '87 study, Stern uses a low-pass filter (order unspecified) with cutoff frequency $f_{lowpass}=0.08 \text{ hz} \approx 4.8 \text{ cpm}$, and a Beckman R611 recorder with a time constant of 10 seconds, which translates into a high-pass frequency cutoff of $.0159 \text{ hz} \approx 1 \text{ cpm}$. If a typical motion artifact created by abdominal movements is modeled as a step input, Figure 5.15 shows both the time domain and frequency domain results if this input is processed by a band-pass filter with single pole behavior at both sides of the band. As shown in the figure, the dominant time constant in the step response is associated with the high-pass side of the filter. The spectrum of this particular response shows a peak around $f_{highpass}$. Thus, unless reasonable stability of the raw input EGG is confirmed, there may be some corruption of the computed spectrum due to the inherent response of the band-pass filter. Stern does not address the possibility of motion artifacts in his subjects, because they are assumed stationary throughout the experiment. However, any quick abdominal movement (a rapid inhalation or exhalation, hiccup, or burp) may cause a step change in the input signal, which might necessarily be misinterpreted during running spectrum analysis. In this study, the auto-balancing circuitry of the DRI pre-amp circumvented the need for high-pass filtering. Also, since motion artifacts are usually concentrated near dc, frequencies below .04 hz were not considered in any visual or quantitative analyses.

A more obvious effect of Stern's filtering technique is the very low cutoff frequency of

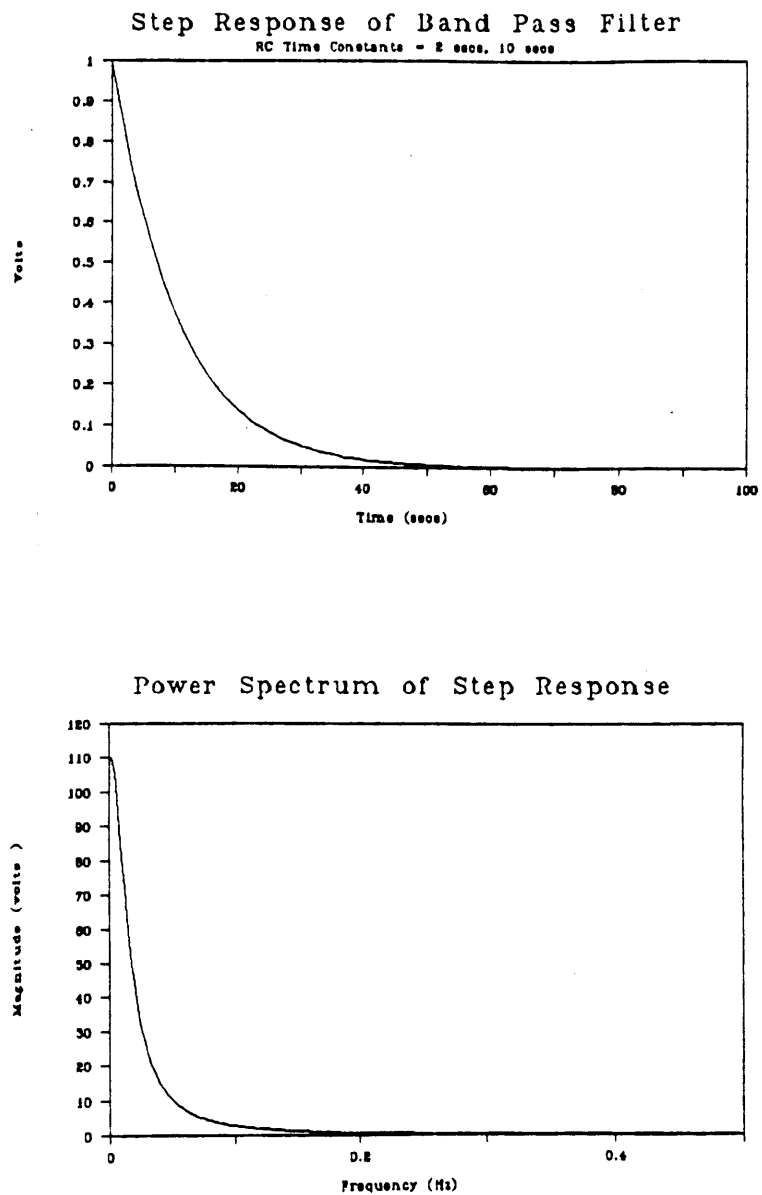


Figure 5.15: Output from single pole band-pass filter given a motion artifact input modeled as a step. $f_{lowpass}=4.8$ cpm. $f_{highpass}=1$ cpm.

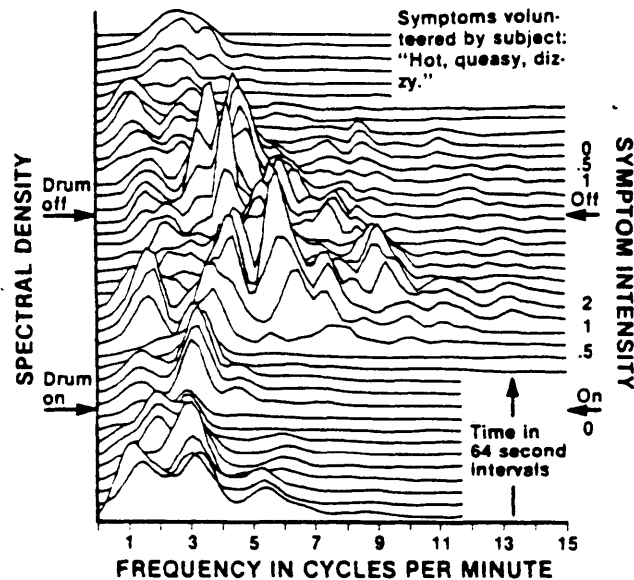


Figure 5.16: Waterfall plot of running spectrum analysis (from Stern, et. al., 1987).

4.8 cpm. The paper reports on and displays frequencies in the range well above 4.8 cpm, up to ~ 10 cpm. However, Hamilton[21] states in a paper on human EGG's that "we feel that this is not a great problem since the amplitude of signals with rates up to 10 cpm would be diminished by no more than 50% in size." In time series analysis of EGG's, this attenuation may not be important, but in the waterfall plots displayed in Stern's paper (see Figure 5.16), the displayed information may be somewhat misleading. Namely, if the frequency components around 10 cpm are increased by a factor of 4 (2^2 because of the power law), the waterfall plot would have a different shape than the one shown.

Another common signal processing method used by Stern was that of averaging adjacent components in the resulting spectra, as illustrated in Figure 5.17. Stern averaged 5 adjacent spectral components within a bandwidth of 0.0195 Hz, resulting in a loss of resolution in the frequency domain. Also, the effect of this smoothing function is to taper or moderate the high peaks and increase the low valleys of the original spectra. As a result, the visual display

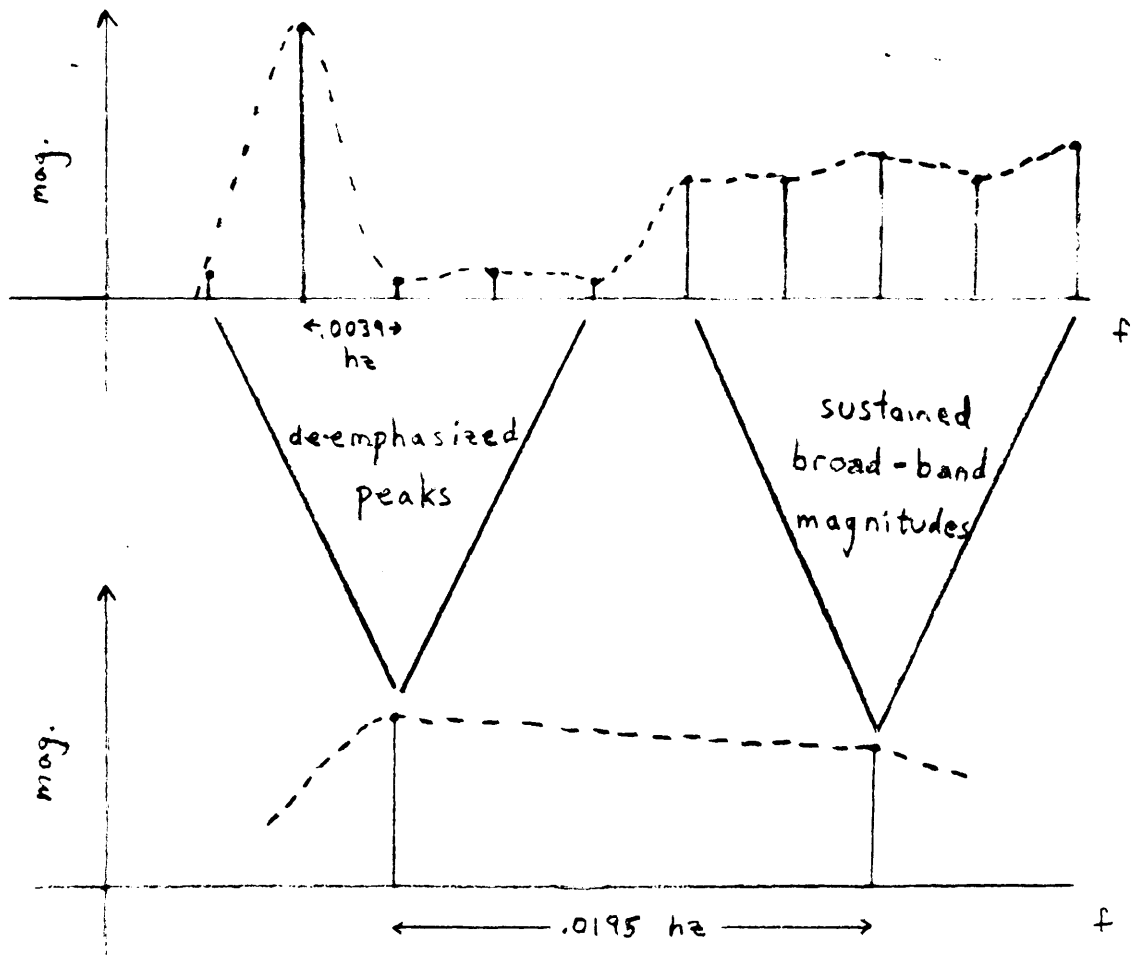


Figure 5.17: Effect of averaging 5 adjacent frequency components.

of information shown in Figure 5.16 may be somewhat misleading in its representation of the actual spectra derived. Sharp, high amplitudes from the original computations are shown here as smoother and wider, and low-level broad band magnitudes are boosted so that differences in peak amplitude values is significantly less. The net effect would be to display more high-level tachygastrias than had actually occurred, which may offer a partial explanation for the disparity between Stern's observations and those presented here.

5.5 Summary

Six healthy volunteers each participated in 5 repetitions of a standard motion sickness experiment using a rotating chair. Subjects showing a prominent resting BER were instructed to make head movements during chair rotation to induce motion sickness via a Coriolis cross-coupled stimulus to the semicircular canals. A velocity staircase stimulus was used. Severe or moderate motion sickness was elicited in all trials. Running spectrum analysis of the recorded EGG signals from all trials show that a consistent and prolonged decrease in BER magnitude occurs during reports of motion sickness. A dimensionless Spectrum Peak Index was proposed that measures the relative height of the most prominent spectral peaks. This Peak Index reflects decreases in the BER magnitude relative to broad-band increases in the frequency range above the BER (tachygastrias).

Because a sick state appeared to be characterized by a prolonged consistent decrease in the spectrum peak index, a running average of these peak indices was calculated to obtain a comprehensive measure of the simple decrease in amplitude, *and* the duration and stability of that decrease. Important parameters used in the running average method are (1) T , the duration of the averaging window, (2) m , the mean of data points within the averaging window, and (3) sd , the standard deviation of data points within the averaging window. Low and stable peak index values during the onset of motion sickness are reflected in a decrease of both the mean and standard deviation of the computed running average of duration T . Thus, to obtain a diagnostic binary (sick/not sick) predictor for the occurrence of motion sickness, threshold criteria were imposed on resulting mean and standard deviation values such that, for a given window duration T , if the computed mean was less than some set value, m_{thresh} , *and* the computed standard deviation was less than some predetermined value, sd_{thresh} , then a 'sick' state was predicted.

For the specific experimental data described in this report, optimum values of T , m_{thresh} ,

and sd_{thresh} were determined based on a minimization of false positives and a maximization of detection time prior to the end of the experiment. The resulting values were a time window length (T) of 4 mins, a mean threshold value (m_{thresh}) of 3, and a standard deviation threshold value (sd_{thresh}) of 1.5. Of the 24 test sessions reported here, these parameter values predicted sickness onset at least 1 minute before the sickness endpoint in 22 of 24 sessions. In resting subjects, false positives (false indications of a symptomatic state) occurred $\sim 10\%$ of the time across all test sessions. False negatives (false indications of an asymptomatic state) occurred $\sim 17\%$ of the time in subjects reporting moderate to severe nausea. The running average method as applied to calculated spectrum peak indices serves well as a first-order indicator of motion sickness, although its reliability, as expressed in the statistics above, is not entirely foolproof. Further evaluation of this method is required to confirm its usefulness as a prediction scheme for motion sickness symptoms.

Although EGG monitoring offers some insight into changes in gastric electrical activity during motion sickness, the true diagnostic value afforded by these measurements has yet to be determined. The usefulness of EGG in clinical situations has not been verified, as indicated by Geldof's appraisal that, based on some set criteria, only half of the patients with unexplained nausea and vomiting showed any "abnormal" EGG's[17]. The motion sickness criteria developed above attempted to encompass all the characteristic EGG responses showed by each of the subjects, but inherent variability in the EGG, as in any physiological measurement, makes discovery of a completely reliable and robust motion sickness indicator extremely difficult. Sources of variability in monitoring EGG's are widespread. Electrode position may be the single biggest factor in determining the strength and frequency content of the signal. Different electrode configurations may enhance detection of tachygastrias, at the expense of decreased BER magnitude. A major step in EGG research would be to unravel the underlying gastric physiological activity to the point of developing a comprehensive electrical model of the stomach. Then, after locating the stomach with

fluoroscopy or ultrasound, what is "seen" by a given pair of electrodes can be verified. A more immediate need is standardization of the EGG recording and processing methods so that more consistent results may be obtained among research groups. In this way, different findings may be correlated or compared and the potential of EGG recording may be fully realized.

Appendix A

Motion Sickness Questionnaire, Pre-Session Questionnaire, Magnitude Estimation Instructions, and Informed Consent Statement

MOTION SICKNESS QUESTIONNAIRE

INSTRUCTIONS

This questionnaire is designed to find out: if there are factors in your medical history which we ought to know about when we interpret the results of our experiments; how susceptible to motion sickness you are; and what sorts of motion have been most effective in causing your motion sickness. The form is divided into three parts. Section A deals with your medical history, section B is concerned with your childhood experiences with motion sickness, that is prior to the age of 12, and section C deals with your experience with motion sickness since the age of 12.

Motion sickness susceptibility is revealed by a wide variety of subjective symptoms and objective signs, and may be experienced over a wide range of severity. Common symptoms are stomach discomfort, nausea, vomiting, pallor, sweating. These symptoms are often accompanied by drowsiness, increased salivation, a feeling of warmth (not associated with exercise), and/or headache.

Your replies to all questions will be treated in the strictest confidence.

Motion Sickness Questionnaire

113

SECTION A

SUBJECT CODE: AF DATE: _____ AGE: _____ (years)

GENDER: _____ WEIGHT: _____ (lbs) HEIGHT: _____ (inches)

OCCUPATION: _____ RIGHT OR LEFT HANDED: _____

If your answer to any of the following questions is yes, please give a brief description. Use reverse side, if necessary.

1. Do you have any vision defects requiring the use of corrective lenses?
2. Do you have any eye muscle defects?
3. Do you have any other vision defects?
4. Have you ever experienced persistent noises in your ears continuing for more than several moments?
5. Do you have a hearing defect?
6. Have you ever been unconscious for more than 5 minutes other than during surgical anesthesia? If so, when and for how long. Briefly describe the circumstances.
7. Have you ever sustained a head injury? If so, describe and indicate the date.
8. Have you ever had persistent stomach trouble or an ulcer?
9. Have you ever experienced repeated episodes of disorientation or vertigo while not in a moving vehicle?
10. Have you experienced motion sickness before?
11. If you have experienced motion sickness, how long does it usually take you to recover completely when the motion stimulus is removed?
12. When you experience motion sickness, what steps do you usually take to control it (other than using drugs or getting off the vehicle)?
13. Do you usually use drugs to control motion sickness? If so, which?
14. Do you experience any side effects, such as drowsiness, when you take an anti-motion sickness drug?
15. If you use an anti-motion sickness drug, do you usually take it before motion exposure or when you begin to feel sick?

SECTION B

All questions refer ONLY to your childhood experiences of motion sickness (if any), where childhood is defined as the period prior to 12 years of age. It is quite possible that you will have difficulty recalling childhood motion sickness; nevertheless, please try to answer the questions to the best of your ability.

Put your answers to question 1 in column 1 of the table below; your answers to question 2 in column 2, etc.

1. Indicate approximately how often you traveled as a passenger on each of the following vehicles (before age 12) by using the following numbers:

- 0 no experience
- 1 less than 5 trips
- 2 between 5 and 10 trips
- 3 more than 10 trips

Considering ONLY those types of transportation that you marked 1, 2, or 3 (i.e. those that you have traveled on as a passenger), go on to answer questions 2 and 3 below. Use the following letters to indicate the appropriate category of responses:

- N never S sometimes A always
- R rarely F frequently

2. How often did you feel sick while traveling, e.g. queasy or nauseated?

3. How often did you actually vomit while traveling?

	1	2	3
CARS			
BUSES OR COACHES			
TRAINS			
AIRLINERS			
AEROBATIC AIRCRAFT			
LIGHT AIRCRAFT			
SMALL OPEN BOATS			
BOATS WITH CABINS			
SHIPS			
GYM SWINGS			
MERRY GO ROUND			
ROLLER COASTER			
OTHER SITUATIONS WHICH MADE YOU MOTION SICK (SPECIFY TYPE)			
Use reverse side if needed.			

SECTION C

This section is concerned solely with your experience of motion sickness (and travel) SINCE the age of 12. Please answer the questions the way you did in Section B.

1. Indicate approximately how often you traveled as a passenger (not driver or pilot) on each of the following vehicles (since age 12) by using the following numbers:
- 0 no experience
 - 1 less than 5 trips
 - 2 between 5 and 10 trips
 - 3 more than 10 trips

Considering ONLY those types of transportation that you marked 1, 2, or 3 (i.e. those that you have traveled on as a passenger), go on to answer questions 2 and 3 below. Use the following letters to indicate the appropriate categories of responses:

- N never S sometimes A always
- R rarely F frequently

2. How often did you feel sick while traveling, e.g. queasy or nauseated?

3. How often did you actually vomit while traveling?

	1	2	3
CARS			
BUSES OR COACHES			
TRAINS			
AIRLINERS			
AEROBATIC AIRCRAFT			
LIGHT AIRCRAFT			
SMALL OPEN BOATS			
BOATS WITH CABINS			
SHIPS			
GYM SWINGS			
MERRY GO ROUND			
ROLLER COASTER			
OTHER SITUATIONS WHICH MADE YOU MOTION SICK (SPECIFY TYPE) Use reverse side if needed.			

4. In general, how would you grade your present susceptibility to motion sickness compared to others? (Circle one)

- TOTALLY IMMUNE LESS SUSCEPTIBLE THAN MOST AVERAGE
- MORE SUSCEPTIBLE THAN MOST EXTREMELY SUSCEPTIBLE

Pre-session Quiz Form

MOTION SICKNESS STUDIES
PRE-SESSION QUESTIONNAIRE

NAME _____
SESSION NUMBER _____
DATE _____

Responses evaluated during this test may be directly or indirectly influenced by factors addressed in the following questions. Please answer each to the best of your ability:

1. Are you in your usual state of physical fitness today? yes no
If no, explain: _____
2. Have you used any medication (e.g. aspirin, cold preparations, prescription or "recreational" drugs) during the past 24 hours? yes no
If yes, what type and how much? _____
3. How much alcohol have you consumed during the past 24 hours?
(No., kinds, & time of drinks) _____
4. How much coffee/tea/cola have you drunk during the past 24 hours?
(No., kinds, and time of drinks) _____
5. How much tobacco have you used during the past 12 hours?
(Number of cigarettes, cigars, pipefuls, etc.) _____
6. How many hours sleep did you get last night? _____ How does this
compare to your usual amount? much less less same more much more
7. How long has it been since your last meal? _____
What did you eat/drink? _____
Subjectively, how hungry do you feel now?
Very hungry slightly hungry normal slightly overfed very overfed
8. Have you felt any stomach awareness, stomach discomfort, or nausea during the
past 24 hours? (if so, when? why?) _____
9. Have you engaged in heavy exercise during the past 6 hours? yes no
10. Have you ever had any lung, heart or circulatory problems, or chronic
stomach trouble? _____

Post session symptom reports (if any):

1992 Magnitude Estimation Instructions

We are interested in studying the time course of motion sickness symptoms and signs created by periods of provocative stimulation. We will attach detectors with tape to your fingers and cheeks to measure the physical signs of motion sickness, such as changes of skin temperature and color, heart rate, and pulse. However, the most important symptoms of motion sickness are uniquely subjective sensations, and cannot be directly measured with an instrument. We therefore have to rely on verbal estimates which you make of the sensation intensity. These can be made using a method called "magnitude estimation". We will ask you to judge the intensity of a sensation by comparing it to a "standard" intensity which you have previously experienced. Involves asking the subject to judge the ratio of between the sensation being experienced and a "standard" intensity, previously presented. Subjects usually find verbal magnitude estimation to be an easy, natural method of reporting the intensity of sensation. Some subjects are at first skeptical of whether meaningful reports can be obtained with such a simple method - until they try it, and see how consistent their reports can be.

To give you the basic idea of magnitude estimation, try the following experiment, which involves estimating the length of a line:

Suppose we say the "standard" line looks like this:

and we call this line length "10".

Now suppose we present you with another line of a different length:

If the standard is 10, how long is this second line?

How accurate would you guess your answer is?

Now, how long is this line?

Finally, how about this line?

On this last one, if you find the line length ratio so small it is difficult to judge, it is better just to say that the sensation is: the line is "present", but too small to judge.

We will ask you to use this same magnitude estimation technique to report the intensity of your sensation in our motion sickness tests today. The only real difference is that we will be able to define the sensation standard level only once at the beginning of the experiment, and you will have to rely on your memory of this level throughout the rest of the experiment when making reports. We expect that it may take a little time before you feel your memory of the standard has stabilized, and you believe your reports are consistent.

Once you begin to make head movements at the start of the experiment, after some time (depending on your susceptibility) you will begin to experience symptoms, which may include stomach awareness or discomfort, nausea, sweating, drowsiness, salivation, headache, and dizziness. We find most people are familiar with

nausea, which can be defined as the unpleasant sensation, usually referred to the stomach, chest, or throat, which at very high levels may eventually be associated with vomiting. Nausea may be due to a variety of causes, such as motion, fever, food poisoning, fear, etc.) The various symptoms may contribute towards your overall discomfort in unequal degrees; e.g. the sensation of nausea may bother you more than the sensation of sweating.

In this experiment today, we want you to use the magnitude estimation technique to tell us about the intensity of your sensation of either nausea or overall discomfort level. (The experimenter will tell you which). We want to work with only slight to moderate sensation levels, in order to minimize any chance that you will reach the point of vomiting, so do your best to tell the experimenter exactly how you feel at all times. Early in the experiment, we will show you that if you (stop moving your head, and close your eyes), after a few moments, symptoms will rapidly subside. Once you have experience with this, you will gain confidence that symptoms can be limited to acceptable levels throughout the duration of the experiment with little difficulty. If at any time during the experiment, despite all precautions, you feel your symptoms are getting intolerably high, stop head movements and close your eyes immediately; do not wait for the experimenter to so instruct you.

Once you have gained some experience with the pattern of rise and fall of your own symptoms, you and the experimenter will pick a sensation magnitude of nausea or overall discomfort in the middle of your range of experience. You should call this standard intensity "10", and try to remember how it feels. Your task will be to estimate the magnitude of your subsequent sensation of nausea: overall subjective discomfort with respect to this standard. In other words, if your sensation now is half the standard, report 5; if it is double, report 20, and so forth. Use whatever numbers seem appropriate - fractions, decimals, or whole numbers. If you are not experiencing the sensation, say "absent". If the sensation is just noticeable (i.e. "threshold"), so that its magnitude ratioed with the standard is infinitely small, just say "sensation present". Try not to worry about being consistent; try to give your report each time regardless of what you may have called some previous sensation level.

Motion sickness susceptibility may be affected by a variety of extraneous factors, which we want to control as much as possible. Because this is important, we have to ask you:

- TO EAT A NORMAL SIZED MEAL AT YOUR NORMAL MEALTIME PRIOR TO THE EXPERIMENT
- TO DRINK ALCOHOL, COFFEE, TEA, COLA, AND OTHER STIMULANTS ONLY IN MODERATION DURING THE DAY PREVIOUS TO THE EXPERIMENT
- TO DRINK NO ALCOHOL ON THE DAY OF THE EXPERIMENT
- TO DRINK NO COFFEE, TEA, COLA, AND NOT TO SMOKE FOR 3 HOURS PRIOR TO THE EXPERIMENT
- TO AVOID HEAVY EXERCISE FOR 6 HOURS PRIOR TO THE EXPERIMENT

Informed Consent Statement

INFORMED CONSENT STATEMENT

STUDY OF DYNAMICS OF SYMPTOMS AND SIGNS IN MOTION SICKNESS

I have been asked to participate as a subject in a quantitative study of the pattern of motion sickness symptoms and signs. The stimuli used are active head movements made during prolonged wearing of left/right vision reversing glasses or while rotating in a computer controlled chair. I have been briefed on the purposes of the study. I will be asked to complete motion sickness history and pre-session questionnaires. I will be asked not to drink alcohol or take any medication for 24 hours prior to testing, and coffee or other stimulants for 12 hours prior to each session. I understand that during the testing I will probably experience slight or moderate motion sickness symptoms, such as stomach discomfort, nausea, pallor, sweating, drowsiness, and other symptoms when I make head movements, and that these symptoms may persist for some time after the end of the experiment, particularly if rapid head movements are made. I will attempt to report my subjective symptoms to the experimenter, who will be simultaneously recording my objective symptoms and head movements. Non-invasive optical (infrared) pallor measurement detectors, and electronic thermometers may be attached to my skin with adhesive tape. Conventional disposable surface recording electrodes may be applied to my abdomen to monitor gastric potentials. The sites of these electrodes may be lightly scratched with a sterile hypodermic needle prior to the application of the electrode.

Although participation in up to 6 two hour sessions may be requested, I understand that I am free to withdraw from further participation in the session or in the entire experiment at any time and for any reason. I realize that there is a slight chance that I may become nauseated to the point of vomiting, although every effort will be made to prevent this by appropriately limiting my head movements. I have no medical history such as heart or lung disease or chronic stomach trouble which would make such an accidental vomiting episode medically undesirable.

I understand that I should not operate a vehicle for three hours after the end of the experiment, and that I should report any persisting motion sickness symptoms to the experimenter.

I understand that my anonymity will be preserved when my questionnaire and experimental results are reported.

In the unlikely event of physical injury resulting from participation in this research, I understand that medical treatment will be available from the MIT Medical Department, including first aid, emergency treatment and follow-up care as needed, and that my insurance carrier may be billed for the cost of such treatment. However, no compensation can be provided for medical care apart from the foregoing. I further understand that making such medical treatment available, or providing it, does not imply that such injury is the Investigator's fault. I also understand that by my participation in this study I am not waiving any of my legal rights.

I understand that I may also contact the Chairman of the Committee on the Use of Humans as Experimental Subjects, Dr. George Wolf (MIT 56-213, 253-6781), if I feel I have been treated unfairly as a subject.

I agree to participate in this experiment.

Signed: _____ Date: _____

Experimenter: _____ Date: _____

Appendix B

Symptom Scoring Definitions

MASSACHUSETTS INSTITUTE OF TECHNOLOGY

MAN VEHICLE LABORATORY

STANDARD DEFINITIONS FOR SCORING ACUTE MOTION SICKNESS
USING THE PENSACOLA DIAGNOSTIC INDEX METHOD

January, 1987

Charles M. Oman, Brian W. Rague, and Ojas U. Rege
Room 37-219
MIT, Cambridge, MA 02139 USA
(617) 253-7508

Pensacola Motion Sickness Index: MVL Definitions. Page 2

STANDARD DEFINITIONS FOR SCORING ACUTE MOTION SICKNESS
USING THE PENSACOLA DIAGNOSTIC INDEX METHOD

I. SUMMARY: The lack of detailed definitions of the various symptoms and signs and distinctions between intensity levels in the open literature descriptions of the Pensacola Diagnostic Index (PDI) has so far prevented the motion sickness research community from achieving a completely consistent implementation of this method between laboratories. PDI test scores obtained in different laboratories are not truly equivalent. This memo establishes definitions for use in the MIT Man Vehicle Lab (MVL), and compares them with those employed by the NASA/JSC Neurophysiology Laboratory, and other groups. Our objectives in circulating this memo are to promote broader awareness of the methodological problem caused by the lack of standards, and to initiate a comparison of definitions and discussion. Our ultimate goal is to develop an appropriate set of practical, referencable standard definitions which reflect the best collective experience of the research community and which can be employed by researchers as is, or alternatively can serve as a point of departure, so that only exceptions from this standard need any elaboration in journal articles. Commentary on current practice in other laboratories, and suggestions for improvements in these definitions are solicited.

II. BACKGROUND

It has become the usual practice in motion sickness research over the past 20 years to score symptoms according to the "Pensacola Diagnostic Index" (PDI) method defined by Graybiel, Wood, Miller, and Cramer of the US Naval Aerospace Medical Institute in Pensacola, Florida in 1968 (Aerospace Medicine 39:453-455). This method was developed so as to allow experimenters to conveniently clinically describe the symptoms and signs of motion sickness in individual subjects and relate the overall intensity of sickness in one subject to that of another showing a somewhat different constellation of symptoms. The method requires no physiological monitoring equipment, only an experienced observer and cooperative subject. The symptoms and signs documented include are those characteristic of acute laboratory motion sickness (i.e. short term, controlled stimulation). The basic approach is to have the subject or observer grade the subjective intensity of eight different modalities of symptoms and signs on a traditional clinical 1-2-3 "slight/moderate/severe" basis, and then to numerically weight the resulting scores to arrive at a weighted "malaise index". Typically, the method is used to establish a numerical endpoint in "time to endpoint" type motion sickness susceptibility test paradigms. In these tests, time or number of head movements, etc. required to reach a particular PDI endpoint under a standardized nauseogenic stimulus condition is taken as a measure of insusceptibility. Prior to the development of the PDI system, vomiting was the only endpoint generally accepted as reliable for motion sickness research. The objective of the PDI method was to allow investigators to systematically define endpoints well short of vomiting which were at once reliable and acceptable to subjects. At the commonly used "Malaise IIa" (5-7 points, sometimes abbreviated "M.IIa") and the "Malaise III" (8 - 15 points, "M.III") symptom levels, the subjects exhibit a few signs or symptoms that are relatively obvious changes from baseline. Subjects usually quickly recover and are able to return to their daily activities.

Although the PDI scoring method is complex, the method has face validity, has

Pensacola Motion Sickness Index: MVL Definitions, Page 3

certainly stood the test of time, and has produced data which appears reasonably repeatable. For example, Pensacola investigators who subsequently used the PDI to develop the Coriolis Sickness Susceptibility Index (CSSI) test showed that in repeat testing of 30 subjects, the correlation coefficient between 1st and 2nd session results using a PDI endpoint of 5 or more points was 0.89. Thus, there is empirical evidence that the PDI is measuring something repeatable. The numerical weighting scheme used in the PDI assures that the malaise index usually corresponds monotonically with the subject's self report of overall sickness intensity. However, we do not yet know exactly how the PDI score covaries with objective measurements of physiological variables, or subjective ratio scaled estimates of overall discomfort of nausea or overall discomfort. The PDI is not constructed so that, for example, a doubling of the PDI score corresponds to a doubling of self reported nausea or overall discomfort.

The PDI method does suffer from certain drawbacks. The most of significant of these is that little detail was provided in the original or subsequent Pensacola publications as to precise definitions of the individual symptom modalities, and within each modality, the exact distinction between slight, moderate, and severe intensity. As a result, other laboratories using the PDI method have informally developed and adopted their own working definitions, albeit sometimes with guidance from Pensacola. To our knowledge, these working definitions have not been published in the open literature. Perhaps as a result, significant differences exist between the working definitions adopted by various research groups. In some cases these definitions depart from the letter or even the spirit of the original Pensacola terminology. When such differences exist, they can have a significant impact on the numerical score achieved by individual subjects. While data from an individual laboratory using the PDI may be internally consistent, the data obtained in different laboratories cannot be directly compared. Attention is rarely drawn to this fact in Journal articles; typically authors say only that "symptoms were scored using the Pensacola Diagnostic Method (Graybiel et al, 1968)", implying that the original Pensacola publication completely specifies the implementation of the technique. Some laboratories - notably the JSC Neurophysiology Laboratory - have carefully documented their procedures in internal memoranda. However, no inter-laboratory comparison of working definitions has previously been attempted.

Below we formally establish working definitions for PDI terminology in the MVL. These definitions are largely similar to those used in previous MVL motion sickness studies including the SL-1 and D-1 Spacelab mission experiments. Except as noted, we have tried to make these MVL definitions conform closely to the working definitions established previously by NAMRL Pensacola and/or the JSC Neuro Laboratory. Shorthand acronyms for the various modalities and levels are retained, because this has historically proven useful to observers writing down symptom reports under time pressure in experimental settings. In bracketed notes following each definition, a detailed comparison is made with working definitions developed in the NASA/JSC Neurophysiology Lab and other groups, and the rationale for the MVL definition is discussed. The JSC definitions are described in detail in a memo provided to MIT/MVL by Patricia Ryan (11/4/86). We thank the staff of the Neurophysiology Lab for making their definitions available to us.

Pensacola Motion Sickness Index: MVL Definitions, Page 4

III. MIT/MVL STANDARD PENSACOLA DIAGNOSTIC INDEX SYMPTOM DEFINITIONS:

Epigastric Awareness ("EA", 1 point) - Epigastric awareness is a sensation that draws attention to the epigastric area (stomach and upper abdomen, and/or substernal area including esophagus, and throat), but which is not uncomfortable, and can be distinguished from the threshold sensation of nausea (see below). The statement "ah, I have a stomach" is descriptive. It should be a symptom that is minimally noticeable.

[Note: the JSC Neuro lab has required that EA be intermittent (i.e., it may be present when head movements are being made, but disappears when the head is held still). In MVL experience, persistent EA which is not uncomfortable and therefore ED (see below) is frequently seen in the early stages of sickness in some individuals.]

Epigastric Discomfort ("ED", 2 points) - Epigastric discomfort is an uncomfortable sensation that is distinguishable from and more intense than epigastric awareness but also distinguishable from nausea (see below). It is referred to the upper abdominal area, stomach, esophagus, and/or throat.

[Note 1: The JSC Neuro lab requires ED to be persistent (i.e., present even with the head held still although it may wax or wane upon starting and stopping head movements). In MVL experience, by the time ED is persistent, the subject often chooses to redefine it as nausea.]

[Note 2: The PDI scale was constructed assuming that EA, ED, and nausea are successively increasing levels of sensation intensity within the same general modality, and that subjects usually progress up this scale in sequence. While this is usually the case, in MVL experience, this is not invariably so. Many experienced subjects recognize their first sensations of stomach discomfort as a low level of nausea, and prefer to use this term to describe it.]

Nausea 1 ("NSA 1", 4 points) - Nausea 1, or "slight nausea" is an unpleasant sensation referred to the stomach, upper abdomen, and/or esophagus or throat which the subject unequivocally recognizes through previous experience as being associated with the act of vomiting and retching when the intensity of sensation reaches higher levels. However, vomiting is not imminent. Nausea 1 sensation levels are defined as those associated with the lowest third of the overall range of nausea sensation which runs from the threshold of nausea up to the most intense levels usually experienced moments before and during the act of vomiting.

[Note 1: We have found that the definition of the boundary between ED, NSA 1 and NSA 2 (below) has a profound effect on when the PDI endpoint is formally reached, since the subject typically accumulates 8 points (Malaise III endpoint) when ED becomes NSA 1 in the presence of several other low level symptoms, or as NSA1 becomes NSA2. Several other labs with whom we have communicated define NSA 1 as "the lowest levels of nausea" or "the first appearance of unequivocal nausea", NSA 3 as "the most intense levels of nausea: just before you reach for the bag", and by exclusion, nausea 2 is usually defined as everything in between. When we have experimented with this definition, we find our subjects are always pressing us to define the boundary between nausea 1 and 2, and they comment that since NSA 1 and 3 levels are just those around the extremes, the NSA 2 range seems very wide indeed. At the very highest nausea intensities,

Pensacola Motion Sickness Index: MVL Definitions, Page 5

vomiting and/or retching are virtually inevitable, and therefore NSA 3 and vomiting/retching are virtually synonymous. In adopting definition above, which splits the range of nausea into thirds, we are attempting to anchor the nausea range using the subject's previous experience, and to provide a more useful range of gradations of nausea intensity.]

[Note 2: In contrast with the original Pensacola definition adopted by most other labs, the JSC Neuro Lab requires nausea 1 to be of moderate (as opposed to slight) intensity, and to persist between head movements. The subject is asked if they feel "that continuing additional head movements might get them close to the point of throwing up". If the answer is 'yes' or 'maybe', Nausea I is considered present. If the answer is 'no', the subject is assumed to be borderline between ED and NSA 1 or below. By using this definition, JSC probably elicits a higher level of sickness when subjects reach the formal MIIa or MIII endpoint. The JSC definition of NSA 1 probably corresponds to the Nausea II definition used by most other laboratories.]

Nausea II/III (NSA 2 or NSA 3, 8 points) - Nausea II, or 'moderate nausea' and Nausea III or 'severe nausea' are more intense, unpleasant sensations referred to the stomach, upper abdomen, and/or esophagus or throat which are associated with the act of vomiting and retching. Nausea II sensation levels are defined as those associated with the middle third of the overall range of nausea sensation experience which runs from the threshold of nausea up to the most intense levels usually experienced moments before and during the act of vomiting. Nausea III is the upper third of this range, and includes those levels at which the subject 'begins to reach for the bag', and for which even one more head movement will probably cause emesis.

[Note: Under the original PDI definition, progressing from NSA2 to NSA3 does not produce an increment in malaise index, since the subject is given 8 points when NSA2 or NSA3 are present. In the past, some labs (including MVL) have deviated from this practice, and score NSA3 and/or vomiting and/or retching as 16 points. This is of little import in many situations, however, since endpoints are usually reached before NSA3 is encountered. Nausea II and III are often (but not always) accompanied by an increased urge to swallow, and by sighing and panting.]

Vomiting (16 points) - Vomiting is the overt act of emesis. Forceful contraction of the abdominal muscles and the diaphragm, closure of the glottis, and expulsion of the stomach contents to the mouth.

Retching (16 points) - Unproductive vomiting; 'dry heaves'. Forceful contraction of the abdominal muscles and the diaphragm, and closure of the glottis, but stomach contents do not reach the mouth.

[Note: belching is a common episodic sign of early motion sickness onset. Occasionally 'wet burping' is encountered, in which a small amount of stomach contents are regurgitated into the mouth, usually because of a transient relaxation of the cardiac (upper gastric) sphincter. It is not associated with a crescendo of nausea. True vomiting always involves forceful contraction of abdominal muscles and diaphragm.]

Flushing/Subjective Warmth 2/3 ('TMP 2/3', 1 point) - Flushing is an increased reddening of the skin, sign detected by the observer, usually starting on the

Pensacola Motion Sickness Index: MVL Definitions, Page 6

face and neck. It may be seen by the test operator as a blushing of the face. Subjective warmth is a symptom reported by the subject, experienced as a gradual or sudden sensation of increased warmth of the surface of the body. The warmth may also be localized to the chest, back, under arms, or thighs. The appearance of either of these two symptoms at moderate or severe levels, but not slight levels, separately or together is given one point. In some subjects, a slight flushing consistently precedes the onset of pallor. Many subjects experience transient flushing shortly after vomiting.

[Note: the JSC Neuro lab also scores slight flushing/subjective warmth as 1 point, although the practice at Pensacola, MIT and elsewhere is usually to score only moderate and severe levels.]

Pallor I (*PAL 1*, 2 points) - Pallor I is the first noticeable blanching or whitening (paling) of the skin color on the face. It may not involve the entire face, but be limited to small areas such as around the nose and mouth or the ear lobes.

[Note: The intensity of this sign is graded by the test observer, not by the subject. The detection of Pallor I is difficult, but may sometimes be aided by noting changes with reference to the subject's clothing or the walls of the room (if appropriately colored). Prior to the start of the test, the test observer should also spend 30 seconds carefully reviewing the color pattern on the subject's face to establish a "visual fix" of the subject's normal facial color. Pallor judgements in dark skinned individuals are extremely difficult to score.] Even experienced observers frequently comment that they have little confidence in the reliability of their judgements of slight pallor. Dr. Graybiel has noted privately that both of the Pensacola rotating room observers generally were agreement when pallor II is manifest, but pallor I was regularly scored by one but not the other technician.]

Pallor II (4 points) - Pallor II is moderate pallor, and by definition is more noticeable than Pallor I. Pallor II is present when the subject's entire face, and possibly ears, neck, and upper chest (if visible) have obviously lost their normal color. A blotchy appearance is common.

Pallor III (8 points) - Pallor III severe pallor, and this term should be reserved for situations where the subject's face and upper torso appear virtually devoid of color. The skin has an ashen white or green appearance. The phrase "white as a ghost" may accurately describes the subject. This severe form of pallor normally is correlated with NSA 3 and vomiting.

Sweat I (*SWT 1*, 2 points) - Sweat I is the first noticeable onset of mild cold (thermally inappropriate) sweating that is sensed by the subject, or visible as small specks. Sweat I is usually not visually apparent to the test operator. Instead, the subject typically becomes aware of a light amount of sweat on the forehead, upper torso or under arms. Sweat I may be experienced as a mild clammy or sticky feeling before the actual appearance of beads of sweat. The subject typically reports his skin feels cooler due to sweat evaporation. The test operator or subject may wipe the forehead with a dry finger to check for dryness. Because sweating on the palms of the hands may be due to arousal or anxiety, sweating there is conventionally ignored.

Pensacola Motion Sickness Index: MVL Definitions, Page 7

[Note: An alternative convenient mnemonic for grading 3 levels of sweating as suggested some years ago by Dr. G. Crampton is: "specks, beads, and sheets". Sweating and sweating sensations are notoriously dependent on environmental temperature and humidity. Best results are obtained when environmental temperature, humidity, breeze and clothing are standardized. Sweating amount also depends to some extent on gender and skin type.]

Sweat II (*SWT 2*, 4 points) - Sweat II is a moderate level of more generalized body sweat that is distinctly felt by the subject and visible to the test observer. Sweat II may be seen as small beads of perspiration, typically on the forehead or face. If the subject is wearing tight fitting clothing it may be visible as a slight dampening of the clothing. Again, the sweat may evaporate causing the subject to feel noticeably cool.

Sweat III (*SWT 3*, 8 points) - Sweat III is a very profuse whole body sweat that can be easily seen as sheets or rivulets of sweat on exposed parts of the subject's body, especially face and neck. With Sweat III, the subject's clothing will become noticeably damp, particularly on the chest, under arms, and back.

Increased Salivation I (*SAL+ 1*, 2 points) - This is the first subjectively noticeable slight increase in the amount of saliva accumulating in the mouth, and consequent need to swallow, as reported by the subject.

[Note 1: Since the observer cannot detect light Salivation I, it is essential for the test operator to ask the subject at the beginning of test if his mouth feels normal or dry and to report any change. Salivation onset is often preceded by a dryness of the lips and front of the mouth. Sighing and panting are also commonly seen at higher symptom levels, and breathing through the mouth often dries the lips.]

Increased Salivation II (*SAL+ 2*, 4 points) - Salivation II is pronounced, increase in the amount of excess saliva accumulating in the subject's mouth. With Saliva II, the subject has a noticeably increased need to swallow more frequently.

[Note: Increased swallowing due to salivation should not be confused with swallowing due to Nausea II/III. If swallowing is present, the test operator should determine whether salivation is also present.

Increased Salivation III (*SAL+ 3*, 8 points) - Severe salivation occurs when copious amounts of saliva are present, potentially leading to drooling of the mouth. Rarely seen.

Drowsiness I (*DRS*, 2 points) - Slight drowsiness occurs when the subject reports a slight decrease in mental alertness, or being slightly sleepy.

[Note 1: Many labs include reports of boredom, apathy and fatigue under this symptom. JSC Neuro lab includes in the drowsiness category: feeling relaxed, slight confusion, slowing of head movements, incorrect head movements, or less verbally responsive to the observer's questions. However, lack of responsiveness can also be due to preoccupation with symptoms, rather than drowsiness, per se. Because judgements of changes in apathy, boredom, confusion etc. are very difficult for the observer to objectively make, MVL prefers to

Pensacola Motion Sickness Index: MVL Definitions, Page 8

retain the simple traditional definition of drowsiness, and to ask the subject to make the drowsiness assessment.]

[Note 2: Yawning is a common episodic sign of early motion sickness onset or other autonomic stress, and is not directly scored under the PDI. Yawning may or may not be associated with drowsiness. If the observer sees the subject yawn, neither the observer (nor the subject) should automatically assume that the subject is drowsy.]

Drowsiness II (*DRS 2*, 4 points) - Moderate drowsiness is drowsiness which is very apparent to both subject and test conductor. The subject feels he could easily fall asleep.

Drowsiness III (*DRS 3*, 8 points) - This symptom is scored when the subject is observed to be literally falling asleep during the test and appears unable to perform required tasks (e.g., head movements) even when prompted by the test operator. This is only rarely seen in laboratory tests where the stimulus exposure is typically short.

Headache II/III (*HAC 2/3*, 1 point) - This symptom is defined as a moderate or severe headache which was not present prior to the test, and which the subject feels is a symptom. Slight headaches are not scored.

[Note 1: It has been the MVL experience that subjects who "get headaches" often experience HAC as a motion sickness symptom. Subjects who have experienced motion sickness before often are aware if they generally experience HAC as a symptom. The headache may be localized to one region of the head or it may involve the entire head. It may be of persistent nature or it may wax and wane.]

[JSC Neuro Lab has chosen to score slight to moderate headaches as 1 point, and severe, intense headaches as 2 points. JSC also considers a self report of "head fullness" as Headache.]

Dizziness II/III (*DIZ 2/3*, 1 point) - This symptom modality includes subject reports of dizziness, "feathers in the head", vertigo, spatial disorientation, wobbliness, unsteadiness. If any of these sensations are present at moderate or severe levels and persist beyond several seconds after the subjects head stops moving, DIZ 2/3 is scored. If these sensations are slight, or are present only when the subject's head is undergoing motion but disappear within seconds after head motion stops, then Dizziness is not scored.

[Note 1: The JSC Neuro Lab has found that in some cases, DIZ may become the "dominant and distressful" symptom. In these cases, they prefer to score 2 symptom points.]

SYMPTOM SCORING: Points for the different reporting modalities are summed at each observation time. At Pensacola, JSC Neuro Lab, and MVL, points are NOT considered cumulative. Thus, when a symptom disappears, the point value of that symptom is subtracted from the previous total. There has been some confusion on this issue in the past, and we are aware of one lab which routinely uses cumulative points.

UNSCORED SYMPTOMS: A variety of symptoms and signs other than those formally

Pensacola Motion Sickness Index: MVL Definitions, Page 9

included in the PDI system frequently occur in motion sickness, and experienced observers often look for them, and make marginal notes concerning their presence when they are seen. These include: loss of appetite, confusion, apathy, loss of concentration, belching, flatulence, desire to defecate, yawning, sighing, and panting.

Supported by NASA Contract NAS9-17371

Appendix C

Lattice-C Programs used for EGG Real-Time Analysis

The main body of the EGG analysis program controls the real time software acquisition and storage of newly sampled data points. These values are read from a real time access file labeled "RTA", provided by *LabTech Notebook*. The raw EGG data is first processed by an offset correction scheme which essentially compensates for any auto-balancing voltage steps incurred by the DRI pre-amp. If the magnitude of the difference between successive 1 hz data samples is greater than 0.5 volts, then a correction voltage equal to the negative of this difference is added to subsequent data points. This correction voltage, stored in the variable *corr*, will reflect the total sum of compensating voltage steps in hardware. DC corrected raw EGG data is stored in the disk file *dfile.prn*.

Initially, 512 data points are sampled and stored in the array $x[i]$, where $1 \leq i \leq 512$. The main program then calls the sub-routine *fft()*. The data are processed by an FFT program, FFT842 (acquired from public domain). The number of points in the FFT is adjustable (must be a power of 2), and can be specified by changing the value of the global variable MAXN. Within the sub-routine *fft()*, (1) a hamming window multiplies the raw data (*hamming()*), (2) the real and imaginary values of the FFT are stored in a file *trans.prn*, (3) frequency components below .042 hz are set to 0, essentially high-pass windowing the data, and (4) energy spectrum components are computed (*squared()*) and stored in a file *spect.prn*.

To realize our specific running spectrum analysis format whereby a window of length 512 points is moved incrementally by 64 points, the main control program moves the last 448 points in processing array $x[i]$ to positions from $i=1$ to $i=448$, then fills the remaining 64 array points with new samples. The first 8 spectra (~15 minutes) are processed by a sub-routine *apex()*, which computes the highest magnitude of any frequency component

within the range .04-.06 hz. This peak is used for calibrating the intensity levels for the real time grey scale plot. Calibration is performed by *calib()*, and involves multiplying the peak value determined in *apex()* by $\frac{2}{3}$, then dividing the resulting value by 6 to produce 7 discrete levels, represented by 7 different intensities in the grey-scale plot.

At this point, the main module calls the *plot()* routine, which essentially draws and labels the axes used for the grey-scale display. Remaining energy spectra are computed in the same way described above, with the exception that resulting spectral components are processed by the routine *convert()*, which converts the magnitudes of each of the frequency components into an integer number from 0 to 6 corresponding to the 7 intensity levels used for grey-scale plotting. After this operation, the main program calls the sub-routine *grey()*, which reads the converted integer values and draws the appropriate 3 x 3 pixel pattern on the grey-scale plot. Integer values used for grey-scale plotting are stored sequentially in the disk file *code.prn*.

Exiting from this EGG processing program can only be accomplished *after* the calibration period. Typing "d" will inform the program that the user wishes to exit. The "d" will not be echoed on the screen. After the program has completed plotting a given spectrum, the main program will search for a keyboard hit. If the keyboard hit is a "d," the main program will store present calibration values, flag indicators, and the most recently acquired data in a stack file, *stack.prn*. If the user wishes to return to the EGG processing program later in the recording session, the main module will read the values from *stack.prn* to update its status, then call the sub-routine *regrey()*, which will redo the grey-scale plot up to the point when the processing program was last exited.

```

#include <stdio.h>
int flag, stop;
int spn, step;
double corr;

main(argc, argv)
int argc;
char *argv[];
{
    extern double x[];
    extern double peak, corr;
    extern int flag;
    int i, n, u, c, hit;
    double j, g, temp;
    float rta_data;
    double z[513];

    FILE *fp, *np, *cp, *sp, *fopen();

    x[0]=0.0;
    z[0]=0.0;
    corr=0.0;
    temp=0.0;
    stop=0;
    fp = fopen("RTA", "r");
    setnbf(fp);
    if (argc != 1)
        goto redo;
    np = fopen("dfile.prn", "w");
    cp = fopen("code.prn", "w");
    for(i=1; i<=512; i++)
        (n = fscanf(fp, "%f", &rta_data);
         if(n == EOF)
             goto end;
         else
             (j = rta_data;
              g = j - temp;
              if(g >= 0.5)
                  corr = corr - g;
              if(g <= -0.5)
                  corr = corr - g;
              temp = j;
              j = j + corr;
              x[i] = j;
              z[i] = j;
              fprintf(np, "%g\n", j);
              printf("%d\tCalibrating\n", i); ))
    flag=0;
    spn=1;
    printf("Executing FFT and Peak analysis\n");
    fft();
    apex();

    for(step=1; step<=7; step++)
        {
            for(i=1; i<=448; i++)
                ( n = i + 64;
                  x[i] = z[n];
                  z[i] = z[n]; )
        }
}

```



```

for(i=449;i<=512;i++)
  ( n = fscanf(fp,"%f",&rta_data);
    if(n == EOF)
      goto end;
    else
      (j = rta_data;
        g = j - temp;
        if(g >= 0.5)
          corr = corr - g;
        if(g <= -0.5)
          corr = corr - g;
        temp = j;
        j = j + corr;
        x[i] = j;
        z[i] = j;
        fprintf(np,"%g\n",j);
        printf("%d\tcalibrating\n",i));)
    flag=1;
    printf("Executing FFT and Peak Analysis\n");
    fft();
    apex();
  )
calib();
plot();

start: for(i=1;i<=448;i++)
  ( n = i + 64;
    x[i] = z[n];
    z[i] = z[n];)

for(i=449;i<=512;i++)
  (n = fscanf(fp,"%f",&rta_data);
    if(n == EOF)
      goto end;
    else
      (j = rta_data;
        g = j - temp;
        if(g >= 0.5)
          corr = corr - g;
        if(g <= -0.5)
          corr = corr - g;
        temp = j;
        j = j + corr;
        x[i] = j;
        z[i] = j;
        fprintf(np,"%g\n",j);
        u = i % 10;
        printf("%d\b",u); ))
    flag=1;
    printf("e\b");
    fft();
    convert();
    for(i=2;i<=101;i++)
      fprintf(cp,"%g\n",x[i]);
    grey();
    if(stop==1)
      goto end;
    hit = kbhit();
    if(hit != 0)

```

Lattice-C Programs

```

(c = getch();
 if (c == 'd')
  (sp = fopen("stack.prn", "w");
   fprintf(sp, "%d\n", spn);
   fprintf(sp, "%g\n", peak);
   for(i=65; i<=512; i++)
    fprintf(sp, "%g\n", z[i]);
   fclose(sp);
   fclose(fp);
   fclose(np);
   fclose(cp);
   printf("\bType 'exit'\n");))
 goto start;
redo: sp = fopen("stack.prn", "r");
     n = fscanf(sp, "%d", &spn);
     n = fscanf(sp, "%lf", &peak);
     for(i=65; i<=512; i++)
      n = fscanf(sp, "%lf", &z[i]);
     fclose(sp);
     np = fopen("dfile.prn", "a");
     cp = fopen("code.prn", "a");
     calib();
     plot();
     regrey();
     goto start;
end:  fclose(fp);
     fclose(np);
     fclose(cp);
     printf("\b");
}

```

Lattice-C Programs

```

#include <stdio.h>
#define MAXN 512

double pi2, p7;
double x[MAXN+1];
double y[MAXN+1];
fft()
(
    FILE *sp,*qp,*fopen();
    int i,k;
    extern int flag;
    extern int spn;
    double r;
    hamming();
    fft842(0, MAXN, x, y);
    for(i=2;i<=101;i++)
        (k = (2*i)-1;
         x[i] = x[k];
         y[i] = y[k]);
    if (flag == 0)
        (qp = fopen("trans.prn","w");
         fprintf(qp,"0\n");
         for(i=2;i<=101;i++)
             (r = .00390625*(i-1);
              fprintf(qp,"%g\t%g\t%g\n",r,x[i],y[i]));
         fclose(qp);)
    if (flag == 1)
        (qp = fopen("trans.prn","a");
         fprintf(qp,"%d\n",spn);
         for(i=2;i<=101;i++)
             (r = .00390625*(i-1);
              fprintf(qp,"%g\t%g\t%g\n",r,x[i],y[i]));
         fclose(qp);)
    squared();
    if (flag == 0)
        (sp = fopen("spect.prn","w");
         fprintf(sp,"0\n");
         for(i=2;i<=101;i++)
             (r = .00390625*(i-1);
              fprintf(sp,"%g\t%g\n",r,x[i]));
         fclose(sp);)
    if (flag == 1)
        (sp = fopen("spect.prn","a");
         fprintf(sp,"%d\n",spn);
         for(i=2;i<=101;i++)
             (r = .00390625*(i-1);
              fprintf(sp,"%g\t%g\n",r,x[i]));
         spn = spn + 1;
         fclose(sp);)
)
hamming()
(
    int i,n;
    double atof(),j;
    char k[20];
    FILE *fp, *fopen();

    y[0]=0.0;
    fp = fopen("hamming.dat","r");

```

```

        for(i=1;i<=MAXN;i++)
            ( n = fscanf(fp,"%s",&k);
              j = atof(k);
              y[i] = j;)
        fclose(fp);

        for(i=1;i<=MAXN;i++)
            (x[i] = x[i] * y[i];
             y[i] = 0.0;)

squared()
{
    int i;

    for(i=1;i<=11;i++)
        x[i] = 0.0;
    for(i=12;i<=101;i++)
        x[i] = (x[i]*x[i])+(y[i]*y[i]);
}

/*
-----
function fft842(inverse, n, x, y)
fast fourier transform for n=2**m
complex input
-----

This program replaces the vector z=x+iy by its finite discrete,
complex fourier transform if inverse==0. The inverse transform is
calculated if inverse=-1. It performs as many base 8 iterations as
possible and then finishes with a base 4 iteration or a base 2
iteration if needed.

The integer n (a power of 2), the n-real-location array x[], and
the n-real-location array y[] must be supplied.
*/

fft842(inverse, N, x, y)
double x[], y[];
{
    int i, j, nt, n2pow, n8pow, nthpo, ipass, nextlt, lengt, ij;
    int j1, j2, j3, j4, j5, j6, j7, j8, j9, j10, j11, j12, j13, j14, ji;
    int l[15+1];
    double r, fi;
    double atan(), sqrt();

    pi2 = 8.0 * atan(1.0);
    p7 = 0.70710678;
    for (i=1, nt=2; i<=15; i++, nt*=2) if (N == nt) goto start;
    fprintf (stderr, "N is not a power of two\n");
    exit(1);

start: n2pow = i;
      nthpo = N;
      if (!inverse) for (i=1; i<=nthpo; i++) y[i] = -y[i];

      n8pow = n2pow/3;
      if (n8pow > 0) { /* radix 8 passes, if any. */
          for ( ipass=1; ipass<=n8pow; ipass++) {

```



```

        y[i] /= nthpo;
    }
    else for ( i=1; i<=nthpo; i++) y[i] = -y[i];
}

/*
-----
function: r2tx
radix 2 iteration subroutine
-----
*/

r2tx(nthpo, cr0, cr1, ci0, cil)
double cr0[], cr1[], ci0[], cil[];

(
    int k;
    double r1, fi1;

    for ( k=1; k<=nthpo; k+=2 ) (
        r1 = cr0[k] + cr1[k];
        cr1[k] = cr0[k] - cr1[k];
        cr0[k] = r1;
        fi1 = ci0[k] + cil[k];
        cil[k] = ci0[k] - cil[k];
        ci0[k] = fi1;
    )
)

/*
-----
function: r4tx
radix 4 iteration subroutine
-----
*/

r4tx (nthpo, cr0, cr1, cr2, cr3, ci0, cil, ci2, ci3)
double cr0[], cr1[], cr2[], cr3[], ci0[], cil[], ci2[], ci3[];

(
    int k;
    double r1, r2, r3, r4, fi1, fi2, fi3, fi4;
    for ( k=1; k<=nthpo; k+=4 ) {
        r1 = cr0[k] + cr2[k];
        r2 = cr0[k] - cr2[k];
        r3 = cr1[k] + cr3[k];
        r4 = cr1[k] - cr3[k];
        fi1 = ci0[k] + ci2[k];
        fi2 = ci0[k] - ci2[k];
        fi3 = cil[k] + ci3[k];
        fi4 = cil[k] - ci3[k];
        cr0[k] = r1 + r3;
        ci0[k] = fi1 + fi3;
        cr1[k] = r1 - r3;
        cil[k] = fi1 - fi3;
        cr2[k] = r2 - fi4;
        ci2[k] = fi2 + r4;
        cr3[k] = r2 + fi4;
    }
)

```

Lattice-C Programs

```

        ci3[k] = fi2 - r4;
    }
}

/*
-----
subroutine: r8tx
radix 8 iteration subroutine
-----
*/

r8tx (nxtlt, nthpo, lengt, cr0, cr1, cr2, cr3, cr4, cr5, cr6, cr7,
      ci0, ci1, ci2, ci3, ci4, ci5, ci6, ci7)
double cr0[], cr1[], cr2[], cr3[], cr4[], cr5[], cr6[], cr7[],
       ci0[], ci1[], ci2[], ci3[], ci4[], ci5[], ci6[], ci7[];
{
    int j, k;
    double scale, arg, cos(), sin();
    double c1, c2, c3, c4, c5, c6, c7, s1, s2, s3, s4, s5, s6, s7;
    double ar0, ar1, ar2, ar3, ar4, ar5, ar6, ar7;
    double ai0, ai1, ai2, ai3, ai4, ai5, ai6, ai7;
    double br0, br1, br2, br3, br4, br5, br6, br7;
    double bi0, bi1, bi2, bi3, bi4, bi5, bi6, bi7;
    double tr, ti;
    extern double pi2, p7;

    scale = pi2/ lengt;
    for ( j=1; j<=nxtlt; j++) {
        arg = (j-1) * scale;
        c1 = cos(arg);
        s1 = sin(arg);
        c2 = c1*c1 - s1*s1;
        s2 = c1*s1 + c1*s1;
        c3 = c1*c2 - s1*s2;
        s3 = c2*s1 + s2*c1;
        c4 = c2*c2 - s2*s2;
        s4 = c2*s2 + c2*s2;
        c5 = c2*c3 - s2*s3;
        s5 = c3*s2 + s3*c2;
        c6 = c3*c3 - s3*s3;
        s6 = c3*s3 + c3*s3;
        c7 = c3*c4 - s3*s4;
        s7 = c4*s3 + s4*c3;
        for ( k=j; k<=nthpo; k+=lengt) {
            ar0 = cr0[k] + cr4[k];
            ar1 = cr1[k] + cr5[k];
            ar2 = cr2[k] + cr6[k];
            ar3 = cr3[k] + cr7[k];
            ar4 = cr0[k] - cr4[k];
            ar5 = cr1[k] - cr5[k];
            ar6 = cr2[k] - cr6[k];
            ar7 = cr3[k] - cr7[k];
            ai0 = ci0[k] + ci4[k];
            ai1 = ci1[k] + ci5[k];
            ai2 = ci2[k] + ci6[k];
            ai3 = ci3[k] + ci7[k];
            ai4 = ci0[k] - ci4[k];
            ai5 = ci1[k] - ci5[k];
            ai6 = ci2[k] - ci6[k];
            ai7 = ci3[k] - ci7[k];

```

```

br0 = ar0 + ar2;
br1 = ar1 + ar3;
br2 = ar0 - ar2;
br3 = ar1 - ar3;
br4 = ar4 - ai6;
br5 = ar5 - ai7;
br6 = ar4 + ai6;
br7 = ar5 + ai7;
bi0 = ai0 + ai2;
bi1 = ai1 + ai3;
bi2 = ai0 - ai2;
bi3 = ai1 - ai3;
bi4 = ai4 + ar6;
bi5 = ai5 + ar7;
bi6 = ai4 - ar6;
bi7 = ai5 - ar7;
cr0[k] = br0 + br1;
ci0[k] = bi0 + bi1;
if (j > 1) {
    cr1[k] = c4*(br0-br1) - s4*(bi0-bi1);
    ci1[k] = c4*(bi0-bi1) + s4*(br0-br1);
    cr2[k] = c2*(br2-bi3) - s2*(bi2+br3);
    ci2[k] = c2*(bi2+br3) + s2*(br2-bi3);
    cr3[k] = c6*(br2+bi3) - s6*(bi2-br3);
    ci3[k] = c6*(bi2-br3) + s6*(br2+bi3);
    tr = p7*(br5-bi5);
    ti = p7*(br5+bi5);
    cr4[k] = c1*(br4+tr) - s1*(bi4+ti);
    ci4[k] = c1*(bi4+ti) + s1*(br4+tr);
    cr5[k] = c5*(br4-tr) - s5*(bi4-ti);
    ci5[k] = c5*(bi4-ti) + s5*(br4-tr);
    tr = -p7*(br7+bi7);
    ti = p7*(br7-bi7);
    cr6[k] = c3*(br6+tr) - s3*(bi6+ti);
    ci6[k] = c3*(bi6+ti) + s3*(br6+tr);
    cr7[k] = c7*(br6-tr) - s7*(bi6-ti);
    ci7[k] = c7*(bi6-ti) + s7*(br6-tr);
}
else {
    cr1[k] = br0 - br1;
    ci1[k] = bi0 - bi1;
    cr2[k] = br2 - bi3;
    ci2[k] = bi2 + br3;
    cr3[k] = br2 + bi3;
    ci3[k] = bi2 - br3;
    tr = p7*(br5-bi5);
    ti = p7*(br5+bi5);
    cr4[k] = br4 + tr;
    ci4[k] = bi4 + ti;
    cr5[k] = br4 - tr;
    ci5[k] = bi4 - ti;
    tr = -p7*(br7+bi7);
    ti = p7*(br7-bi7);
    cr6[k] = br6 + tr;
    ci6[k] = bi6 + ti;
    cr7[k] = br6 - tr;
    ci7[k] = bi6 - ti;
}
}

```


Lattice-C Programs

```

#include <stdio.h>
double peak;
apex()
{
    extern double x[];
    extern int flag;
    int i,hi;
    double freq,npeak;

    if(flag==0)
        (peak = x[2];
         hi = 1;
         for(i=3;i<=101;i++)
             (if(x[i] > peak)
              (peak = x[i];
               hi = i - 1;))
         freq = 0.00390625 * hi;
         printf("Freq = %g\tMag = %g\n",freq,peak);
         if(freq < 0.04 || freq > 0.06)
             (printf("Freq outside EGG Baseline Range: Peak Disregarded\n");
              peak = 0.0;)
        )

    if(flag==1)
        (npeak = x[2];
         hi = 1;
         for(i=3;i<=101;i++)
             (if(x[i] > npeak)
              (npeak = x[i];
               hi = i - 1;))
         freq = 0.00390625 * hi;
         printf("Freq = %g\tMag = %g\n",freq,npeak);
         if(freq < 0.04 || freq > 0.06)
             (printf("Freq outside EGG Baseline Range: Peak Disregarded\n");
              goto finish;)
         if(npeak > peak)
             peak = npeak;
        )
    finish: ;
}

```

```
#include <stdio.h>
double lim1,lim2,lim3,lim4,lim5,lim6;
calib()
(
    extern double peak;
    lim6 = peak * 2.0;
    lim6 = lim6/3.00000;
    lim1 = lim6/6.00000;
    lim2 = 2 * lim1;
    lim3 = 3 * lim1;
    lim4 = 4 * lim1;
    lim5 = 5 * lim1;
)
```

```

#include <stdio.h>
plot()
{
    int c,a,b,d,i,j,k;
    extern double x[];
    extern int p,q;
    char *n;
    static char device[]="HALOIBM.DEV";
    static char mess1[]="Frequency in Hz";
    static char mess2[]="64 Mins";
    setdev(device);

    p=20;
    q=177;
    initgraphics(&(a=0));
    setipal(&(a=0), &(b=0));
    a=20;
    b=181;
    movabs(&a, &b);
    lnabs(&(a=319), &b);          /*Draw abscissa*/
    movabs(&(a=20), &b);
    lnrel(&(a=0), &(b=1));
    movtcurabs(&(a=17), &(b=191)); /*Draw hashmarks w/numbers*/
    text("0");
    a=58;
    b=181;
    movabs(&a, &b);
    lnrel(&(a=0), &(b=2));
    for(i=1; i<=3; i++)
        (a=(20+(i*78))-1;
         b=181;
         j=10;
         stci_d(n, i, j);
         movabs(&a, &b);
         movtcurabs(&a, &b);
         lnrel(&(a=0), &(b=2));
         movtcurrel(&(a=-9), &(b=10));
         text(".");
         movtcurrel(&(a=8), &(b=0));
         text(n);
         a=(58+(i*78))-1;
         b=181;
         movabs(&a, &b);
         lnrel(&(a=0), &(b=2));
        )

    a=110; /*Label x-axis*/
    b=199;
    movtcurabs(&a, &b);
    text(mess1);
    deltcu();
    movabs(&(a=8), &(b=0)); /*Draw ordinate*/
    lnrel(&(a=5), &(b=0));
    movabs(&(a=10), &(b=0));
    lnrel(&(a=0), &(b=179));
    movabs(&(a=8), &(b=179));
    lnrel(&(a=5), &(b=0));
    a=7;
    b=116; /*Label y-axis*/
}

```

```
settext(&(c=1), &(d=1), &(j=1), &(k=1));  
movtcurabs(&a, &b);  
text(mess2);  
deltcur();  
)
```

```
convert()
{
    extern double x[],lim1,lim2,lim3,lim4,lim5,lim6;
    int i;

    for(i=2;i<=101;i++)
    (if (x[i] <= lim1)
        x[i] = 0;
    else if (x[i] > lim1 && x[i] <= lim2)
        x[i] = 1;
    else if (x[i] > lim2 && x[i] <= lim3)
        x[i] = 2;
    else if (x[i] > lim3 && x[i] <= lim4)
        x[i] = 3;
    else if (x[i] > lim4 && x[i] <= lim5)
        x[i] = 4;
    else if (x[i] > lim5 && x[i] <= lim6)
        x[i] = 5;
    else if (x[i] > lim6)
        x[i] = 6;
    else printf("Invalid Input for Conversion\n");)
}
```

Lattice-C Programs

```

#include <stdio.h>

int p,q;

grey()
(
    int a,i;
    extern double x[];
    extern int stop;

    startgraphics(&(a=0));
    for(i=2;i<=101;i++)
        ( if (x[i] == 6)
            six(p,q);
          else if (x[i] == 5)
            five(p,q);
          else if (x[i] == 4)
            four(p,q);
          else if (x[i] == 3)
            three(p,q);
          else if (x[i] == 2)
            two(p,q);
          else if (x[i] == 1)
            one(p,q);
          else zero(p,q);
          next();)
    )

next()
(
    if(p == 317 && q == 0)
        stop=1;
    else
        (if(p != 317)
            p = p + 3;
          else
            (p = 20;
             q = q - 3;))
    )

six(p,q)
int p,q;
(
    int i,j,z;
    z=3;
    setcolor(&z);
    for(i=0;i<=2;i++)
        (for(j=0;j<=2;j++)
            (movabs(&p,&q);
             ptrel(&i,&j);))
    )

four(p,q)
int p,q;
(
    int i,j,z;
    z=1;

```

```

        setcolor(&z);
        for(i=0;i<=2;i++)
            (for(j=0;j<=2;j++)
                (movabs(&p,&q);
                    ptrrel(&i,&j);))
    )

two(p,q)
int p,q;
(
    int i,j,z;
    z=2;
    setcolor(&z);
    for(i=0;i<=2;i++)
        (for(j=0;j<=2;j++)
            (movabs(&p,&q);
                ptrrel(&i,&j);))
    )

zero(p,q)
int p,q;
(
    int i,j,z;
    z=0;
    setcolor(&z);
    for(i=0;i<=2;i++)
        (for(j=0;j<=2;j++)
            (movabs(&p,&q);
                ptrrel(&i,&j);))
    )

five(p,q)
int p,q;
(
    int i,j,z;
    z=3;
    for(i=0;i<=2;i++)
        (for(j=0;j<=2;j++)
            (if (z==3)
                (z=1;
                    goto skip;)
                if (z==1)
                    z=3;
                skip: setcolor(&z);
                    movabs(&p,&q);
                    ptrrel(&i,&j);))
    )

three(p,q)
int p,q;
(
    int i,j,z;
    z=1;
    for(i=0;i<=2;i++)
        (for(j=0;j<=2;j++)
            (if(z==1)
                (z=2;
                    goto skip;)
                if(z==2)
                    z=1;
                skip: setcolor(&z);
            )
        )
    )

```

```
        movabs(&p,&q);
        ptrel(&i,&j);}
    )
one(p,q)
int p,q;
(
    int i,j,z;
    z=2;
    for(i=0;i<=2;i++)
        (for(j=0;j<=2;j++)
            (if(z==2)
                (z=0;
                 goto skip;)
                if(z==0)
                    z=2;
            skip: setcolor(&z);
                 movabs(&p,&q);
                 ptrel(&i,&j);}))
    )
```



```

#include <stdio.h>

regrey()
{
    int a,i,c,n;
    FILE *cp, *fopen();
    extern int p,q;
    double j;

    startgraphics(&(amp;a=0));

    cp = fopen("code.prn","r");
    while((n = fscanf(cp,"%lf",&j)) != EOF)
    {
        if (j == 6)
            sixr(p,q);
        else if (j == 5)
            fiver(p,q);
        else if (j == 4)
            fourr(p,q);
        else if (j == 3)
            threer(p,q);
        else if (j == 2)
            twor(p,q);
        else if (j == 1)
            oner(p,q);
        else if (j == 0)
            zeror(p,q);
        else printf("No good\n");
        nextr();
    }
    fclose(cp);
}

nextr()
{
    if(p == 317 && q == 0)
        ;
    else
        (if(p != 317)
         p = p + 3;
         else
         (p = 20;
          q = q - 3;))
}

sixr(p,q)
int p,q;
{
    int i,j,z;
    z=3;
    setcolor(&z);
    for(i=0;i<=2;i++)
        (for(j=0;j<=2;j++)
         (movabs(&p,&q);
          ptrel(&i,&j);))
}

fourr(p,q)
int p,q;

```

```

    int i,j,z;
    z=1;
    setcolor(&z);
    for(i=0;i<=2;i++)
        (for(j=0;j<=2;j++)
            (movabs(&p,&q);
                ptrel(&i,&j);))
    )

twor(p,q)
int p,q;
(
    int i,j,z;
    z=2;
    setcolor(&z);
    for(i=0;i<=2;i++)
        (for(j=0;j<=2;j++)
            (movabs(&p,&q);
                ptrel(&i,&j);))
    )

zeror(p,q)
int p,q;
(
    int i,j,z;
    z=0;
    setcolor(&z);
    for(i=0;i<=2;i++)
        (for(j=0;j<=2;j++)
            (movabs(&p,&q);
                ptrel(&i,&j);))
    )

fiver(p,q)
int p,q;
(
    int i,j,z;
    z=3;
    for(i=0;i<=2;i++)
        (for(j=0;j<=2;j++)
            (if (z==3)
                (z=1;
                    goto skip;))
            if (z==1)
                z=3;
            skip: setcolor(&z);
                movabs(&p,&q);
                ptrel(&i,&j);))
    )

threer(p,q)
int p,q;
(
    int i,j,z;
    z=1;
    for(i=0;i<=2;i++)
        (for(j=0;j<=2;j++)
            (if(z==1)
                (z=2;
                    goto skip;))
            )
    )

```

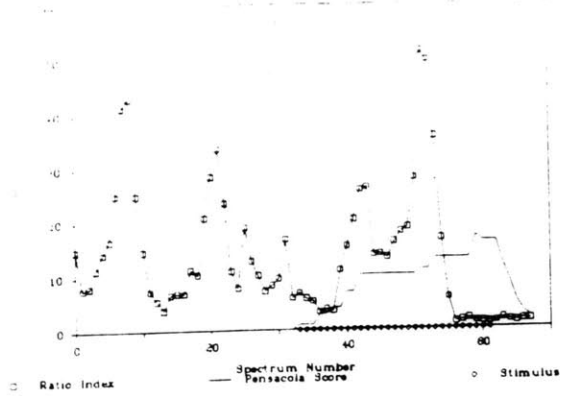
```
        if(z==2)
            z=1;
        skip: setcolor(&z);
            movabs(&p,&q);
            ptrel(&i,&j);))
    )
oner(p,q)
int p,q;
(
    int i,j,z;
    z=2;
    for(i=0;i<=2;i++)
        (for(j=0;j<=2;j++)
            (if(z==2)
                (z=0;
                 goto skip;)
                if(z==0)
                    z=2;
                skip: setcolor(&z);
                    movabs(&p,&q);
                    ptrel(&i,&j);))
            )
        )
    )
```

Appendix D

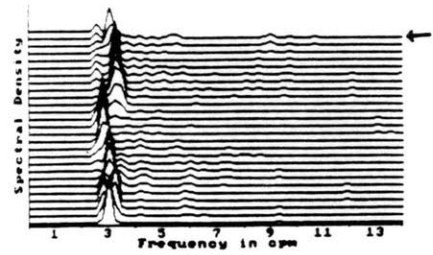
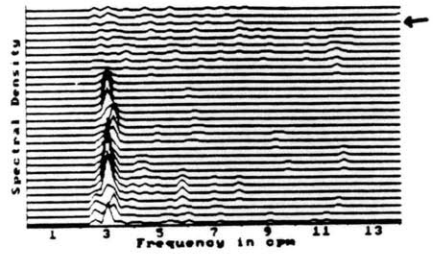
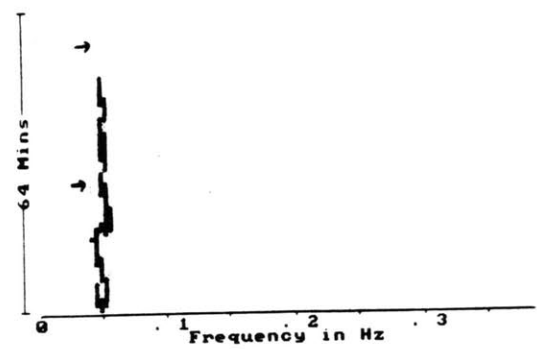
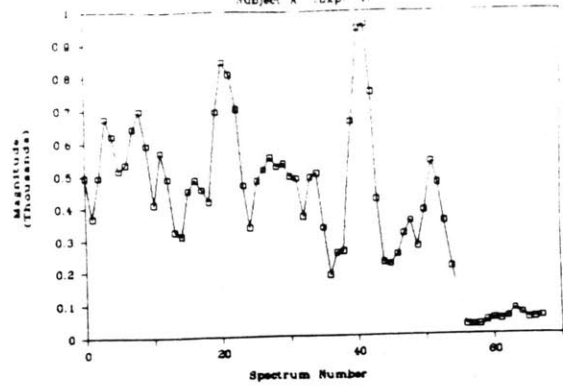
Data

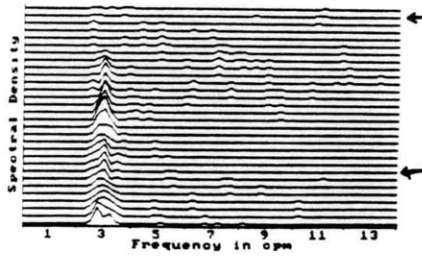
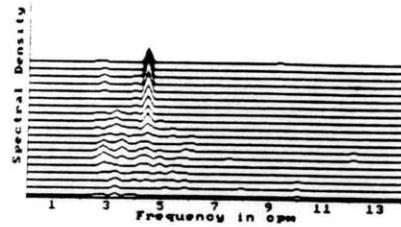
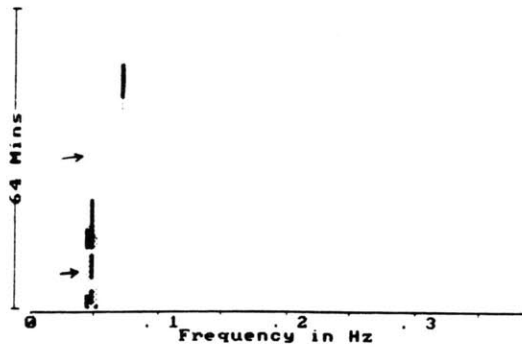
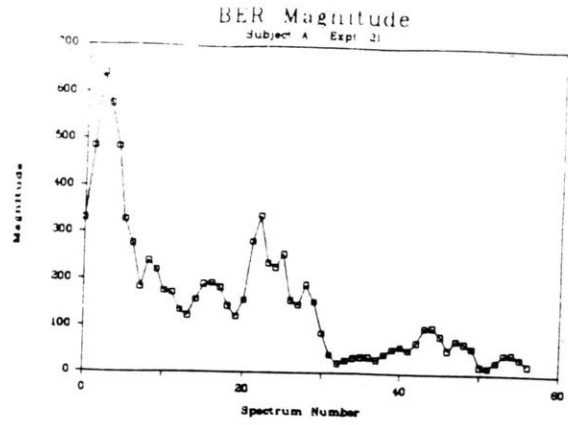
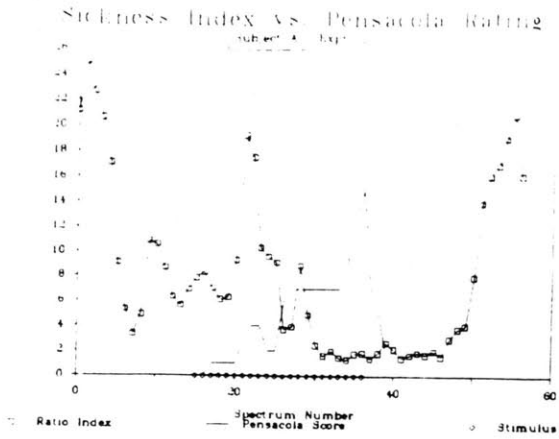
This section presents the data acquired from all 24 test sessions (6 subjects x 4 sessions) listed by subject and experiment number. The data are presented in four ways: (upper left) a graph of spectrum peak index (or sickness index or ratio index), Pensacola Score, and presence of stimulus as a function of Spectrum Number; (upper right) BER magnitude as a function of Spectrum Number; (lower left) grey-scale plot of computed spectra (darker pixels correspond to higher magnitudes); (lower right) waterfall plot of computed spectra. Grey-scale and waterfall plots are normalized to the value N. The first spectrum graphed on the grey-scale and waterfall plots is spectrum number 8. Spectra 0-7 were used to determine normalizing factor N. Arrows in lower graphs signify the beginning and end of the stimulus (chair rotation).

Success Index vs. Pensacola Rating
Subject A, Exp. 1



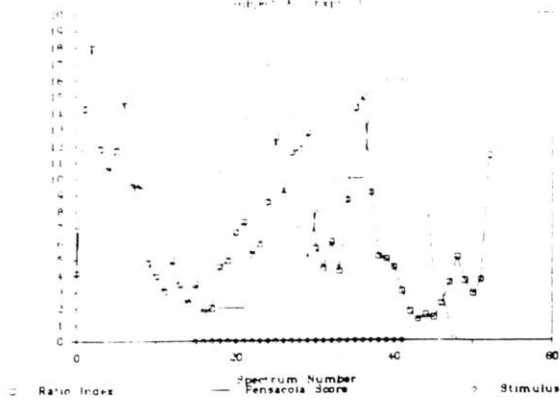
BER Magnitude
Subject A, Exp. 1



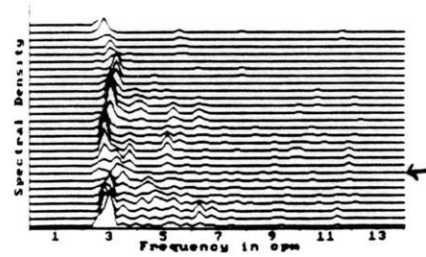
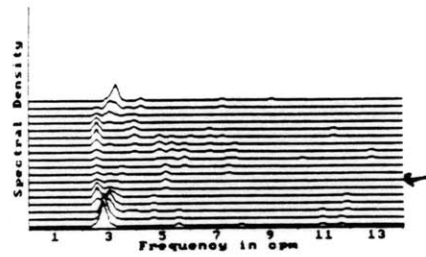
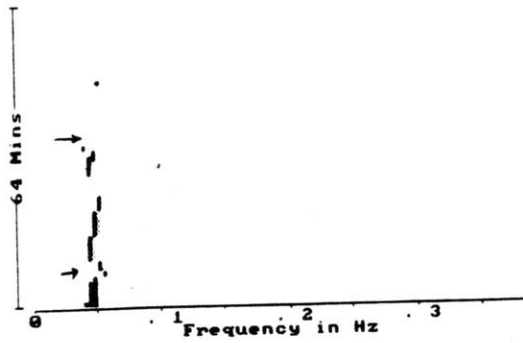
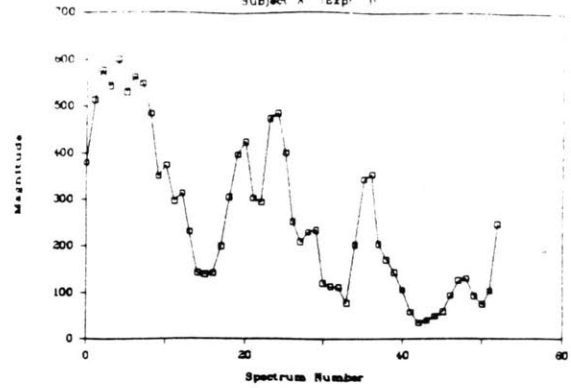


Subject A, Expt. 2 (N = 639)

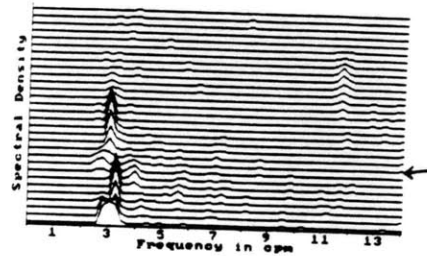
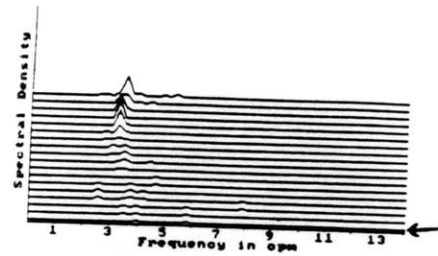
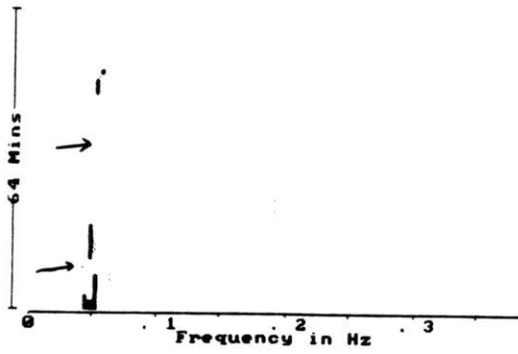
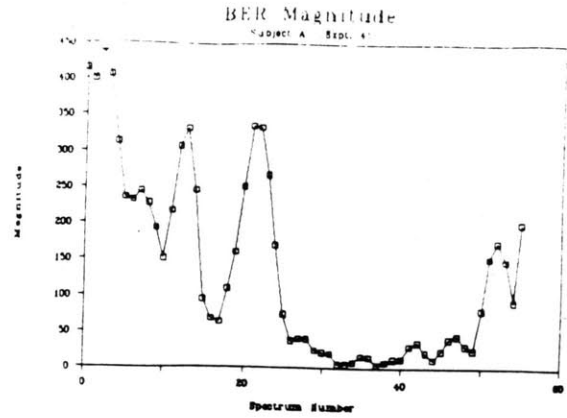
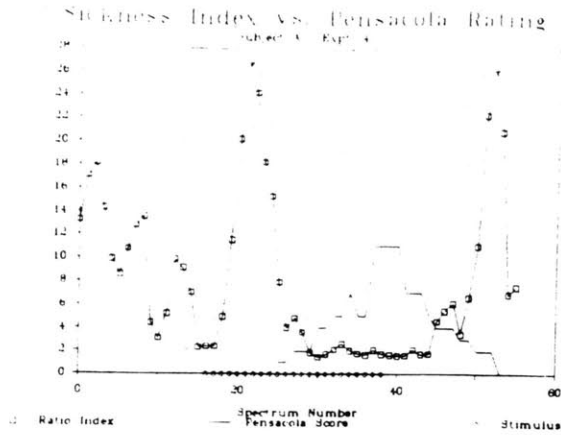
Sickness Index vs. Pensacola Rating



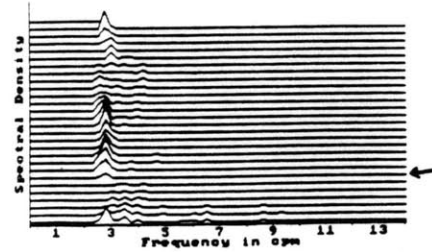
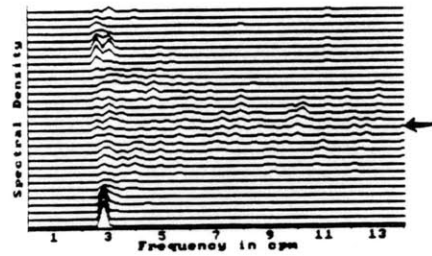
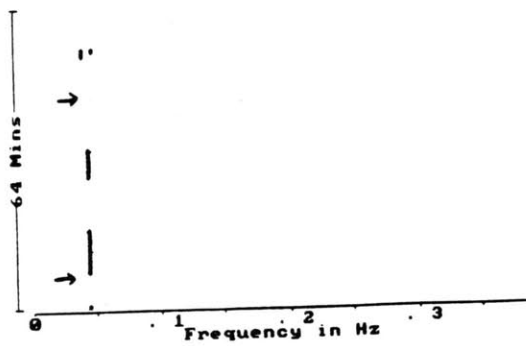
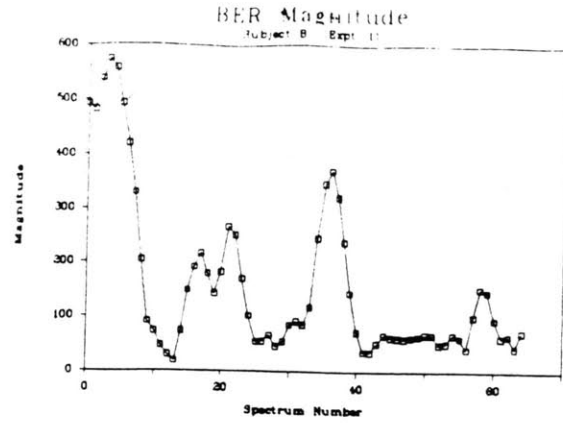
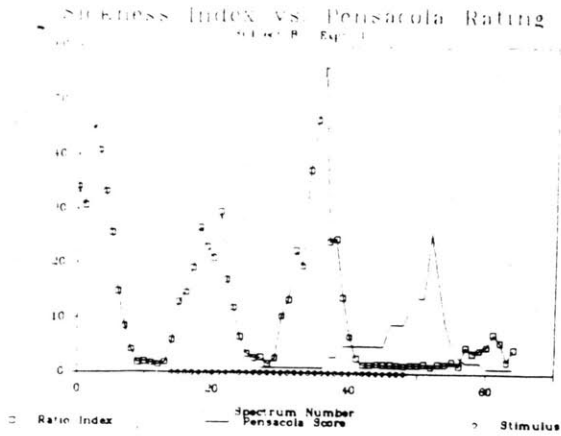
BER Magnitude



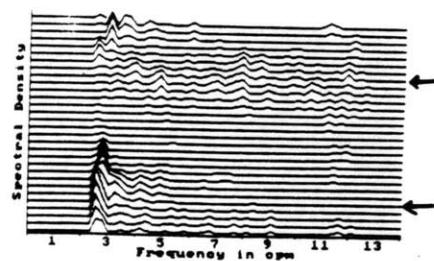
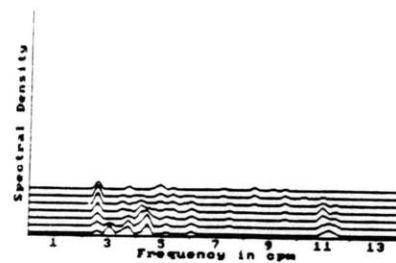
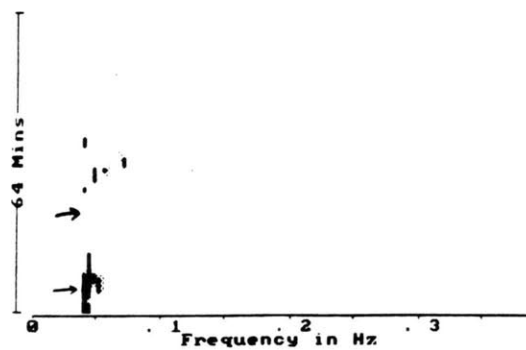
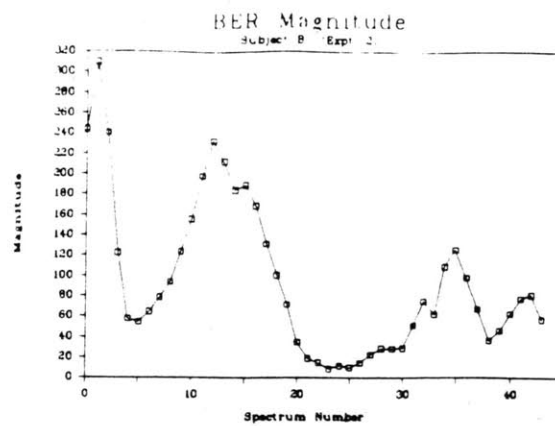
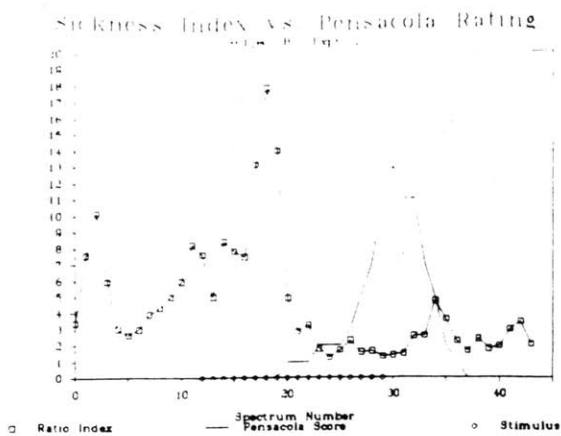
Subject A, Expt. 3 (N = 600)



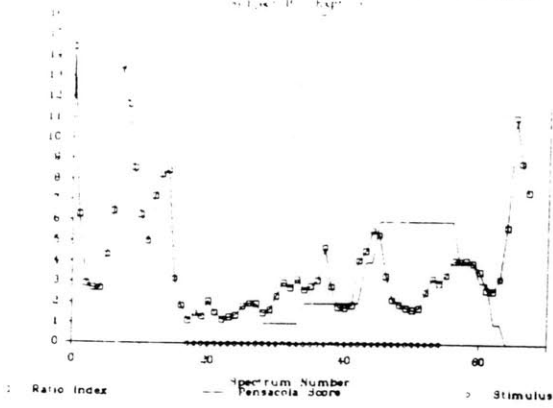
Subject A, Expt. 4 (N = 442)



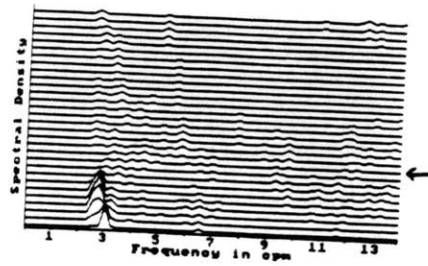
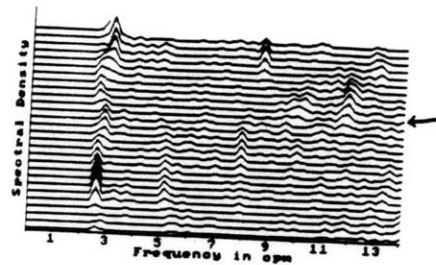
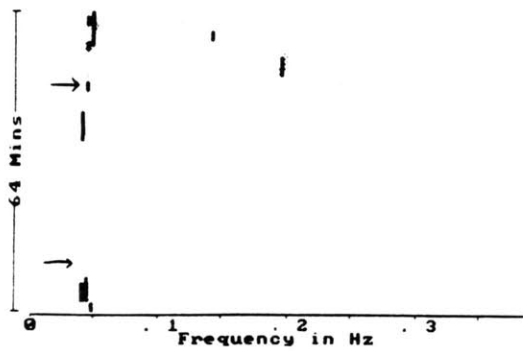
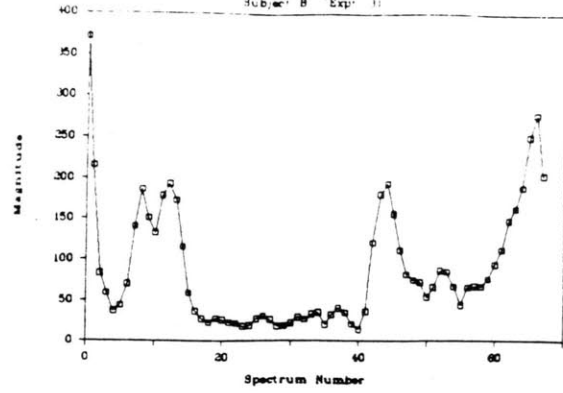
Subject B, Expt. 1 (N = 573)



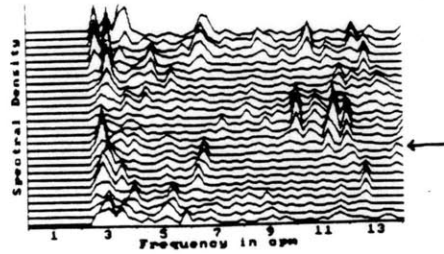
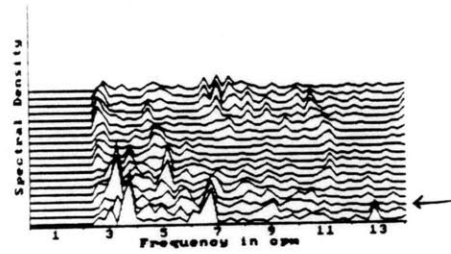
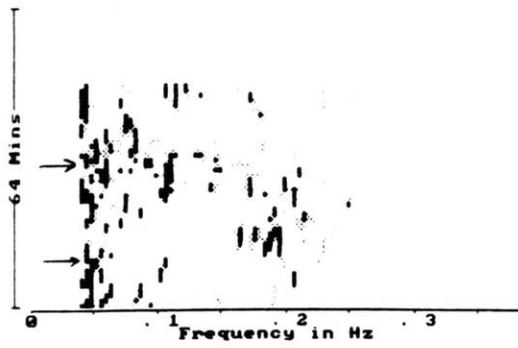
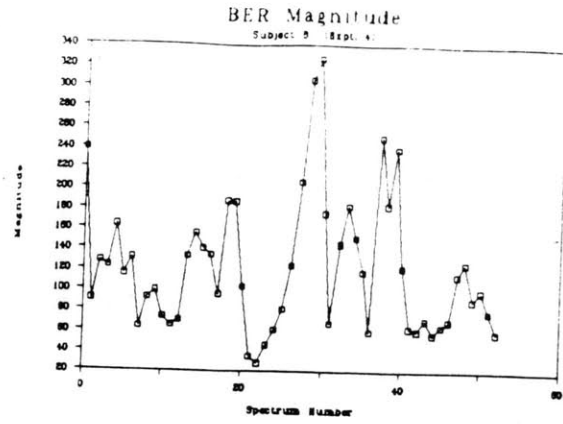
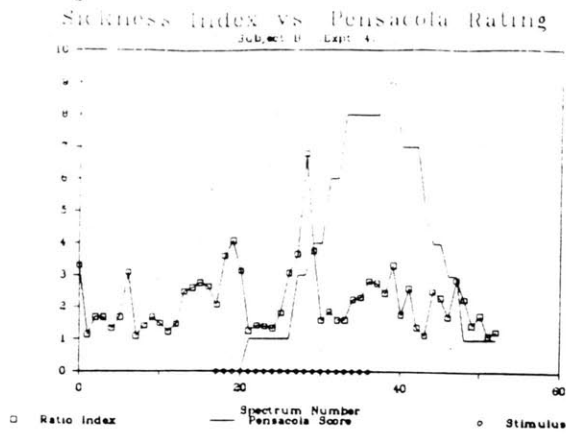
Sickness Index vs Pensacola Rating



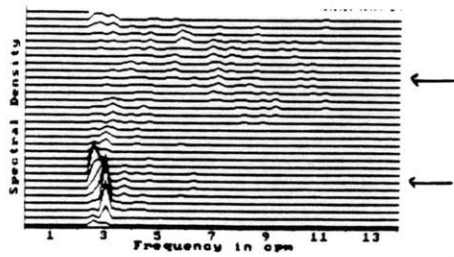
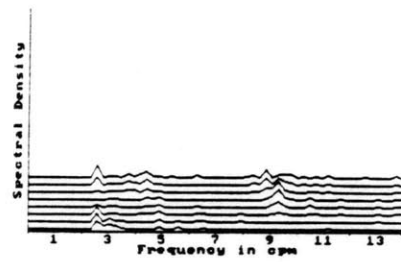
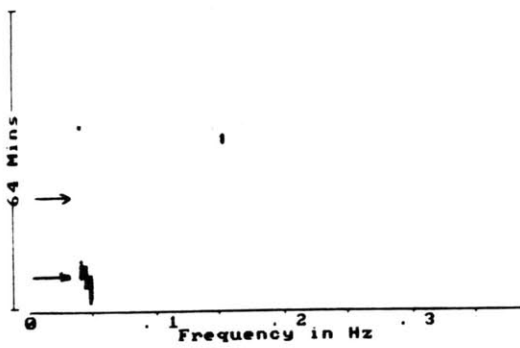
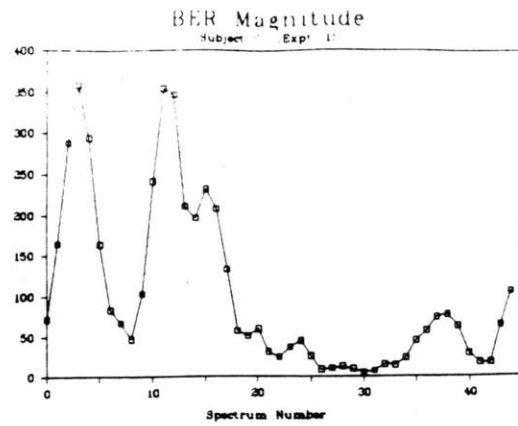
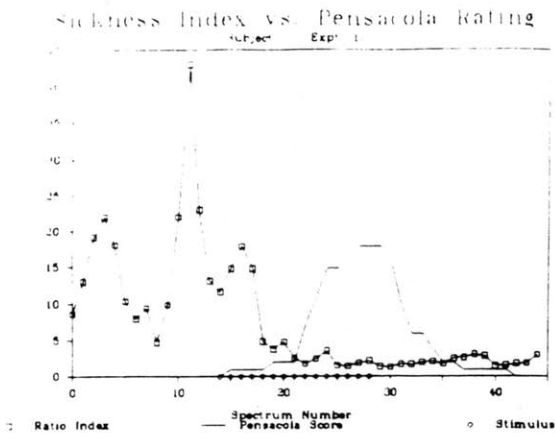
BER Magnitude



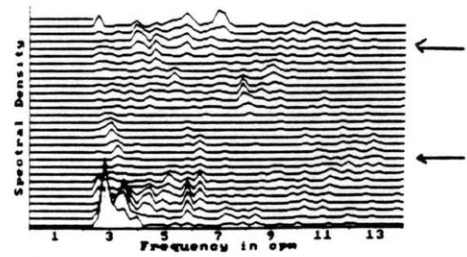
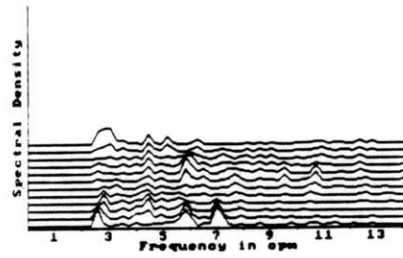
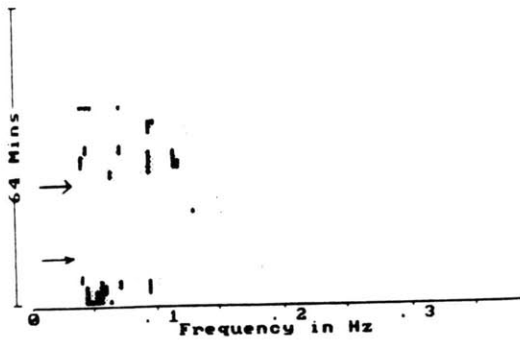
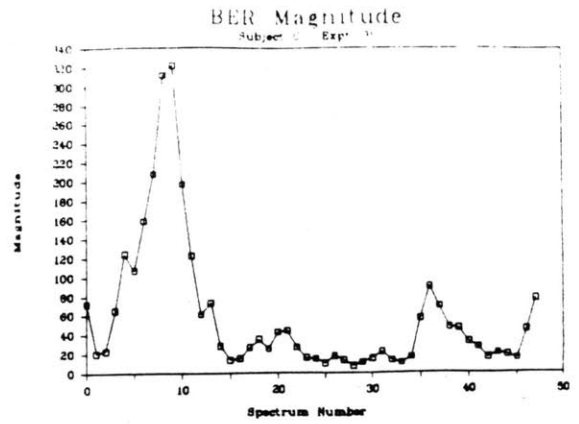
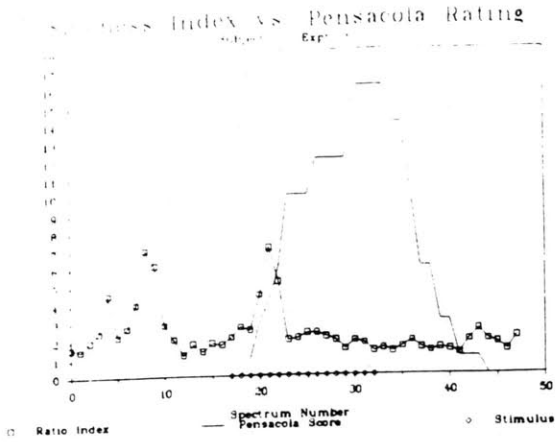
Subject B, Expt. 3 (N = 371)

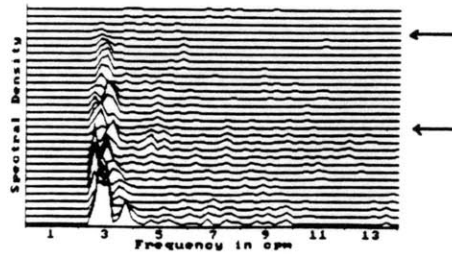
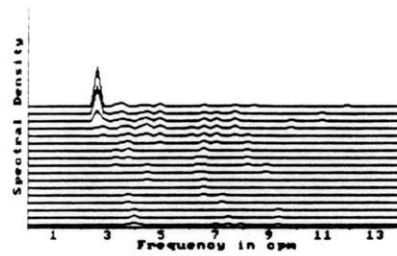
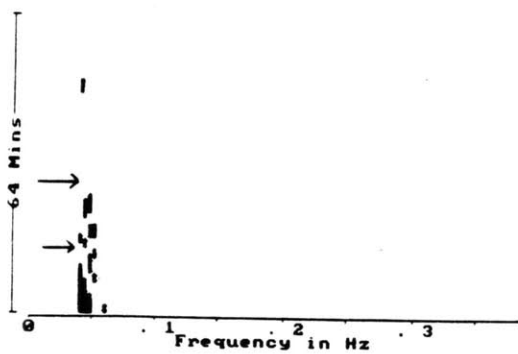
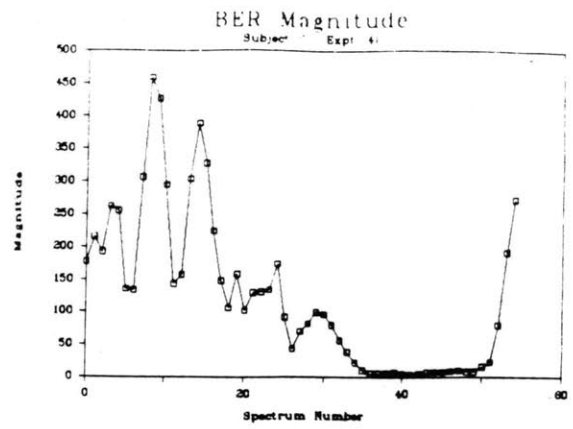
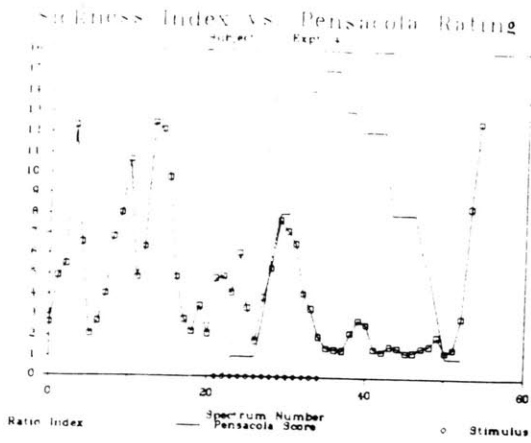


Subject B, Expt. 4 (N = 238)



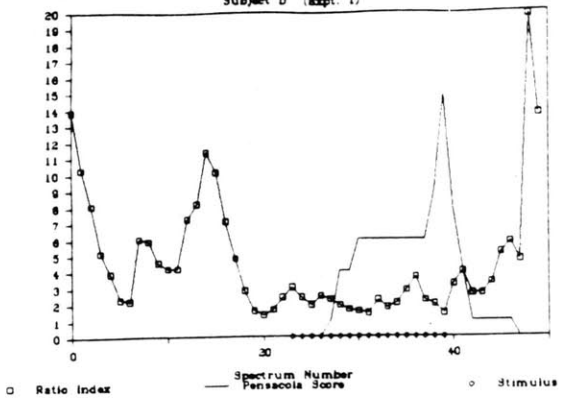
Subject C, Expt. 1 (N = 357)



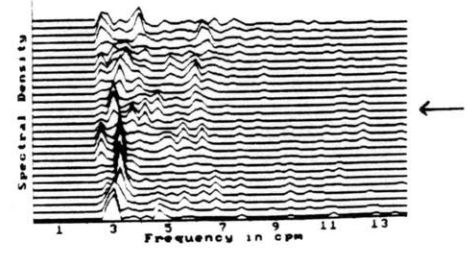
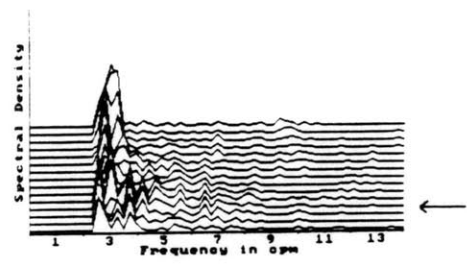
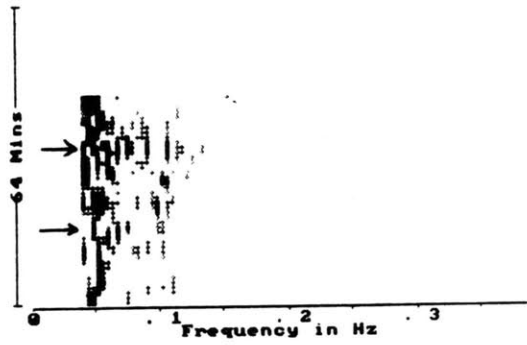
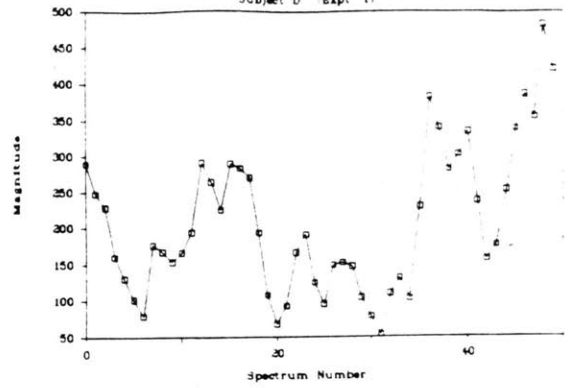


Subject C, Expt. 4 (N = 306)

Sickness Index vs. Pensacola Rating

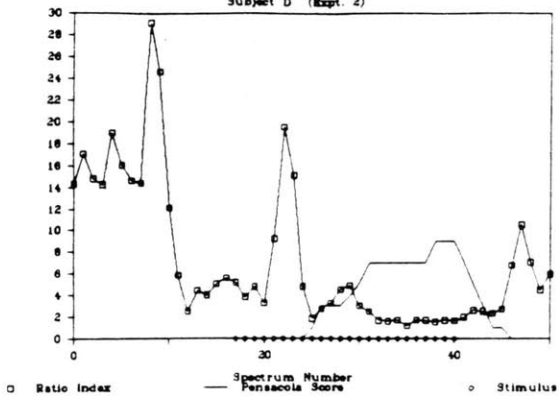


BER Magnitude

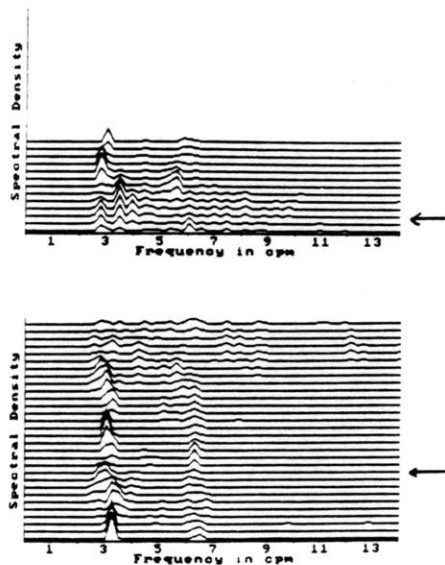
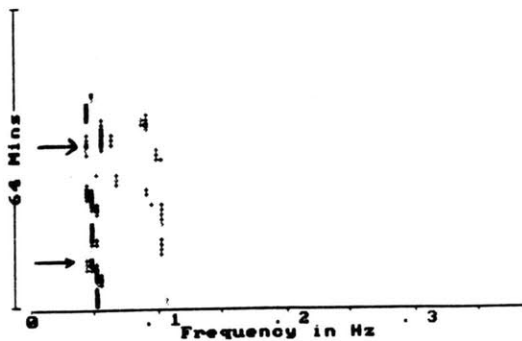
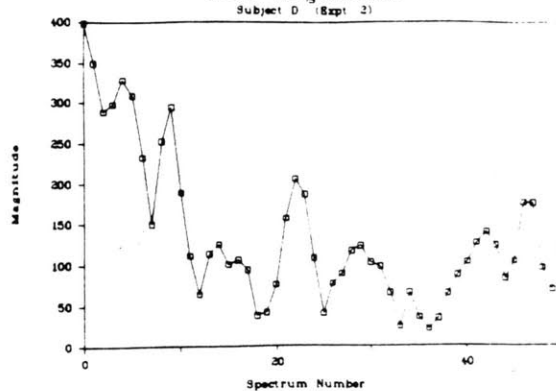


Subject D, Expt. 1 (N = 289)

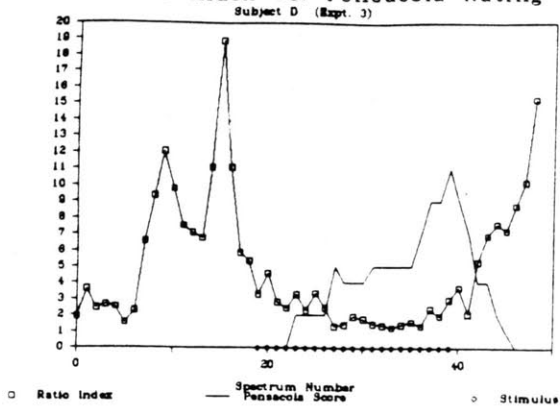
Sickness Index vs. Pensacola Rating
Subject D (Expt. 2)



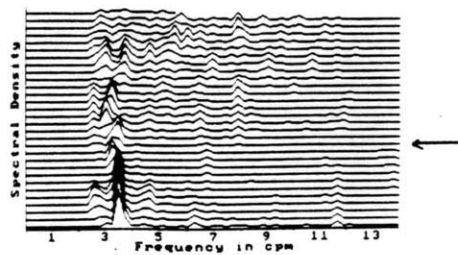
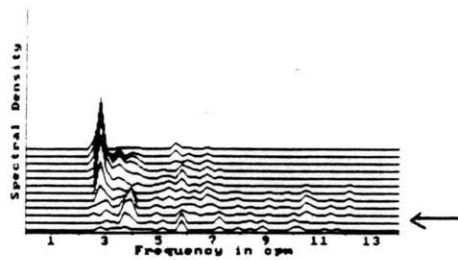
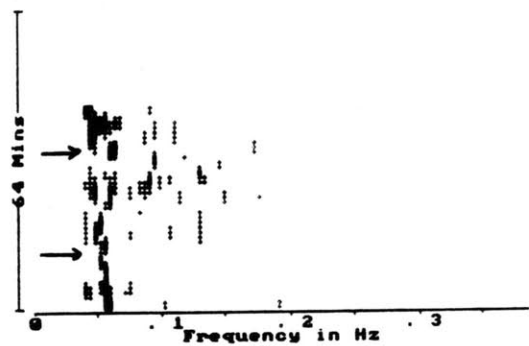
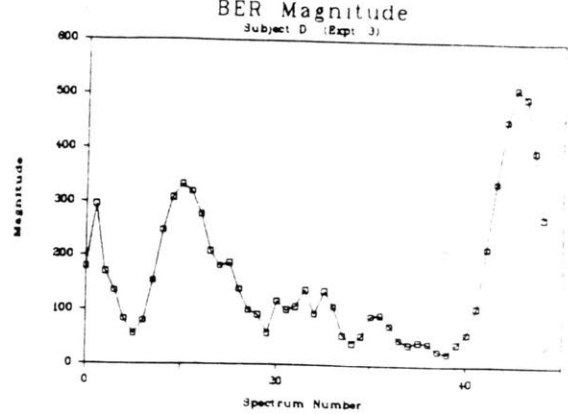
BER Magnitude
Subject D (Expt. 2)



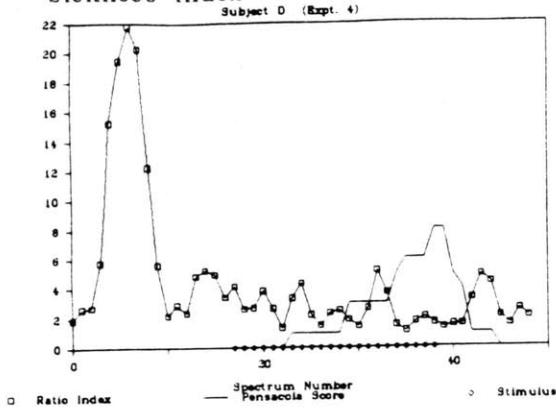
Sickness Index vs. Pensacola Rating



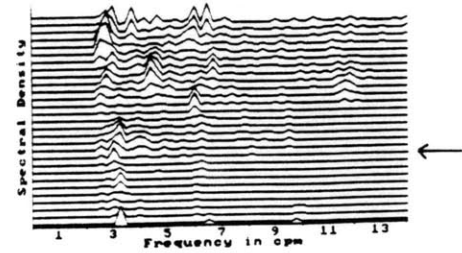
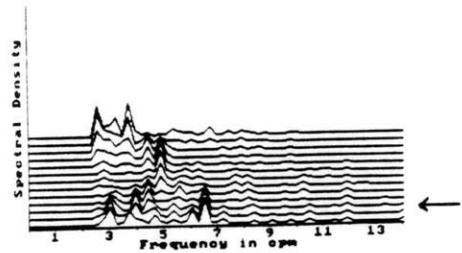
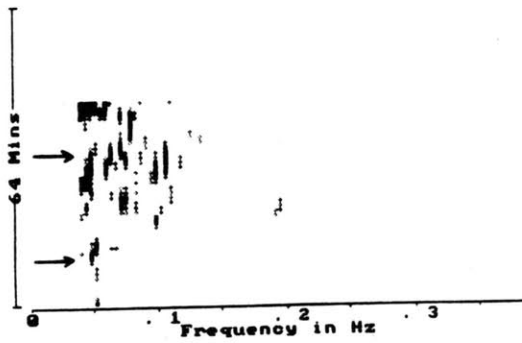
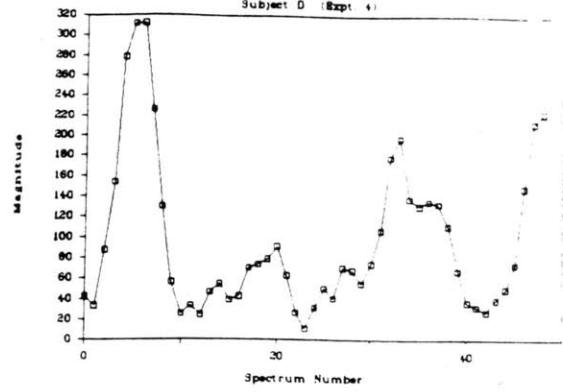
BER Magnitude



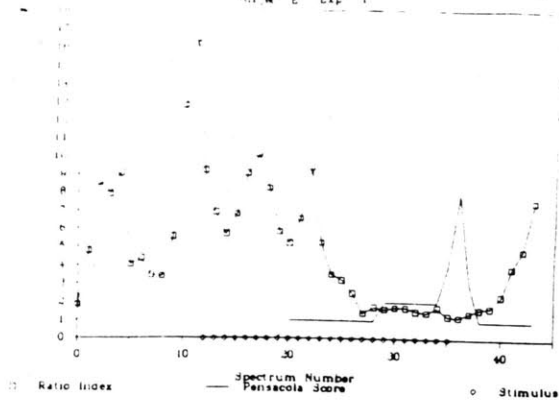
Sickness Index vs. Pensacola Rating



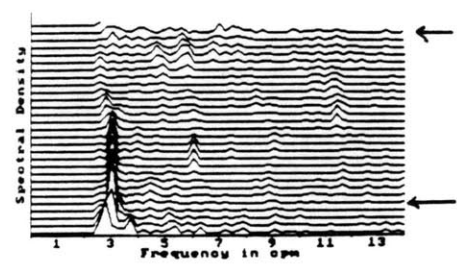
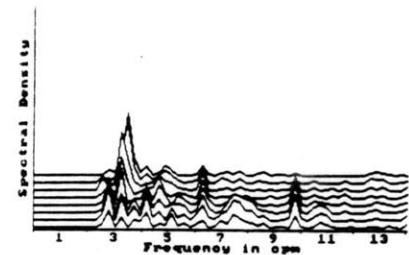
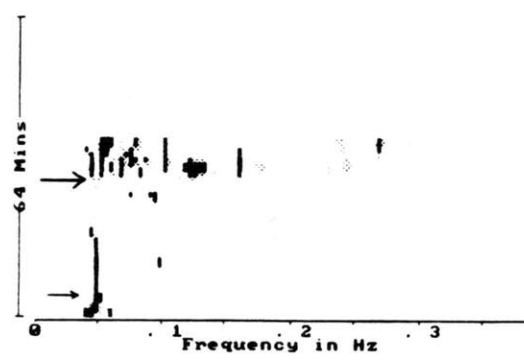
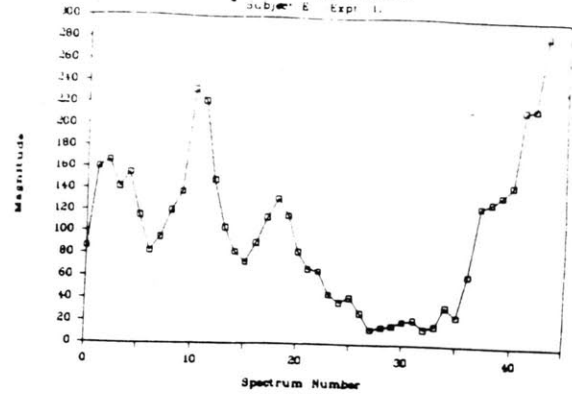
BER Magnitude



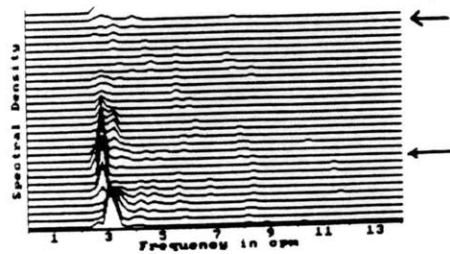
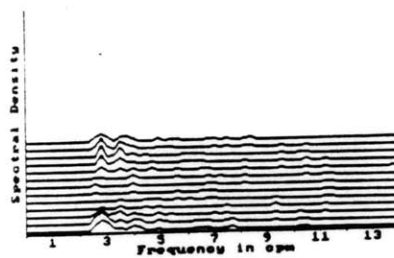
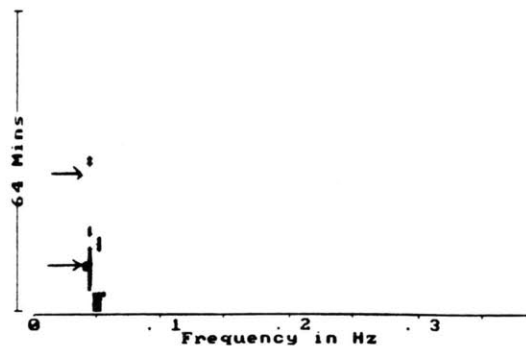
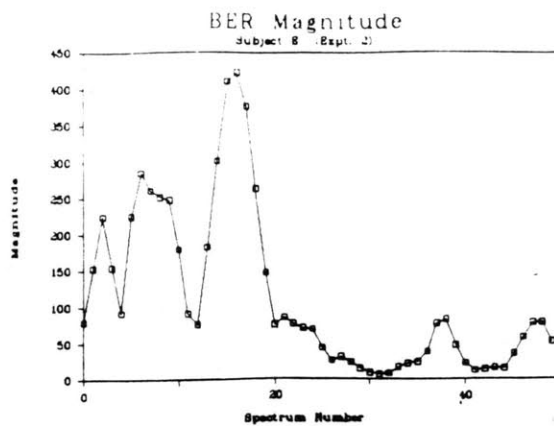
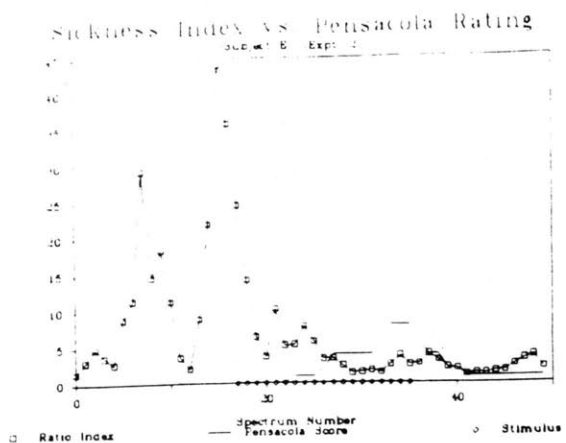
Sickness Index vs. Pensacola Rating



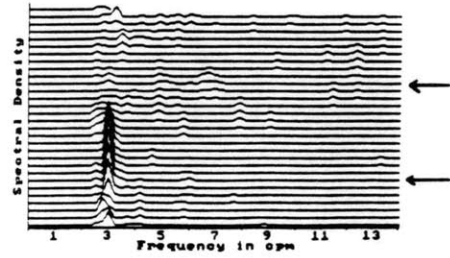
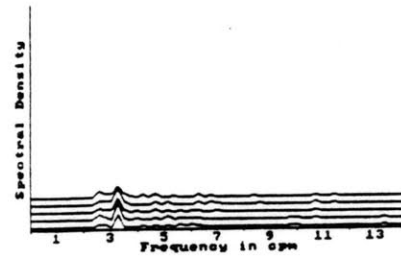
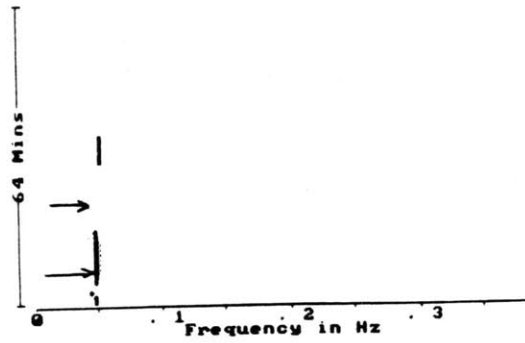
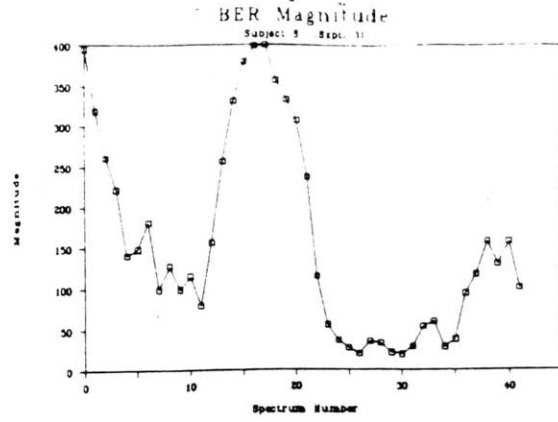
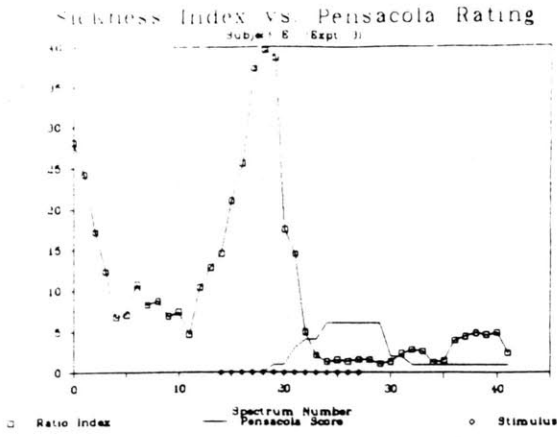
BER Magnitude



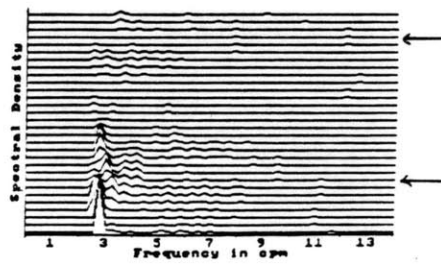
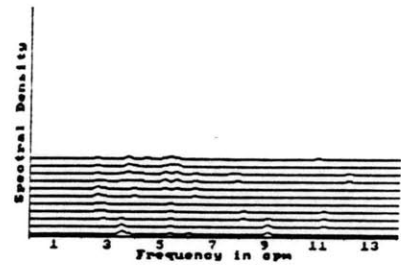
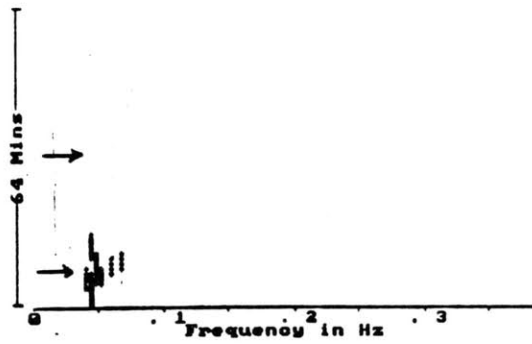
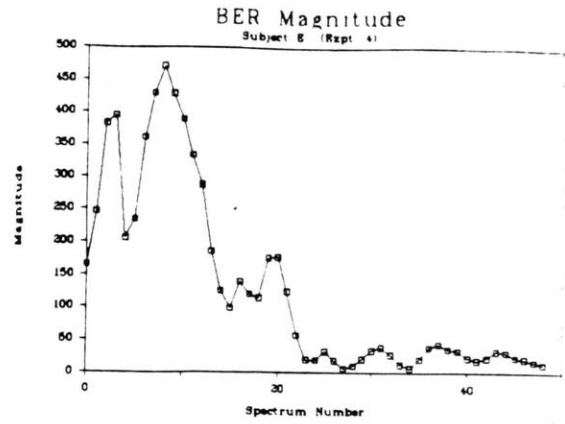
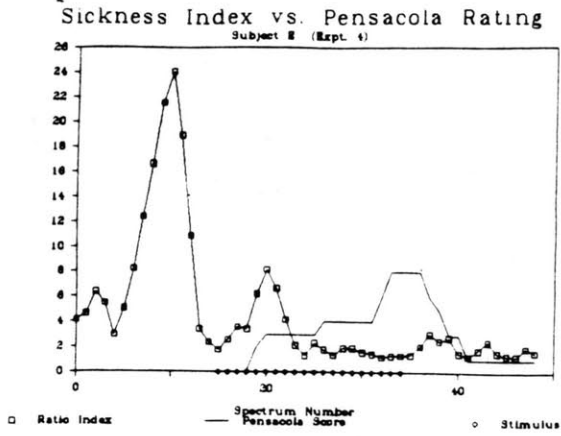
Subject E, Expt. 1 (N = 165)



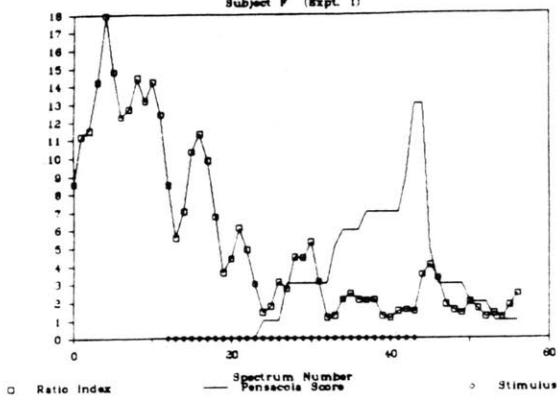
Subject E, Expt. 2 (N = 284)



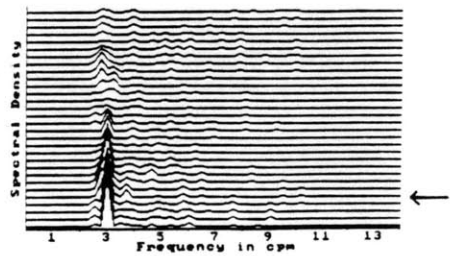
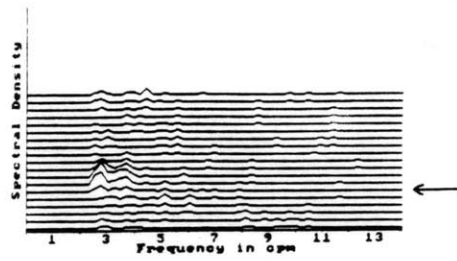
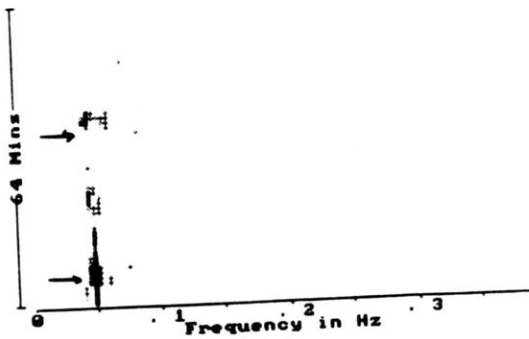
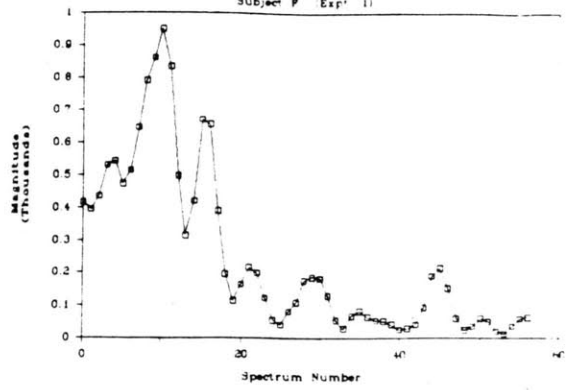
Subject E, Expt. 3 (N = 395)



Sickness Index vs. Pensacola Rating

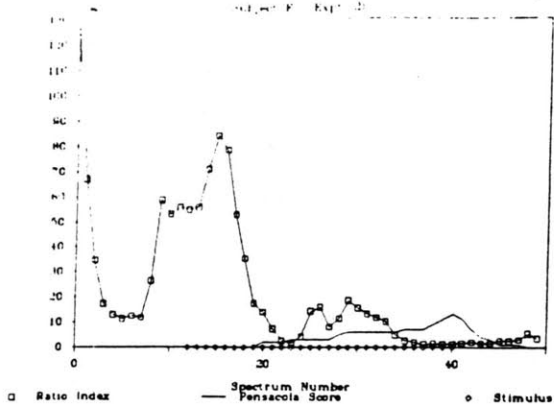


BER Magnitude

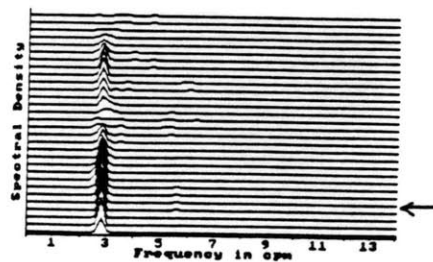
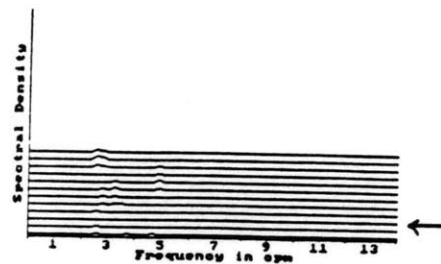
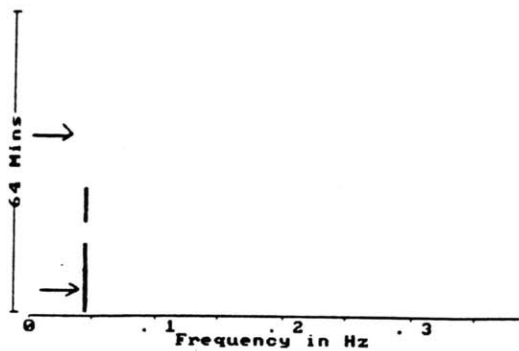
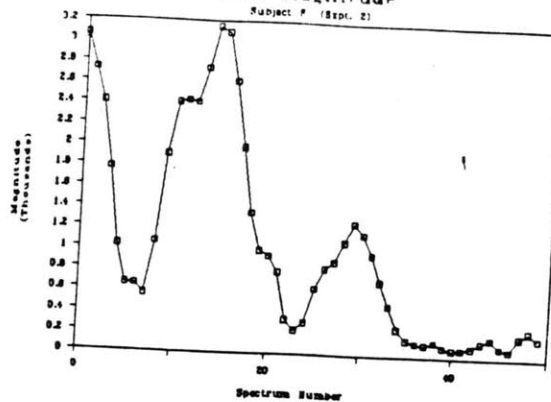


Subject F, Expt. 1 (N = 645)

Sickness Index vs. Pensacola Rating

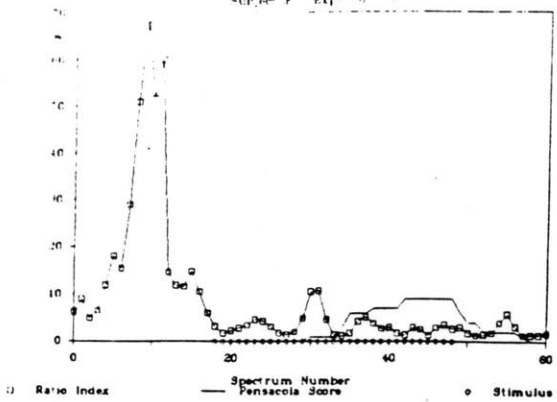


BER Magnitude

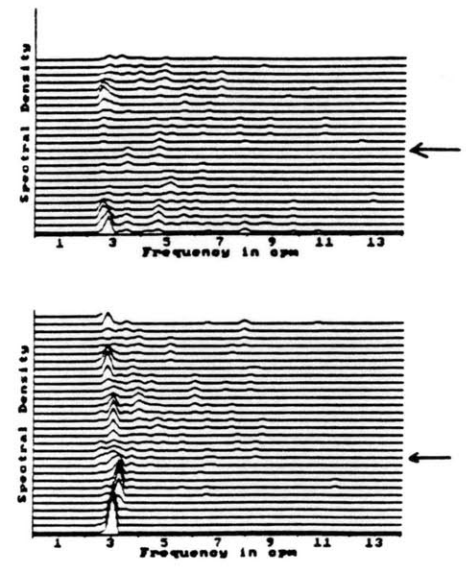
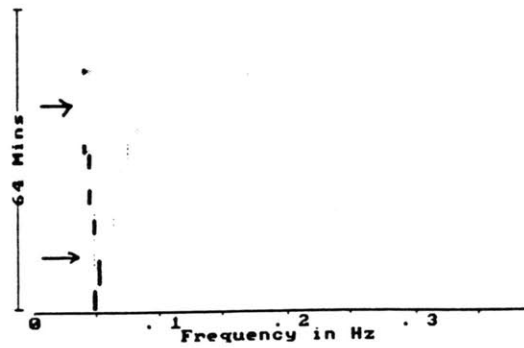
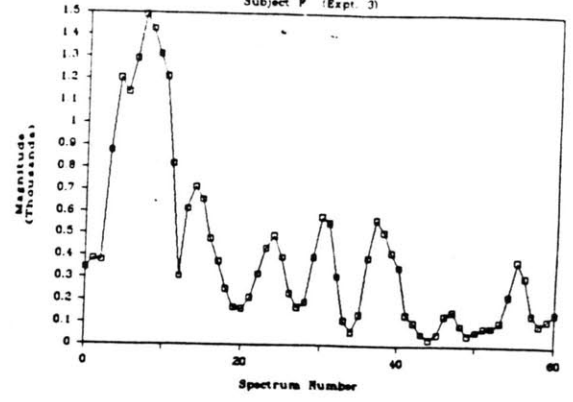


Subject F, Expt. 2 (N = 3056)

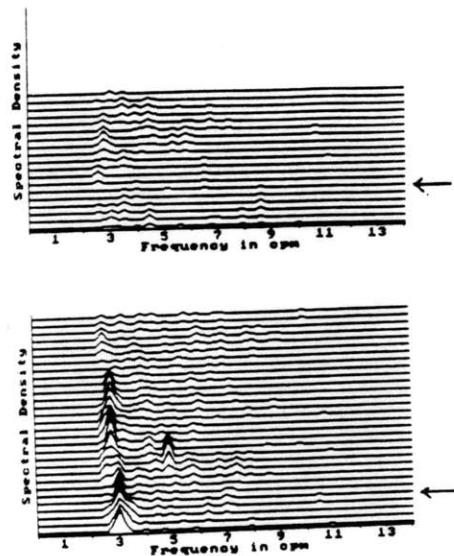
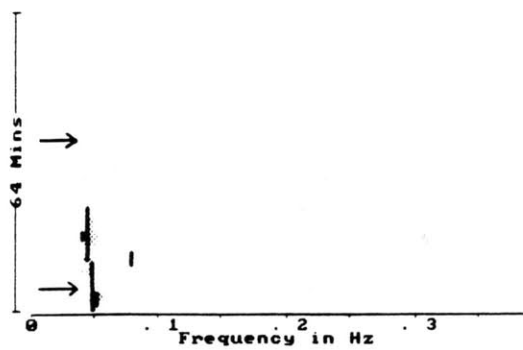
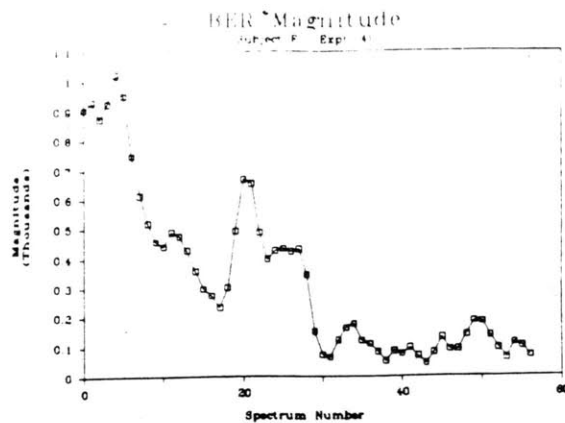
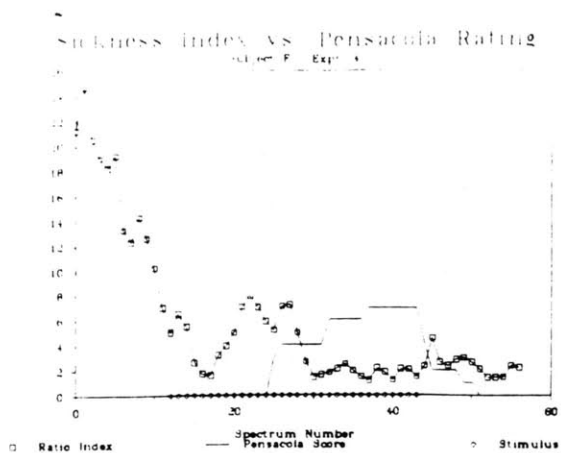
Sickness Index vs. Pensacola Rating



BER Magnitude



Subject F, Expt. 3 (N = 1490)



Subject F, Expt. 4 (N = 1024)

Bibliography

- [1] Abell, T.L., Malagaleda, J-R. "Glucogen-evoked gastric dysrhythmias in humans shown by an improved electrogastrographic technique," *Gastro.* 88; 1932-1940,1985.
- [2] Abell, T.L., Tucker R., Malagaleda, J-R. "Simultaneous gastric electromanometry in man," *Electrogastrography: methodology, validation, and application*,ed. Stern R.M., Koch, K.L., Praeger, New York, 78-88,1985.
- [3] Alvarez, W.C. "The electrogastrogram and what it shows,"*J.A.M.A.*, 78; 1116-1119,1922.
- [4] Bellahsene, B.E., Hamilton, J.W., Webster, J.G., Bass, P., Reichelderfer, M. "An improved method for recording and analyzing the electrical activity of the human stomach," *IEEE Trans.Biomed.Eng.*,Vol. 32, 11; 911-915,1985.
- [5] Bendat, J.S., Piersol, A.G. *Random Data: Analysis and Measurement Procedures*, John Wiley and Sons, N.Y.,1971.
- [6] Blackman, R.B., Tukey, J.W. *The Measurement of Power Spectra*, Dover,N.Y.,1959.
- [7] Bock, O.L., Oman, C.M. "Dynamics of subjective discomfort in motion sickness as measured with a magnitude estimation method," *Aviat. Space Environ.Med.* 53; 773-777,1982.
- [8] Brown, B.H., Smallwood, R.H., Duthie, H.L., Stoddard, C.J. "Intestinal smooth muscle electrical potentials recorded from surface electrodes," *Med.Biol.Eng.* 13; 97-103,1975.
- [9] Code, C.F., Marlett, J.A. "The interdigestive myo-electric complex of the stomach and small bowel of dogs," *J.Physiol.* 246; 289-309,1975.
- [10] Daniel, E.E., Irwin, J. "Electrical activity of gastric musculature," *Handbook of Physiology*, Section 6, Alimentary Canal, Volume IV, Am.Physiol.Soc., Washington,1968.

- [11] Davis, R.C., Garafolo, L., Gault, F. "An exploration of abdominal potentials," *J.Comp.Physiol.Psychol.* 50; 529-532,1957.
- [12] Davis, R.C., Garafolo, L., Kolnjorn. "Conditions associated with gastrointestinal activity," *J.Comp.Physiol.Psychol.* 52; 466-475,1959.
- [13] Durrani, T.S., Nightingale, J.M. "Data windows for digital spectral analysis," *Proc.Inst.Elec.Eng.* Vol. 119, 3; 343-352,Mar.1972.
- [14] Durrani, T.S., Nightingale, J.M. "Probability distributions for discrete Fourier spectra," *Proc.Inst.Elec.Eng.* Vol. 120, 2; 299-311,Mar.1973.
- [15] El-Sharkaway, T.Y., Morgan, K.G., Szurszewski, J.H. "Intracellular electrical activity of canine and human gastric smooth muscle," *J.Physiol.* 279; 291-307,1978.
- [16] Finch, P., Ingram, D., Henstridge, J., Catchpole, B. "The relationship of sleep stage to the migrating gastrointestinal complex of man," *Gastrointestinal Motility*, ed. J.Christensen, Raven Press, New York; 261-265,1980.
- [17] Geldof, H., Van Der Schee, E.J., Van Blankenstein, M., Grashuis, J.L., "Electrogastrographic study of gastric myoelectrical activity in patients with unexplained nausea and vomiting," *Gut* 27; 799-808,1986.
- [18] Grashuis, J.L., Van Der Schee, E.J., Geldof, H. "Electrogastrography in dog and man," *em/ Electrogastrography: methodology, validation, and application*, ed. Stern, R.M., Koch, K.L., Praeger, New York, 57-77,1985.
- [19] Graybiel, A., Wood, C.D., Miller, E.F., Cramer, D.B. "Diagnostic criteria for grading the severity of acute motion sickness," *Aerospace Med.* 39; 453-455,1968.
- [20] Guedry, F.E., Benson, A.J. "Coriolis cross-coupling effects: disorienting and nauseogenic or not?" *Aviat.Sp. Environ.Med* 49; 29-35,1978.
- [21] Hamilton, J.W., Bellahsene, B., Reichelderfer, M., Webster, J.G., Bass, P. "Human electrogastrograms: comparison of surface and mucosal recordings," *Dig.Dis.Sci.* 31; 33-39,1986.
- [22] Hamilton, J.W., Bellahsene, B.E., Cascio, D.S., Webster, J.G., Bass, P. "Human electrogastrograms: comparison of techniques of recording," preprint,1987.
- [23] Hamming, R.W. *Digital Filters*, Prentice-Hall Inc, N.J.,1977.
- [24] Harris, F.J. "On the use of windows for harmonic analysis with the discrete Fourier transform," *Proc.IEEE*, Vol. 66, 1; 51-83,Jan.1978.

- [25] Held, R. *Journal of Nervous and Mental Diseases* 132; 26-32,1961.
- [26] Homick, J.L., Reschke, M.F., Vanderploeg, J.M. "Space adaptation syndrome: incidence and operational implications for the space transportation system program," paper 36, Proc. NATO AGARD Sym.on Mot.Sick.: Mech., Pred., Prev.,and Treat., Williamsburg, VA, May,1984.
- [27] Itoh, Z., Aizawa, I., Takeuchi, S., Takayanagi, R. "Diurnal changes in gastric motor activity in conscious dogs," *Am.J.Dig.Dis.* 22; 117-124, 1977.
- [28] Kay, S.M., Marple, S.L. "Spectrum analysis - a modern perspective," *Proc.IEEE*, Vol. 69, 11; 1380-1419,Nov.1981.
- [29] Kelly, K.A., Code, C.F., "Canine gastric pacemaker," *Am.J.Physiol.* 220; 112-118,1971.
- [30] Kentie, M.A., Van Der Schee, E.J., Grashuis, J.L., Smout, A.J.P.M. "Adaptive filtering of canine electrogastrographic signals. Part 1: system design," *Med.Biol.Eng.Comput.* 19; 759-764,1981.
- [31] Kohl, R.L. "Failure of metoclopramide to control emesis or nausea due to stressful angular or linear acceleration," *Aviat.Space Environ.Med.* 58; 125-131,1987.
- [32] Linkens, D.A., Cannell, A.E. "Interactive graphic analysis of gastrointestinal electrical signals," *IEEE Trans.Biomed.Eng.* 21; 335-339,1974.
- [33] Linkens, D.A., Datarina, S.P. "Estimation of frequencies of gastrointestinal electrical rhythms using autoregressive modeling," *Med.Biol.Eng.Comput.* 16; 262-268,1978.
- [34] McDonough, F.E., Schneider, M. "Effect of motion on roentgenographic appearance of stomach and small bowel," *Gastro.* 2; 32-45,1944.
- [35] Miller, E.F., Graybiel, A. "A standardized laboratory means of determining susceptibility to coriolis (motion) sickness," Pensacola, FL, Naval Aerospace Medical Institute, NAMI-1058,1969.
- [36] Miller, E.F., Graybiel, A. "Motion sickness produced by head movement as a function of rotational velocity," Pensacola, FL, Naval Aerospace Medical Institute, NAMI-1101,1970.
- [37] Noll, A.M. "Cepstrum pitch determination," *J.Acoust.Soc.Am.* 41; 293-309,1967.
- [38] Oman, C.M. "A heuristic mathematical model for the dynamics of sensory conflict and motion sickness," *Acta Oto.Suppl.* 392,1982.

- [39] Oman, C.M. "Space motion sickness and vestibular experiments in Spacelab," SAE Tech. Paper 820833; 12th Intersoc. SAE Conf. on Environ. Systems, San Diego, GA,1982.
- [40] Oman, C.M. "Spacelab experiments on space motion sickness," Paper IAF 85-312, pp. 1-16,1985.
- [41] Oman, C.M., Lichtenberg, B.K., Money, K.E., McCoy, R.K. "Space motion sickness: symptoms, stimuli, and predictability," EBR,1986.
- [42] Oman C.M. "Experiments on the etiology and time course of motion sickness," Space Adapt.Res.Prog.Proposal, Submitted Sept.,1986.
- [43] Oman C.M. "Vestibular Organs," Class notes, Quantitative Physiology, March 15,1983.
- [44] Oppenheim, A.V., Schafer, R.W. *Digital Signal Processing*, Prentice-Hall, N.J.,1975.
- [45] Pederson, J.E. "Real time analysis of doppler signals reflected from blood vessels with a dedicated micro-processor," Proc.Bio.Eng. 80; 346-349,1980.
- [46] Reason, J.T., Graybiel, A. "Changes in subjective estimates of well-being during the onset and remission of motion sickness symptomatology in the slow rotation room," Pensacola, FL, Naval Aerospace Medical Institute, NAMI-1083,1969.
- [47] Reason, J.T., Brand, J.J. *Motion Sickness*, Academic Press, London,1975.
- [48] Reason, J.T. "Motion sickness adaptation: a neural mismatch model," J.Roy.Soc.Med. 71; 819-829,1978.
- [49] Smallwood, R.H. "Analysis of gastric electrical signals from surface electrodes using phase-lock techniques. Part 1: system design. Part 2: system performance with gastric signals," Med.Biol.Eng.Comput. 16; 507-518,1978.
- [50] Smallwood, R.H., Brown, B.H., Duthie, H.L. "An approach to the objective analysis of intestinal smooth muscle potentials recorded from surface electrodes," *Proc. 5th Int. Symposium on Gastrointestinal Motility*, Leuven, Belgium,1975.
- [51] Smout, A.J.P.M. *Thesis*, Erasmus University, Rotterdam, The Netherlands, 1980.
- [52] Smout, A.J.P.M., Van Der Schee, E.J., Grashuis, J.L. "What is measured in electro-gastrography?" *Dig.Dis.Sci.* 25; 179-187,1980.
- [53] Smout, A.J.P.M., Van Der Schee, E.J., Grashuis, J.L. "Postprandial and interdigestive gastric electrical activity in the dog recorded by means of cutaneous electrodes," *Gastrointestinal Motility*, ed. J.Christiansen, 187-194, Raven Press, N.Y.,1980.

- [54] Sobakin, M.A., Privalov, I.A. "Multichannel recording of human gastric electrical activity from body surface," *Bull.Exp.Biol.Med.* 81; 636-638,1976.
- [55] Stanley, W.D., Dougherty, G.R., Dougherty, R. *Digital Signal Processing*, Reston, Va.,1984.
- [56] Stern, R.M., Koch, K.L., Leibowitz, H.W., Lindblad, I.M., Shupert, C.L., Stewart, W.R. "Tachygastria and motion sickness," *Aviat.Space Environ.Med.* 56; 1074-1077,1985.
- [57] Stern, R.M., Koch, K.L., Stewart, W.R., Lindblad, I.M. "Spectral analysis of tachygastria recorded during motion sickness," *Gastro.* 92; 92-97,1987.
- [58] Stevens, S.S. "The direct estimation of sensory magnitudes-loudness," *Am.J.Psychol.* 69; 1-25, 1956.
- [59] Stevens, S.S. "On the psychophysical law," *Psychol.Rev.* 64; 153-184,1957.
- [60] Stevens, S.S. "Cross-modality validation of subjective scales for loudness, vibration and electric shock," *Exp.Psychol.* 57; 201-209,1959.
- [61] Szurszewski, J.H. "A migrating electrical complex of the canine small intestine," *Am.J.Physiol.* 217; 1757-1763,1969.
- [62] Szurszewski, J.H. "Mechanism of action of pentagastrin and acetylcholine on the longitudinal muscle of the canine antrum," *J.Physiol.* 252; 335-361,1975.
- [63] Telander, R.L., Morgan, K.G., Kreulen, D.L., Schmalz, P.F., Kelly, K.A., Szurszewski, J.H. "Human gastric atony with tachygastria and gastric retention," *Gastro.* 75; 497-501,1978.
- [64] Thompson, D.G., Richelson, E., Malagaleda, J-R. "Perturbation of gastric emptying and duodenal motility through the central nervous system," *Gastro.* 83; 1200-1206,1982.
- [65] Thouvenot, J., Tonkovic, S., Penaud, J. "Electrosplanchnography: method for electrophysiological exploration of the digestive tract," *Acta Med., Yugosl.* 27; 227-247,1973.
- [66] Tiemann, F., Reichertz, P. "Experiments using the electrointestinogram," *Med.Exptl.* 1; 17-26,1959.
- [67] Urkowitz, H. *Signal Theory and Random Processes*, Artech House, MA.,1983.

- [68] "Utricular and saccular otoliths," Class Notes, Quantitative Physiology, March 17, 1983.
- [69] Van Der Schee, E.J., *Thesis*, Erasmus University, Rotterdam, The Netherlands, 1984.
- [70] Van Der Schee, E.J., Smout, A.J.P.M., Grashuis, J.L. "Application of running spectrum analysis to electrogastrographic signals recorded from dog and man," *Motility of the Digestive Tract*, ed. M. Weinbeck, 241-250, Raven Press, N.Y., 1982.
- [71] Van Der Schee, E.J., Grashuis, J.L. "Contraction-related, low-frequency components in canine electrogastrographic signal," *Am.J.Physiol.* 245; 470-475, 1983.
- [72] Van Der Schee, E.J., Kentie, M.A., Grashuis, J.L., Smout, A.J.P.M. "Adaptive filtering of canine electrogastrographic signals. Part 2: filter performance," *Med.Biol.Eng.Comput.* 19; 765-769, 1981.
- [73] Vantrappen, G., Janssens, J., Hellemans, J., Ghooos, Y. "Interdigestive motor complex of normal subjects and patients with bacterial overgrowth of small intestine," *J.Clin.Invest.* 59; 1158-1166, 1977.
- [74] Volkers, A.C.W., Van Der Schee, E.J., Grashuis, J.L. "Electrogastrography in the dog: waveform analysis by a coherent averaging technique," *Med.Biol.Eng.Comp.* 21; 56-64, 1983.
- [75] Weber, J., Kohatsu, S. "Pacemaker localization and electrical conduction patterns in the canine stomach," *Gastro.* 59; 717-726, 1970.
- [76] Webster, J.G. *Medical Instrumentation: Application and Design*, Houghton Mifflin Co., 1978.
- [77] Wolf, S. "The relation of gastric function to nausea in man," *J.Clin.Invest.*, 22; 877-882, 1943.
- [78] You, C.H., Chey, W.Y., Menguy, R. "Electrogastrographic study of patients with unexplained nausea, bloating and vomiting," *Gastro* 79; 311-314, 1980.
- [79] You, C.H., Chey, W.Y., Lee, K.Y., Menguy, R., Bortaff, A. "Gastric and small intestinal myoelectric dysrhythmia associated with chronic intractable nausea and vomiting," *Ann.Int.Med.* 95; 449-451, 1981.

Acknowledgements

I would like to express my thanks to my thesis advisor, Dr. Charles M. Oman, whose guidance and support helped me throughout this research project. Without the financial support provided through our NASA contract, I don't believe I would even be writing this. I'd like to thank Alan Natapoff, who soundly counseled me when I approached him with tons of unintelligible data. Here's to the staff and graduate students of the MVL, best in Aero/Astro. I would especially like to thank Gina Gonzalez, my fiancée, for being there at my most difficult times and for tolerating my most unpleasant moods. And I cannot forget Justin. May he someday read this with interest and pride, and maybe with some realization that, yea, maybe the old man isn't so stupid after all.